Formation and Evolution of X-ray Binaries in Globular Clusters

A Thesis

Submitted to the
Tata Institute of Fundamental Research, Mumbai
for the degree of Doctor of Philosophy
in Physics

by

Sambaran Banerjee

Department of Astronomy & Astrophysics
Tata Institute of Fundamental Research
Mumbai

May, 2008

DECLARATION

This thesis is a presentation of my original research work. Wherever contributions of others are involved, every effort is made to indicate this clearly, with due reference to the literature, and acknowledgement of collaborative research and discussions.

The work was done under the guidance of Professor Pranab Ghosh, at the Tata Institute of Fundamental Research, Mumbai.

Sambaran Banerjee

In my capacity as supervisor of Mr. Sambaran Banerjee, I certify that the above statements are true to the best of my knowledge.

Pranab Ghosh

Date:

To my Parents

Acknowledgements

It is difficult to express my thankfulness and gratitude in words to the people whom I owe for the work during my days as a graduate student at TIFR, Mumbai, which accumulates to this thesis. A number of individuals have been on my side, in many different ways, during these years of wonderful learning experience.

To begin with, I wish to take this opportunity to thank my thesis advisor Prof. Pranab Ghosh without whom I cannot imagine of any fraction of this work. Prof. Ghosh is an eminent scientist and an extremely knowledgeable person, but more than that he is a warm and very friendly person to encounter with. His efficient guidance, friendly approach and constant encouragement is the root of my enthusiasm throughout this work. I enjoyed the discussion sessions with him wholeheartedly, often several times a day, which not only generated most of the ideas employed in this work but also have greatly helped me to have a broader view of the subject as a whole, which, I believe, is the most important part of my learning. His suggestions and criticisms have been extremely helpful in each phase this study. Apart from science, I am also thankful to him for his help in improving my capacity of writing and oral presentations.

I wish to express my gratitude to Prof. H.M. Antia for many scientific discussions and assistance. Antiaji's discussions and suggestions have been extremely helpful while developing the numerical codes for the computations. I am also very much thankful to him for his help in various institutional matters.

Special thanks to Prof. A.R. Rao for his lively company. Apart from discussions on astrophysics, Rao has also encouraged me in various other activities, particularly attending gym and the Marathon! While nobody could provide me more encouragement, running the Mumbai Marathon still remains to be materi-

alized. Thanks to Subhada (Dr. S. Majumdar) for enthusiastic discussions on many topics — science, food, trips. I am very much thankful to Pankaj (Prof. Pankaj S. Joshi) for teaching me general relativity and for the lively discussions during my project with him. I am thankful to DNA (Prof. D. Narashimha) for his discussions at various occasions.

Many thanks to my thesis synopsis examiners Prof. H.M. Antia, T.P. Singh, Prof. B.S. Acharya, A. Dighe and Prof. J.S. Yadav for many interesting discussions and helpful suggestions.

I am very much thankful to the Dept. of Astronomy & Astrophysics (DAA) at TIFR for its excellent environment for research and various facilities. I enjoyed the computing facility at DAA very much and I wish to thank Antiaji once more for maintaining such an excellent facility so efficiently. I am grateful to Kadam, Sobha and Magnes for their help in many departmental and technical matters and making life in the department so easy going.

So many thanks to my friends and colleagues at DAA for their friendship and pleasant company. Special thanks to my officemates Aseem, Anya and Tarak for their cheerful company and many lively discussions and debates. Thanks to Shasideep, Rakesh, Ashutosh, Satej, Harshal, Swastik, Surajit, Anandamayee for their happy company and numerous discussions. Many thanks to my former officemates Rituparno (rituda) and Poonam for their friendship. I relished their company very much. Apart from discussions on general relativity, rituda has encouraged me in various activities. I greatly enjoyed with him the treks through the Sahyadri mountains, the Mumbai film festival and general chat on many irrelevant and relevant issues. I am thankful to Poonam for sharing many happy moments with me and for creating additional recreation at our workplace while messing up with computers!

Many thanks to the staff of the administrative sections of TIFR, who has been extremely cooperative with me in all official matters. My special thanks to the Public Relations & Travel section officials who helped me a lot in my Visa applications while travelling abroad. Thanks to the Dispatch section officials for sending out loads of my stuff. Many thanks to the TIFR library staff for maintaining such a wonderful library and being so much polite while returning books as lately as three years! Thanks to the TIFR Canteen staff for feeding me.

My early days during my B.Sc. at Presidency college, Kolkata are memorable *for lifetime. My heartiest thanks to Prof. Dipanjan Raychaudhuri (DRC), Debapriyo Shayam (DS) and Mira Dey (miradi) for their excellent lectures, many discussions and advice and above all for their constant encouragement and support for being in this career. So many thanks to my batchmates Sudeep, Rajdeep, Supti, Ritaban, Shubhojit, Saiti, Chayan, Sohini, Kunal, Sanghamitra, Shyamal, Swati, Soumya for their friendship and sharing of many joyful moments. I am also thankful to them, particularly to Sudeep and Rajdeep, for many interesting discussions on physics. I express my admiration to College Street, Kolkata, for its books, history and its passionate touch!*

I am extremely thankful to Prof. Douglas C. Heggie (Univ. Edinburgh) for his enlightening and thought-provoking discussions at several meetings, which has greatly helped me in my work. Interaction with such an eminent astronomer like Douglas is indeed a very pleasant experience. My heartiest thanks to Prof. F.W.M. Verbunt (Univ. Utrecht) for many interesting and lively discussions. Many thanks to Simon Portegies Zwart (Univ. Amsterdam) for arranging my visit at the Astronomical Institute "Anton Pannekoek", Univ. Amsterdam. We had many interesting discussions during this visit, particularly on dynamical formation of hypervelocity stars. I am grateful to Holger Baumgardt (Univ. Bonn) for many lively discussions at several occasions, particularly those on N-body simulations. I am thankful to Prof. Pavel Kroupa (Univ. Bonn) for his discussions and helpful comments. Many thanks to Sverre J. Aarseth (IoA, Cambridge) for his discussions and suggestions. Many thanks to Piet Hut (IAS, Princeton) for discussions and introducing me to the "Virtual World". The "MICA" (Meta Institute for Computational Astrophysics) online meetings using the remarkable software "Qwaq" are awesome and I am very much pleased to take part in this entirely new way of scientific communications. I am thankful to Prof. S.L.W. McMillan (Univ. Drexel) for interesting discussions.

I wish to thank DAA, TIFR, Council for Scientific & Industrial Research (CSIR), Indian National Science Academy (INSA), International Astronomical Union (IAU), The Netherlands Research School for Astronomy and Astrophysics (NOVA) and European Science Foundation (ESF) for providing me grants for participating in several scientific events abroad which has been extremely helpful in my work and brought to me opportunities to interact with the experts from all over the world. I am thankful to the MODEST (Modelling Of DEnse STel-

lar systems) collaboration for holding such excellent workshops and providing me financial assistance and hospitality for attending them.

My days at TIFR were made colourful by several individuals, without whose introduction, this episode of acknowledgement would remain incomplete. My heartiest thanks to Swagato (mamu) for his friendship. Swagato has been with me in many good and bad times. I am grateful to him for all his help and advice in many matters with which I loved to bother him (even sometimes when it was not at all necessary, sorry mamu), be it life, photography, latex or physics. His company has always been a source of encouragement for me. I am also thankful to him for introducing me to photography which has now become my most favorite hobby. Many thanks to Anindita (mami) for her cheerful company in many occasions. So many thanks to Rajarshida (dadu) for his company and elderly advice on life, physics and diet. I am very sorry dadu, that I failed to follow your diet instructions while the others still seem fine. I am so much thankful to Shamik (comrade) for his friendship and wise advice in many occasions. Many thanks to Rajdeep, Sakuntala, Suman, Debanjan, Anandada, Sourin, Shamayita for their joyful company.

Special thanks to Anindya for his company, many discussions and above all, for his help with computers. Anindya has been the unparalleled mastermind in Linux at TIFR and I am grateful to him for teaching me about Linux. Thanks to Pallab for his help with computers and his voracious company at many restaurants. Cheers to Khadu, Tridib, Basu, Arnab, Partha, Aniket, Shamik (Gupta), Manna, Bela, Girish, Rahul for their joyful company.

Most of all, so many thanks to my parents for their endless love and care and for their support and encouragement which I find difficult to express in words. My parents are my greatest source of encouragement in whatever good I do and I owe to them the most for every success that I have achieved. Many thanks to my sister Tina for her affection and cheerful company.

Contents

List of Figures

Synopsis

Introduction

Globular clusters (henceforth GC) form a very interesting and challenging class of astrophysical systems, from both observational and theoretical points of view (Ashman & Zepf, 1998). A typical GC consists primarily of $10^4 - 10^6$ low-mass stars, gravitationally bound to a size of a few parsecs, which makes a GC several orders of magnitude richer in stellar content compared to the environment outside it, *i.e.*, the galactic field. GCs constitute one of the major components of the halos of both elliptical and spiral galaxies (Ashman & Zepf, 1998; Heggie & Hut, 2003), and for the Milky Way, the observed kinematic, photometric and dynamical properties have been catalogued in detail (Harris, 1996, revised in 1999; Pryor & Meylan, 1993) for many of them.

A GC usually has a core-halo structure, consisting of a core of radius typically less than 1 pc and density $10^4 - 10^5 M_\odot$ pc^{-3}, and an extended halo, in which the stellar density decreases outwards rapidly. For the Milky Way galaxy, and also many other elliptical and spiral galaxies, the GCs consist of old stellar populations (Ashman & Zepf, 1998) with age of the order of a Hubble time (Narlikar, 1993), consisting of low-mass stars within the range $0.1 M_\odot - 1 M_\odot$, typical for old stellar populations. For the Milky way and the Andromeda galaxy, the colour distribution of the GCs has been observed to be *bimodal* (Ashman & Zepf, 1998), so that they can be classified into *red-clusters* and *blue-clusters*. Whether the origin of such difference in colour is age or metallicity or both is a debated question (see Ashman & Zepf (1998) for a discussion). Dense star clusters with young stellar population have also been observed (*e.g.*, in the Antennae merging galaxies), known as the *young massive star clusters*, which are believed to be young phases of GCs. Apart from ordinary stars, GCs also contain compact stellar remnants like neutron stars (henceforth NS) and white dwarfs (henceforth WD). Stellar mass black holes (henceforth BH) however have not been observed in GCs. It is argued that BHs, being generally heavier than the single stars, easily form very tight binaries between them in GC cores through *mass-segregation* and *exchange encounters* (Miller, 2007), which are eventually kicked out of the GC due to recoils from encounters (Spitzer, 1987; Heggie & Hut, 2003) with single stars and binaries. However, intermediate mass black-holes (IMBH) with mass $\sim 10^3 M_\odot$, which can be formed in GC cores through runaway merger of stars as has been observed in several N-body simulations (Portegies Zwart et.al., 2004; Gürkan et.al, 2004), can be retained in GCs. Indirect observational evidences of presence of IMBHs in GCs have been obtained, the most recent one being that described by Maccarone et.al (2007).

It has been realized for about 30 years now that a GC core being a dense concentration of single stars, stellar binaries and compact objects, compact binaries and merger products are produced efficiently in GCs through dynamical encounters like tidal capture, exchange and direct collisions, which, unlike the situation in the field, can proceed at a significant rate in the dense core of a GC. A GC is therefore a "factory" for dynamically producing different kinds of compact binaries. By the term *compact binary*, we mean one that has at least one of its members as a compact star. The compact binaries that are formed dynamically can be *hard* in the sense that their binding energy is larger than the mean kinetic energy of a single star. Such hard binaries can in turn influence the overall dynamical evolution of GC significantly through dynamical processes like mass segregation and "binary-heating" (Spitzer, 1987; Heggie & Hut, 2003) (see below). One of the most interesting and important kind of compact binaries are the X-ray binaries in which we are primarily interested in this thesis. Among other interesting kinds dynamical products are double-NS systems which are very promising sources of gravitational waves and short-period GRBs. Binaries with IMBHs are also widely discussed and are potentially important sources of gravitational radiation. We shall however confine our discussion on X-ray binaries in

GCs, with particular attention to their population evolution through dynamical formation, destruction and binary-orbit shrinkage or "hardening" as they undergo encounters with the surrounding stars. Before proceeding further, we give a brief introduction to the observed properties of X-ray binaries in GCs.

Observing compact binaries in GCs poses extra challenge because, being heavier than the single stars or binaries consisting of two low-mass GC stars, these are segregated into the GC core and hence require very high spatial resolution for optical detection. Thus, GC compact binaries have been best observed in X-rays. X-ray binary populations in GCs of our Galaxy and external galaxies have been detected through observations of high resolution X-ray observatories like CHANDRA, which has discovered a large number of X-ray sources in several GCs in the Galaxy (Pooley et al., 2003) and in several elliptical galaxies (Angelini et.al., 2001). These observations indicate that the Milky Way GCs contain about 100 times more X-ray binaries (per stellar mass) compared to the field and the ratio is much higher for elliptical galaxies. The dynamical processes in GCs are believed to be responsible for this observed overabundance of GC X-ray sources (see Hut et.al. (1992) for a review).

Pooley et al. (2003) found that the number of X-ray sources (mainly low to medium luminosity) in Galactic GCs has a strong positive correlation with the estimated two-body encounter rates of these GCs. It was also found that the probability of finding a bright X-ray source among all the GCs is about 4 percent and remains approximately same for different Galaxy types (Kundu et.al., 2002). Interestingly, it has also been observed that the redder/younger GCs (see above) are more likely to host an X-ray binary than the bluer/older GCs indicating that the formation and evolution of the X-ray binary population may be affected either by age or by metallicity of the cluster (Sarazin et al., 2003). It it also observed that the total number of LMXBs and CVs in different galaxies increase in proportion with the total number of GCs hosted by them rather than the optical luminosity of the galaxies, leading to the possibility that most or all of such binaries in a galaxy may have been formed in the GCs (White et.al., 2002). This is further supported by the lack of evidence of any significant difference between GC and non-GC LMXB/CV populations (Sarazin et al., 2003).

A population of very bright ($L_X \sim 10^{37} - 10^{39}$ erg s^{-1}) and short orbital period ($P < 1$hr) X-ray binaries have been observed in Galactic GCs and massive elliptical galaxies, known as ultra-compact X-ray binaries (UCXB). A significant number of such objects is found in massive elliptical galaxies and for our Galaxy the $(4-7) \times 10^{37}$ erg s^{-1} source 4U 1820-30 in the GC NGC 6624 is the best known example. Such an object is predicted to be a tight binary between a low-mass ($< 0.1 M_\odot$) C/O or He white dwarf donor and a neutron star (Verbunt, 1987; Bildsten & Deloye, 2004). They are predicted to be formed due to physical collisions between a red giant star (henceforth RG) and a neutron star, which results in a common envelope (henceforth CE) inspiral of the latter and subsequent ejection of the RG envelope, forming a narrow binary between the NS and the degenerate core (Verbunt, 1987; Ivanova et.al., 2005). Dense GC cores are therefore believed to be exclusive locations for forming them. UCXBs may well dominate the bright end of the X-ray luminosity function of elliptical galaxies, as argued by Bildsten & Deloye (2004), although they constitute a tiny fraction numerically (Ivanova et.al., 2005; Banerjee & Ghosh, 2007).

Compact binaries, consisting of a compact star and a non-compact companion are formed and destroyed in GC cores through three dynamical processes, *viz.*, (a) *tidal capture* (b) *exchange* mechanisms and (c) *dissociation*, as we discuss below. Such a dynamically formed binary will in general be detached and become an X-ray binary only after the non-degenerate companion fills its Roche-lobe through evolution of the binary (van den Heuvel, 1991). Evolution of such *pre X-ray binaries* or PXBs is not only governed by "natural" mechanisms, namely, orbital angular momentum loss and evolution of the companion, but as well by repeated encounters with the surrounding stars in the GC core.

The dynamical properties of a GC core, with mean density ρ, core radius r_c and dispersion velocity v_c, can be described by two quantities, namely, $\Gamma \equiv (\rho^2/v_c)r_c^3$ and $\gamma \equiv \rho/v_c$, as pointed out by Verbunt (2003). Γ is a measure of the total two-body encounter rate within a GC core and γ measures the rate of encounter of a *single* binary with the surrounding stars (Verbunt, 2003). Γ is a basic scaling parameter for the formation rate of compact binaries (as well as other two-body dynamical processes) and the dynamical binary destruction rate (as well as other binary single-star encounter events) scales as γ. We shall jointly refer to them as *Verbunt parameters* (Banerjee & Ghosh, 2007).

One of the most important channels for the formation of compact binaries is tidal capture. A compact star, during a close passage by an ordinary star, raises tidal deformation on the latter and sets non-radial oscillations in it. The energy dissipated due to the consequent viscous heating of the star, which is extracted from the kinetic energy of relative motion, can be enough to make them bound, provided their first periastron separation r_p is smaller than a critical value r_p^{max} (Fabian et.al., 1975). After getting bound, the binary is usually highly eccentric, and circularizes within several periastron passages to the semi-major-axis $a \approx 2r_p$. The value of r_p^{max} depends on the mass ratio of the two stars and their relative speed, as studied by several authors with various degrees of details, *e.g.*, Spitzer (1987) (impulsive approximation), Lee & Ostriker (1986) (considering detailed modes of stellar oscillations). The total tidal capture rate in a GC is obviously proportional to the two-body encounter rate Γ.

Compact binaries can also be formed by *exchange encounters* (Spitzer, 1987) between a compact star and a non-compact stellar binary. During a close encounter between the compact star and the stellar binary, the compact star, being generally heavier, preferentially replaces one of the binary members to form a PXB. The three stars can initially form an unstable triple system if the relative speed of approach v of the binary and the compact star is less than a critical value $v_{\rm crit}$, defined to be the relative speed that gives the triple system the kinetic energy just enough to dissociate the binary (Heggie & Hut (2003); also see below). Such a temporary phase is called a *resonance*, which breaks up into the exchanged binary and the single star after $\sim 10-100$ orbits. On the other hand, if $v > v_{\rm crit}$, only direct exchange can take place. Exchange is more probable for wider binaries and its cross-section scales with a.

PXBs can be destroyed by exchange encounters also. This occurs when the non-compact companion of a PXB is exchanged with a (heavier) incoming compact star, resulting in a double-compact binary. Such compact binaries are generally not XBs, since both of the stars are degenerate. A PXB can also be destroyed by dissociation in a close encounter with a fast moving star with $v > v_{\rm crit}$. Since the PXBs are significantly hard, $v_{\rm crit}$ is very high and only a few stars in the high-speed tail of the Maxwellian velocity distribution are able to dissociate the binary. Thus destruction by dissociation is negligible for hard binaries in general. Dissociation is important only for much softer compact binaries with $a > 500R_\odot$.

The processes that harden binaries are of two types, *viz.*, (a) those which operate in isolated binaries, and are therefore always operational, *viz.*, *gravitational radiation* and *magnetic braking* and (b) those which operate only when the binary is in a globular cluster, *viz.*, *collisional hardening*. As discussed in detail in (Banerjee & Ghosh, 2006) (henceforth BG06), it is these processes that harden or shrink a compact binary from its detached or PXB phase to the state where the ordinary stellar companion fills its Roche lobe. At this point, the companion begins transferring mass to the compact primary, and the system turns on as an X-ray binary (XB) — either a CV or a LMXB, depending on the nature of the degenerate accretor.

In gravitational radiation process (d'Inverno, 1992), the binary orbit shrinks due to loss of orbital angular momentum J due to the emission of gravitational waves (GW) from the system. The relative angular momentum loss rate due to GW radiation is given by:

$$j_{GW}(a) \equiv \left(\frac{\dot{J}}{J}\right)_{GW} = -\alpha_{GW} a^{-4}, \qquad \alpha_{GW} \equiv \frac{32G^3}{5c^5} m_c m_X (m_c + m_X). \qquad (1)$$

Here, m_X is the mass in solar units of the degenerate primary (neutron star or white dwarf), m_c is the mass of its low-mass companion in solar units, and the unit of the binary orbital radius a is the solar radius. We shall use these units throughout this thesis.

Orbital angular momentum of the binary is carried away primarily by magnetic braking process (Verbunt & Zwaan, 1981) for narrower systems ($a < 2R_\odot$ for typical values, see below), in which the magnetized stellar wind of the companion, co-rotating with the star upto several stellar radii, carries away the spin angular momentum of the star significantly. As the spin of the star is *tidally locked* with the orbital motion, orbital angular momentum is ultimately reduced. Among different suggested prescriptions for magnetic braking (van der Sluys et.al., 2005), we choose the following one suggested by van der Sluys et.al. (2005) which preserves the original Verbunt-Zwaan scaling (Verbunt & Zwaan, 1981), but with reduced strength:

$$j_{MB}(a) \equiv \left(\frac{\dot{J}}{J}\right)_{MB} = -\alpha_{MB}a^{-5}, \quad \alpha_{MB} \equiv 9.5\times10^{-31}GR_c^4\frac{M^3}{m_X m_c}, \quad M \equiv m_c+m_X \tag{2}$$

Here, R_c is the radius of the companion.

The above two mechanisms affect the orbital evolution irrespective of whether the binary is inside a GC. However, inside a dense GC core, the binaries are subjected to frequent scatterings with the background stars, unlike when they are outside the GC. According to *Heggie's law* (Heggie, 1975), the hard binaries *preferentially* shrink or harden as a result of dynamical encounters. It is important to note that while a single scattering can result in expansion or shrinkage of the binary orbit, a hard binary becomes harder *statistically* due to many 3-body scatterings. This has been shown theoretically by Heggie (1975) and later verified in many numerical scattering experiments. It has been shown by Banerjee & Ghosh (2006) that it is this *collisional hardening* which shrinks a wider PXB (say, $a > 20R_\odot$) upto a point where further hardening upto Roche-lobe overflow can be taken over by gravitational radiation and magnetic braking. Approximate analytical *mean* rate of collisional hardening rate has been obtained by Shull (1979) by fitting analytic hardening cross section formulae with results from numerical scattering experiments, according to which the relative rate of increase of binding energy is:

$$\left(\frac{\dot{E}}{E}\right)_C = A_C a\gamma, \qquad A_C \equiv 18G\frac{m_f^3}{m_c m_X} \tag{3}$$

Here, m_f is the mass of the background stars. We shall use $M_\odot\mathrm{pc}^{-3}$ and km sec^{-1} as the units of ρ and v_c respectively. In the above units, the values of γ for Galactic globular clusters typically lie between $\sim 10^3$ and $\sim 10^6$ (BG06). In the detached (*i.e.*, PXB) phase, $\dot{E}$ and $\dot{J}$ are simply related as:

$$\frac{\dot{J}}{J} = -\frac{1}{2}\frac{\dot{E}}{E} \tag{4}$$

so that,

$$j_C(a) \equiv \left(\frac{\dot{J}}{J}\right)_C = -\frac{1}{2}\left(\frac{\dot{E}}{E}\right)_C = \alpha_C a\gamma, \quad \alpha_C \equiv \frac{A_C}{2} = 9G\frac{m_f^3}{m_c m_X} \tag{5}$$

The total rate of loss of orbital angular momentum due to the above three processes is:

$$j_{TOT}(a) \equiv \left(\frac{\dot{J}}{J}\right)_{TOT} = j_{GW}(a) + j_{MB}(a) + j_C(a) \tag{6}$$

Note that while $j_{GW}(a)$ and $j_{MB}(a)$ increase strongly with decreasing a, so that they dominate at small orbital radii ($a < 10R_\odot$ for typical values, see below), collisional hardening is proportional to a and dominates at larger radii. The orbital radius shrinkage rate is given by,

$$\frac{\dot{a}}{a} = 2\frac{\dot{J}}{J} - 2\frac{\dot{m}_c}{m_c} - 2\frac{\dot{m}_X}{m_X} \tag{7}$$

The $\dot{m}_c$ and $\dot{m}_X$ terms on the right-hand side of Eqn. (7) are nonzero during mass transfer in the XB phase. In the PXB phase, $\dot{m}_c = \dot{m}_X = 0$, so that $\dot{a}$ is simply related to $\dot{J}$ as (cf. BG06):

$$\frac{\dot{a}}{a} = 2\frac{\dot{J}}{J} \tag{8}$$

In the XB phase, mass transfer occurs from the low-mass companion to the heavier compact star which tends to expand the binary radius (due to conservation of angular momentum; see van den Heuvel (1992)) so that the orbit shrinkage rate is reduced. The companion *always* fills the Roche-lobe of radius R_L during the mass transfer which is given by the well known Paczyński approximation:

$$R_L/a = 0.462\left(\frac{m_c}{M}\right)^{1/3}, \tag{9}$$

which holds for $0 < m_c/m_X < 0.8$. If we take typical initial values to be $m_X = 1.4M_\odot$, $m_c = 0.6M_\odot$ and $R_c = 0.6R_\odot$ (see below), the first Roche-lobe contact occurs at $a_L \approx 1.94R_\odot$.

It can be shown that for a companion with mass-radius relation $m_c \sim R_c^s$, and assuming no mass loss from the binary, the orbit shrinkage rate during mass transfer is given by:

$$\dot{a} = \frac{j_{tot}(a)a\left(s - \frac{1}{3}\right)}{\left[\frac{s}{2} + \frac{5}{6} - \left(\frac{m_c}{M - m_c}\right)\right]} \qquad (a < a_L) \tag{10}$$

Here, $j_{tot}(a) = j_{GW}(a) + j_{MB}(a)$ is the effective total rate of loss of angular momentum, since the collisional-hardening contributions are negligible, as explained above.

In the majority of our work as described below, we consider a simplified dynamical environment consisting of a *static* and *uniform-density* background of stars with density ρ having a Maxwellian distribution of velocities of the stars with dispersion v_c representing a GC core of radius r_c. Such a model of GC core has been utilized in several important contributions to the subject (*e.g.*, Hut, McMillan & Romani (1992), Portegies Zwart et.al. (1997b)). It essentially represents a GC core in the *quasi-steady* phase (Gao et.al., 1991), where the collapse of the core is temporarily halted due to "binary-heating" (Heggie & Hut, 2003) and the core radius and density remains practically constant with time. In all of our works, we consider equal-mass main-sequence background stars of mass $m_f (= m_c) = 0.6M_\odot$ and an appropriate fraction k_X of compact stars with mass $m_X = 1.4M_\odot$ and a fraction k_b of stellar binaries with the components of mass m_f in equipartition representing a mass-segregated core (Banerjee & Ghosh (2006) and references therein). However, we also consider later the effects of time-evolution of the GC core in Banerjee & Ghosh (2008b), as discussed below.

Collisional hardening of compact binaries in GCs

We first consider the above-discussed mechanisms for hardening of compact binaries in globular clusters to the point of Roche-lobe contact and X-ray emission phase, focussing on the process of collisional hardening due to encounters between binaries and single stars in the cluster core. Our objective is to examine the consequences of collisional hardening in the number of X-ray binaries N_{XB} in a GC and also detect its possible observational signatures.

As discussed above, while the hardening of PXBs at large a is essentially entirely due to collisional hardening, magnetic braking and gravitational radiation takes over for small a ($a < 10R_\odot$). We find that this interplay between collsional hardening (cf. Eqn. (3)) and gravitational radiation (cf. Eqn. (1)) produces a characteristic scaling of the orbit-shrinkage timescale τ_{PXB} of a PXB with the single-star binary encounter rate γ. The orbit shrinkage time from an initial radius a_i upto the Roche-lobe contact point a_L is given by:

$$\tau_{PXB}(a_i, \gamma) \equiv \int_{a_i}^{a_L} \frac{da}{\dot{a}_{\rm GW} + \dot{a}_{\rm MB} + \dot{a}_{\rm C}} \approx \int_{a_i}^{a_L} \frac{da}{\dot{a}_{\rm GW} + \dot{a}_{\rm C}} \tag{11}$$

which is essentially the lifetime of the PXB after which it becomes an XB. Note that magnetic braking is negligible throughout the detached phase so that it can be ignored. We show that (Banerjee & Ghosh, 2006),

$$\tau_{PXB}(a_i, \gamma) \sim \gamma^{-4/5} \tag{12}$$

We investigate possible effects of this scaling on populations of X-ray binaries in globular clusters within the framework of a simple "toy" scheme for describing the evolution of pre-X-ray binaries (PXB) in globular clusters. We simply model the total formation rate as proportional to the two-body encounter rate Γ which is the sum total of the rates of tc and ex1 processes as discussed above. Similarly, the total destruction rate *per binary* due to ex2 and dss processes is $\propto \gamma$. We follow the Ghosh-White evolution scheme (White & Ghosh, 1998; Ghosh & White, 2001) to estimate the evolution of total number of PXBs (N_{PXB}) and X-ray binaries (N_{XB}):

$$\frac{\partial N_{PXB}}{\partial t} = \alpha\Gamma - \beta\gamma N_{PXB} - \frac{N_{PXB}}{\tau(\gamma)} \tag{13}$$

$$\frac{\partial N_{XB}}{\partial t} = \frac{N_{PXB}}{\tau(\gamma)} - \frac{N_{XB}}{\tau_{XB}} \tag{14}$$

Here τ_{XB} is the typical lifetime of in the mass-transferring phase ($\sim$ 2 Gyr). $\tau(\gamma)$ is the mean shrinkage time over a distribution of a_i $f(a_i)$ is given by,

$$\tau(\gamma) \equiv \langle \tau_{PXB} \rangle \equiv \int_{a_i^{\rm min}}^{a_i^{\rm max}} \tau_{PXB}(\gamma, a_i) f(a_i) da_i \tag{15}$$

As the form of $f(a_i)$ is not well-known, we consider four "test cases", *viz.*, (a) $f(a_i) \sim 1/a_i$, (b) $f(a_i) =$ constant, (c) $f(a_i) \propto a_i$ and (d) a Gaussian distribution. α and β are proportionality constants which depend on the cross-sections of the dynamical events and remain constant for an unevolving background.

We find that the expected qualitative trends as obtained from Eqn. (13) and Eqn. (14) are sufficiently supported by data on X-ray binaries in galactic globular clusters (Pooley et al., 2003) for all the four cases. Specifically, we fit our computed N_{XB} with the observed values in a $\Gamma/N_{XB} - \gamma$ plane and find reasonable agreement with the observed trends (Banerjee & Ghosh, 2006), which encourages us towards a more quantitative study.

Evolution of compact-binary population in GCs: A Boltzmann study. The continuous limit

With the binary hardening, formation and destruction processes described above, we explore a Boltzmann scheme for studying the evolution of compact binary populations in GCs, where we utilize a Boltzmann equation in compact binary radius a and time t for studying the evolution of a compact binary population in an unevolving GC core. The compact binary population is described by a distribution function $n(a, t)$, which is defined as the number of compact binaries in the GC core of radius a per unit interval of a at the evolution time t. For a smaller than the Roche-lobe contact point ($a_L \approx 2R_\odot$, for m_X and m_c as indicated earlier) it represents X-ray binaries and larger a values represent PXBs. The evolution of $n(a, t)$ is described by the *collisional Boltzmann equation*:

$$\frac{\partial n}{\partial t} = R(a) - nD(a) - \frac{\partial n}{\partial a} f(a), \tag{16}$$

where $R(a)$ is the total formation rate in the GC core per unit a of compact binaries with radius a, $D(a)$ is the destruction rate *per binary* of compact binaries of radius a and $f(a) \equiv da/dt$ is the total orbital evolution rate of the compact binaries due to the mechanisms mentioned above. This scheme quite generic in the sense that it does not assume any particular dynamical model, so that any suitable model for $R(a)$, $D(a)$ and $f(a)$ can be included to evolve the distribution function. Unlike Fokker-Planck scheme (Spitzer (1987) and references therein), such approach automatically takes into account both the effect of *frequent, weak* and *rare, strong* encounters (Spitzer, 1987). This approach is also computationally very efficient, so that the computations can be performed on any basic workstation in small time (see below). It is however important to note that the dynamical processes are intrinsically discrete and stochastic in nature, and through our continuous Boltzmann equation approach, we are basically studying the *continuous limit*, wherein the probability of occurrence of an event of a given type is treated as a continuous function of the essential variables involved.

As discussed above, compact binaries can be formed by tc and ex1 encounters. If $r_{tc}(a)$ and $r_{ex1}(a)$ represents the rates of these processes respectively, then

$$R(a) = r_{tc}(a) + r_{ex1}(a), \tag{17}$$

where a is the radius of the compact binary so formed. Similarly, as the compact binaries can be destroyed by ex2 and dss processes, we have:

$$D(a) = r_{ex2}(a) + r_{dss}(a) \tag{18}$$

We consider a simplified analytical approach involving the *impulsive approximation* (Spitzer, 1987) which assumes that all the dissipated energy is deposited on the stellar surface *instantly* at the first periastron passage. We show that under impulsive approximation, the *Maxwellian averaged* total tc rate $r_{tc}(a)$ is given by (Banerjee & Ghosh, 2007):

$$r_{tc}(a) = \sqrt{\frac{32\pi^3}{3}} k_X \Gamma G M \left[1 - \exp(-\beta v_0^2(a))\right], \tag{19}$$

where $v_0(a)$ is the maximum speed of approach for tidal capture to occur for $r_p = a/2$, given by (Spitzer, 1987),

$$v_0(r_p) = \left(\frac{4}{3} G m_X R_m^2\right)^{\frac{1}{2}} r_p^{-\frac{3}{2}} \tag{20}$$

The rate function, Eqn. (19) is uniform in a for small a and falls off fairly sharply from about $a \approx 7R_\odot$ (Banerjee & Ghosh, 2007). In this reference, we also discuss the results of various subsequent numerical calculations of tc.

We use the Heggie, Hut & McMillan (1996) exchange cross-section to estimate ex1 and ex2 rates. These authors performed detailed numerical scattering experiments involving exchange encounters with various mass ratios and obtained a semi-analytical fit for the exchange cross section as a function of the particle masses. The Maxwellian averaged ex1 rate is given by,

$$r_{ex1}(a) = \frac{4}{3}\pi r_c^3 k_X \rho^2 f_b(a) \langle \sigma_{ex1}(a) v \rangle = \sqrt{\frac{8\pi^3}{3}} k_X f_b(a) \Gamma G M_{tot} a \overline{\sigma}_{ex1}(m_c, m_X) \tag{21}$$

Here, $f_b(a)$ is the distribution function of the orbital radii of the primordial stellar binaries in the cluster core and $\overline{\sigma}_{ex1}(m_c, m_X)$ is the Heggie, Hut & McMillan (1996) exchange cross-section appropriate for this case. For primordial binaries, we take the widely-used distribution $f_b(a) \propto 1/a$ (*i.e.*, a uniform distribution in $\log a$) (Kraicheva et.al., 1978), upon which the ex1 rate becomes constant in a. Similarly, using the appropriate exchange cross section formula of Heggie, Hut & McMillan (1996) and averaging over Maxwellian distribution,

$$r_{ex2}(a) = k_X \rho \langle \sigma_{ex2}(a) v \rangle = \sqrt{\frac{3\pi}{2}} k_X \gamma G M_{tot} a \overline{\sigma}_{ex2}(m_c, m_X), \tag{22}$$

which is proportional to a. As discussed above, dynamical compact binaries are significantly hard so that they can be dissociated only by the few stars in the high-speed tail of the Maxwellian distribution. We find that the dss rate is negligibly small throughout the range of a of our interest ($a < 80R_\odot$) (see Hut & Bahcall (1983) and Banerjee & Ghosh (2007) for details).

As discussed above, the binary hardening rate $f(a)$ is due to gravitational radiation, magnetic braking and collisional hardening, which have been discussed above (Eqns. (1), (2) and (3)). In the X-ray binary phase (*i.e.*, $a < a_L$), the shrinkage rate is modified according to Eqn. (10).

Using the above models for compact binary formation, destruction and evolution, we solve the Boltzmann Eqn. (16) utilizing the *Lax-Wendorff* scheme (Press et.al., 1992). This scheme has the advantage of having negligible *numerical dissipation* (Press et.al., 1992) so that the evolution of $n(a,t)$ can be computed very accurately. In this work, we focus on (a) the evolution of the period distribution of compact binaries, and (b) the number of X-ray sources N_{XB} in GCs as a function of Verbunt parameters. Furthermore, we restrict ourselves only to CVs and short period LMXBs, where the companion fills its Roche-lobe in its main sequence or early subgiant phase.

We find that the period distribution of X-ray binaries is expected to be such that $n(a) = dN_{XB}/da$, the number of X-ray binaries per unit interval of the orbital radius a, is roughly constant for a smaller than the Roche-lobe overflow point $a_L \approx 2R_\odot$ (see above). For $a > a_L$, which represent PXBs, $n(a)$ is constant upto $a \approx 7R_\odot$, and falls off sharply for larger a. Using typical values of Galactic

GC parameters, *e.g.*, binary fraction in the core, the compact star fraction and the age of the cluster, we find that the model number of X-ray binaries N_{XB} and its expected scaling with Verbunt parameters are in good agreement with observations of Galactic globular clusters (Pooley et al., 2003). We also find that for a *given* Γ, the $\Gamma/N_{XB}(\gamma)$ curve is nearly *independent* of the choice of Γ over the observed ranges of Γ and γ, reflecting a *universal* behavior with γ, as already indicated by the toy model of BG06.

Evolution of compact-binary population in GCs: A Boltzmann study. Introducing stochasticity

We next introduce stochasticity into our Boltzmann scheme for evolving compact binary population in GCs. For this, we consider all the dynamical rate functions, *viz.*, $R(a)$, $D(a)$ and $f(a)$, as *randomly fluctuating* with time about their respective means (Banerjee & Ghosh, 2008a). In order to introduce stochasticity, we consider the full time-dependent Boltzmann equation:

$$\frac{\partial n(a,t)}{\partial t} = R(a,t) - n(a,t)D(a,t) - \frac{\partial n(a,t)}{\partial a} f(a,t), \tag{23}$$

with,

$$\left.\begin{array}{l} R(a,t) = \overline{R}(a) + \zeta^t_{atc} + \zeta^t_{aex1} \\ D(a,t) = \overline{D}(a) + \zeta^t_{aex2} + \zeta^t_{adss} \\ f(a,t) = \overline{f}(a) + \zeta^t_{acoll} \end{array}\right\} \tag{24}$$

Here, $\overline{R}(a)$, $\overline{D}(a)$ and $\overline{f}(a)$ are the same mean formation, destruction and hardening rate functions as in the continuous-limit Boltzmann scheme. ζ^t_{aX} is the random fluctuation from the mean rate of events of type 'X' and $X \Rightarrow$ tc/ex1/ex2/dss/coll by turn. In general, ζ^t_{aX}s are functions of both a and t, of course, which we model as discussed below.

In this introductory work, we use the standard normally-distributed model

$$\zeta^t_{aX} = S_X(a)\eta^t, \tag{25}$$

where $S^2_X(a)$ is the variance of ζ^t_{aX} at a given a and η^ts at each t are independent normal deviates. By adopting a normally-distributed variation, we are, in effect, considering a *Wiener process*, which is the standard mathematical description of Brownian motion. In other words, we are studying a situation wherein the variations in the above dynamical rates about their respective mean values constitute a Brownian motion.

To estimate the variances $S_X^2(a)$, we consider Monte-Carlo simulations where the so-called *rejection method* is widely used to determine whether an event of the above type occurs in a given time interval (Portegies Zwart et.al., 1997a; Sigurdsson & Phinney, 1993). Such a method basically involves a "coin-tossing experiment" to determine the number of occurrences of an event 'X' with mean rate $\overline{R}_X$ within a time $\Delta t < \Delta t_X \equiv 1/\overline{R}_X$, Δt_X being the timescale of occurrence of event 'X'. The number of events within Δt follows a binomial distribution with the following mean and variance (Banerjee & Ghosh, 2008a):

$$\left.\begin{array}{rl} \text{mean} = & \overline{R}_X(a)\Delta t \\ \text{varience} = S_X^2(a)\Delta t^2 = & \overline{R}_X(a)\Delta t(1 - \overline{R}_X(a)\Delta t). \end{array}\right\} \tag{26}$$

Notably, the above variance depends on a, since the mean rates depend on a. When several different types of events are considered simultaneously, as in the present problem, we must, of course, so choose Δt that it is shorter than the shortest dynamical timescale occurring in the problem. Hence for our case, we choose the computational time-step Δt_d as (Banerjee & Ghosh, 2008a),

$$\Delta t_d < \min\left\{\frac{1}{\overline{R}_{tc}(a_{min})}, \frac{1}{\overline{R}_{ex1}(a_{max})}, \frac{1}{\overline{R}_{ex2}(a_{max})}, \frac{1}{\overline{R}_{dss}(a_{max})}, \frac{1}{\overline{\dot{a}_{coll}}(a_{max})}\right\}, \tag{27}$$

Moreover, for the stability of solution of Eqn. (23), the time-step should also obey *Courant condition* (Press et.al., 1992) throughout the range of a under consideration (*i.e.*, $0.6R_\odot$-$60R_\odot$):

$$\Delta t_c = \epsilon\frac{\Delta a}{\overline{f}_{\max}}, \qquad \epsilon < 1. \tag{28}$$

Here, Δa is step-size in a, and $\overline{f}_{\max}$ is the largest value of $\overline{f}(a)$ over the range of a under consideration (Banerjee & Ghosh, 2008a). Hence, we finally have the time step Δt for solving Eqn. (23) to be

$$\Delta t = \min\{\Delta t_d, \Delta t_c\}. \tag{29}$$

The stochastic Boltzmann Eqn. (23) can be looked upon as the earlier continuous equation with additional stochastic terms, which turns it into a *stochastic partial differential equation* or SPDE. It it well-known that ordinary calculus cannot be applied to the handling of stochastic terms in a SPDE, since these terms are non-differentiable in the ordinary sense, and the classical definition of an integral does not apply to them. Rather, one has to modify the methods of calculus suitably, and redefine appropriate integrals. One such modified calculus is the *Itô Calculus*, which has been widely used for solution of SPDEs over the last two decades (Øksendal, 2004; Kloeden et.al., 1994). The corresponding integrals involving the stochastic terms are then called the *Itô integrals*, which have properties appropriately different from those of the ordinary integrals. Different numerical algorithms have been explored by different authors (Gaines, 1995) for numerical solution of SPDEs. The particular algorithm we use is a hybridization of the two-step Lax-Wendorff scheme for the continuous terms (as in the continuous limit case) and the second order stochastic Taylor expansion according to the *Milshtein scheme* for the stochastic terms (Milshtein, 1974; Gaines, 1995) (see Banerjee & Ghosh (2008a) for details).

To make a direct comparison with the continuous-limit case, we perform the same set of computations as in that case with identical sets of parameters. All the results are found to statistically agree with the continuous-limit results in the sense that the former represent random fluctuations about the latter results in all the cases. Specifically, we find that the resulting $n(a,t)$ surface fluctuates randomly about the continuous-limt surface, the details of the fluctuations being different for different runs (*i.e.*, runs with different random number seeds). This is further evident from the observation that an average surface of several independent runs are much smoothed out and tends to coincide with the continuous-limit surface. The XB distribution function dN_{XB}/da is, in this case, a randomly fluctuating distribution about the corresponding uniform mean distribution. As in the case of the continuous limit described above, we also explored the dependence of the computed number of XBs N_{XB} on the Verbunt parameters using the same choices of GC parameters as in that case, and found similar trends and agreement with observations.

Evolution of compact-binary population in GCs: A Boltzmann study. Evolving clusters in the continuous limit

In the works discussed above, we have confined ourselves to a static GC core, in keeping with the works of many previous authors in the subject. In reality, however, a GC evolves dynamically as a result of two-body relaxation processes (Spitzer, 1987; Heggie & Hut, 2003). Simulation of evolution of such many-body systems have been performed by several authors through semi-analytic or approximate methods like Monte-Carlo and Fokker-Planck methods (Spitzer (1987) and references therein) or through the more detailed and computationally intensive direct N-body integration (Aarseth (1999) and references therein). Such simulations show that beginning from an initial model like the Plummer model or the King's model (Heggie & Hut, 2003), a GC, containing a significant fraction of stars in binaries, evolves dynamically through three phases (Gao et.al., 1991), *viz.*, (a) the initial collapse or *pre-collapse*, (b) *quasi-steady* phase (c) *core-collapse* and *gravothermal oscillation* (GTO), which we briefly discuss below.

In the pre-collapse phase, the GC core shrinks rapidly through two-body relaxation process and this phase lasts about 10 initial half-mass relaxation time $t_{rh}(0)$. As the core collapses, the stellar density in the core increases and also the binaries in the GC segregate in the core due to *dynamical friction* (Chandrasekhar, 1942; Heggie & Hut, 2003), so that the "binary-heating" (Spitzer, 1987) due to single-star-binary encounter becomes significant enough to stall the collapse temporarily, which is called the quasi-steady phase. Binary-heating refers to the process of preferential increase of the K.E. of the single-stars in their encounters with the hard binaries due to collisional hardening (see above). Typically after several tens of $t_{rh}(0)$, most of the binaries recoil out of the core, making the central "energy source" inefficient so that the collapse of the GC core resumes. However, it is found that (Sugimoto & Bettwieser, 1983; Goodman, 1987; Makino, 1996) for $N > 7000$ the GC undergoes what is known as the gravothermal oscillations or GTO, in which the GC core undergoes alternate collapsed and expanded phases arising from the significant difference in relaxation times between the core and its surroundings (Heggie & Hut, 2003). During GTO, the core can expand by about two orders of magnitude and time spent in the expanded phase is much longer than that in the collapsed phase.

In this work, we investigate the effect of time evolution of the GC core on X-ray binaries in GCs in the continuous limit. As the ρ, r_c and v_c of the core vary during its dynamical evolution described above, so do the Verbunt parameters, which modifies the evolution of the GC compact binary population. We utilize the time-dependent Boltzmann equation (23) to compute the evolution of GC compact binary population using the same models for binary formation, destruction and hardening as in the continuous-limit case (see above) with time-varying ρ, r_c and v_c. We analytically model the evolution of r_c to have its overall nature similar to that of having the three distinct phases of evolution as mentioned above and the resulting evolution of ρ and v_c are derived from the simplifying assumptions of constancy of core-mass and virialization respectively.

We find that the formation of the compact binaries begins approximately when the core shrinks to the quasi-steady state. However, the formation of compact binaries halts almost completely as soon as the GTO phase starts. This is because, during GTO, the GC core spends most of the time in an expanded phase when the core radius is considerably larger than its quasi-steady value, so that the core density becomes much smaller and the encounter rates drop appropriately. In other words, we find that the dynamical formation of compact binaries is primarily restricted to the quasi-steady phase. Assuming typical values of half-mass relaxation time of GCs, the compact binaries can be formed only upto $\sim 8-10$ Gyrs, although the lifetime of the GC itself can be longer — of the order of a Hubble time. This implies that the assumption of static core would overestimate the compact binary population, if the evolution were continued with this assumption well beyond $8-10$ Gyr, say upto a Hubble time. This in turn justifies our extending the static-core evolution only upto ≈ 8 Gyr, as in the two works described above.

Publications

In Refereed Journals

1. **Sambaran Banerjee** and Pranab Ghosh: "Evolution of Compact-Binary Populations in Globular Clusters: A Boltzmann Study III. Effect of Globular Cluster Evolution". In preparation for submission in The Astrophysical Journal.

2. **Sambaran Banerjee** and Pranab Ghosh (2008): "Evolution of Compact-Binary Populations in Globular Clusters: A Boltzmann Study II. Introducing Stochasticity". The Astrophysical Journal, 680, 1438-1449.

3. **Sambaran Banerjee** and Pranab Ghosh (2007): "Evolution of Compact-Binary Populations in Globular Clusters: A Boltzmann Study I. The Continuous Limit". The Astrophysical Journal, 670, 1090-1103.

4. **Banerjee, S.** and Ghosh, P. (2006): "Collisional Hardening of Compact Binaries in Globular Clusters". Monthly Notices of Royal Astronomical Society, 373, 1188-1194.

In Proceedings

1. **Sambaran Banerjee** and Pranab Ghosh: "Evolution of Compact-Binary Population in Globular Clusters: A Boltzmann Study". To appear in Astronomische Nachrichten, "Galactic and Stellar Dynamics in the era of high resolution surveys" at Strasbourg, France, March 2008.

2. Pranab Ghosh and **Sambaran Banerjee** (2008): “Evolution of X-ray Binary Populations of Globular Clusters: A Boltzmann study”. Bulletin of the American Astronomical Society, HEAD Meeting no.10.

3. **Sambaran Banerjee** and Pranab Ghosh (2008): “Evolution of Compact-Binary Population in Globular Clusters: A Boltzmann Study”. Proceedings of “Dynamical Evolution of Dense Stellar Systems” (IAU Symposium 246) at Capri, Italy, September 2007.

4. Pranab Ghosh and **Sambaran Banerjee** (2007): “Evolution of Compact-binary Populations in Globular Clusters: A Boltzmann Study”. Bulletin of the American Astronomical Society, AAS Meeting no.211.

5. **Banerjee, S.** and Ghosh, P. (2006): “Effects of Encounters on Compact Binaries Inside Globular Cluster”. Proceedings of “The COSPAR Colloquium on Spectra and Timing of Compact X-ray Binaries” at Mumbai, India, January 2005.

Chapter 1

Introduction

1.1 Globular clusters

Globular clusters (henceforth GCs) are dense star clusters with large numbers ($10^4 - 10^6$) of stars gravitationally confined within ~ 10 pc. GCs constitute an important component of a galaxy (spiral or elliptical), and play significant roles in finding clues to several important astrophysical questions, *e.g.*, formation of galaxies, star formation mechanisms and stellar evolution theory. One of the key aspects which makes GCs such an important constituent of a galaxy is their extreme old age, comparable to the age of their host galaxy, as confirmed by detailed observations of GC stellar populations of the Milky Way (Bolte & Hogan, 1995) and M31 (Tripicco, 1993). Because of this, GCs carry fossil-records of the environment during formation of a galaxy, which is of fundamental significance in understanding galaxy formation and evolution. Also, as their constituent stars are nearly at the same distance from us as observers, their relative magnitudes can be measured accurately, which can be reliably compared with the predictions of stellar evolution theory.

On the other hand, a GC, being an densely-packed ensemble of a large number of stars, is in itself a very interesting dynamical system, the physics of which has been explored from as early as the 1960s (von Hoerner, 1960). Various dynamical interactions GCs manifest themselves through their effect on overall dynamical evolution of GCs, and also through formation of different types of encounter products, *e.g.*, tidal binaries, exchange binaries, merger products, and so on, which have many observational signatures. For example, the Milky Way GCs host about 100 times more X-ray binaries per stellar mass than compared to the Galactic field, which has been known since the mid-1970s, and the enhancement is even higher for elliptical galaxies (Angelini et.al., 2001). GCs also harbor many other types of exotic systems, which have recently received considerable attention. Examples are binary millisecond pulsars (Di Stefano & Rappaport, 1992), double neutron star systems (Grindlay et.al., 2006) (which are very promising sources of gravitational waves and possibly short gamma-ray bursts), intermediate-mass black holes (IMBH) (Portegies Zwart et.al., 2004), and so on.

GCs are therefore systems rich in physical phenomena that are of significant interest in various parts of astrophysics. In this thesis, we primarily concentrate on X-ray binaries in GCs, which are of great current interest, and detailed studies of which have become possible in recent years with the advent of subarcsecond-resolution X-ray observatories like *Chandra*. Our aim here is to model the formation and evolution of populations of compact binaries in GCs, and to compare our results with the observed properties of GC X-ray binaries. We do so through a Boltzmann scheme which we have constructed, and which is discussed in the following chapters. Before doing so, we briefly discuss in this chapter various aspects of the astrophysics of GCs, and different directions of previous study in GC dynamics, to put our work in proper context.

1.2 Structure of globular cluster

GCs have a core-halo structure with a dense central core, typically of size less than a parsec, and an extended, low-density halo of size ~ 10 pc (see Fig. 1.1). Detailed observations have been made on many of the Galactic GCs, and their structural, spectrophotometric and kinematic properties have been catalogued in detail (Harris, 1996, revised in 1999; Pryor & Meylan, 1993). GCs in SMC and LMC (van den Bergh, 1991; Stuntzeff et.al, 1992; Elson, Fall & Freeman, 1987) as well as those in the M31 galaxy (Reed et.al, 1994), have also been observed in much detail.

A spherically symmetric, isotropic star cluster in dynamical equilibrium can be modelled using the energy-distribution function of its constituent stars $f(E)$

Figure 1.1: *Globular cluster* NGC 6397. [Courtesy: Antilhue-Chilie]

(Heggie & Hut, 2003). Such equilibrium models are often used for modelling a particular observed GC, which is very important for understanding its structure and properties. They also serve as initial conditions for GC simulations (Gao et.al., 1991; Makino, 1996). Among the numerous possible equillibrum distribution functions (Spitzer, 1987), most popular ones are the *isothermal model*, *King's model* and *Plummer's model*, which we briefly discuss below.

1.2.1 Isothermal model

For the isothermal model (Chandrasekhar, 1942), as its name suggests, $f(E)$ is given by the Maxwellian distribution,

$$f(E) = f_0 \exp(-2j^2 E), \tag{1.1}$$

where, f_0 and j are constants. j is related to the one-dimensional velocity dispersion,

$$\sigma^2 = \frac{1}{2j^2} \tag{1.2}$$

It can be noted from Eqn. (1.1), that the isothermal model is a two-parameter model, with free parameters f_0 and j (alternatively, the central density and velocity dispersion of the GC). While the isothermal model is important because of its thermodynamic significance (Lynden-Bell & Wood, 1968), *e.g.*, in the study of thermal stability of a star cluster, its practical applications are limited because of other unphysical features. Among them the most noticeable one is that it necessarily yields an infinite mass of the cluster, as stars with infinite velocity should remain in the cluster, according to Eqn. (1.1).

1.2.2 King's model

An important improvement over the isothermal model, as least in practical terms, is to "lower" the energy distribution in Eqn. (1.1) as follows,

$$f = \begin{cases} f_0(\exp(-2j^2E) - \exp(-2j^2E_0)) & (E < E_0), \\ 0 & (E > E_0), \end{cases} \tag{1.3}$$

where, E_0 is the escape energy for the cluster. Eqn. (1.3) is called the King's model (King, 1962). Apart from having finite mass and radius, it has several other attractive features. Well inside the GC, we have $E << E_0$, so that the distribution is close to Maxwellian, representing a relaxed core, as can be expected. Moreover, Eqn. (1.3) turns out to be a good approximation to a solution of the Fokker-Planck equation (see Sec. 1.6.1).

Apart from the central density and the velocity dispersion, King's model is characterized by a third parameter $W_0 = 2j^2(E_0 - E_c)$, where, E_c is the energy of a star at rest at the center. In the context of this model, the size of the central region of a cluster, whose central density and velocity dispersion are ρ_c and v_c ($v_c^2 = 3\sigma^2$) respectively, is characterized by the core radius r_c, commonly defined as (Heggie & Hut, 2003),

$$\frac{4\pi G}{3}\rho_c r_c^2 = v_c^2, \tag{1.4}$$

although other definitions exist. King's model is a milestone in stellar dynamics because of its versatility and physically appealing properties and is widely used to model individually observed clusters (Trager et.al, 1995). It has also been extended to incorporate anisotropy (Michie & Bodenheimer, 1963), mass spectrum (Gunn & Griffin, 1979) and an external gravitational field (Heggie & Ramamani, 1995).

1.2.3 Plummer's model

Plummer's model (Plummer, 1911) is the most popular among all the equilibrium star-cluster models, which is partly because its structure can be expressed in terms of very simple functions (see Heggie & Hut (2003) for an excellent comprehension). It is given by the following distribution function:

$$f(E) = \frac{3.2^{7/2}}{7\pi^3}\frac{a^2}{G^5M^4m}(-E)^{7/2}. \tag{1.5}$$

Here, a is the lengthscale of the cluster density distribution [1], called the Plummer radius, M is the total mass of the cluster and m is the mass of the constituent stars. The above distribution function is essentially the solution for the polytropic equilibrium equation of a spherically symmetric and isotropic star cluster (Spitzer, 1987) with index $n = 5$. Because of its analytical simplicity, Plummer's model is widely used as initial conditions for numerical simulations of GCs (Spitzer & Shull, 1975; Gao et.al., 1991; Makino, 1996).

1.3 Globular cluster constituents

In this section, we discuss the host of stellar ingredients of a GC.

1.3.1 Stellar population

The majority of the constituents of a GC are old low-mass main-sequence stars resembling Population II. For the Milky Way and M31, the GCs are as old as 10^{10}

[1] The plummer density distribution is given by, $\rho(r) = \frac{3M}{4\pi a^3}\left(1 + \frac{r^2}{a^2}\right)^{-5/2}$

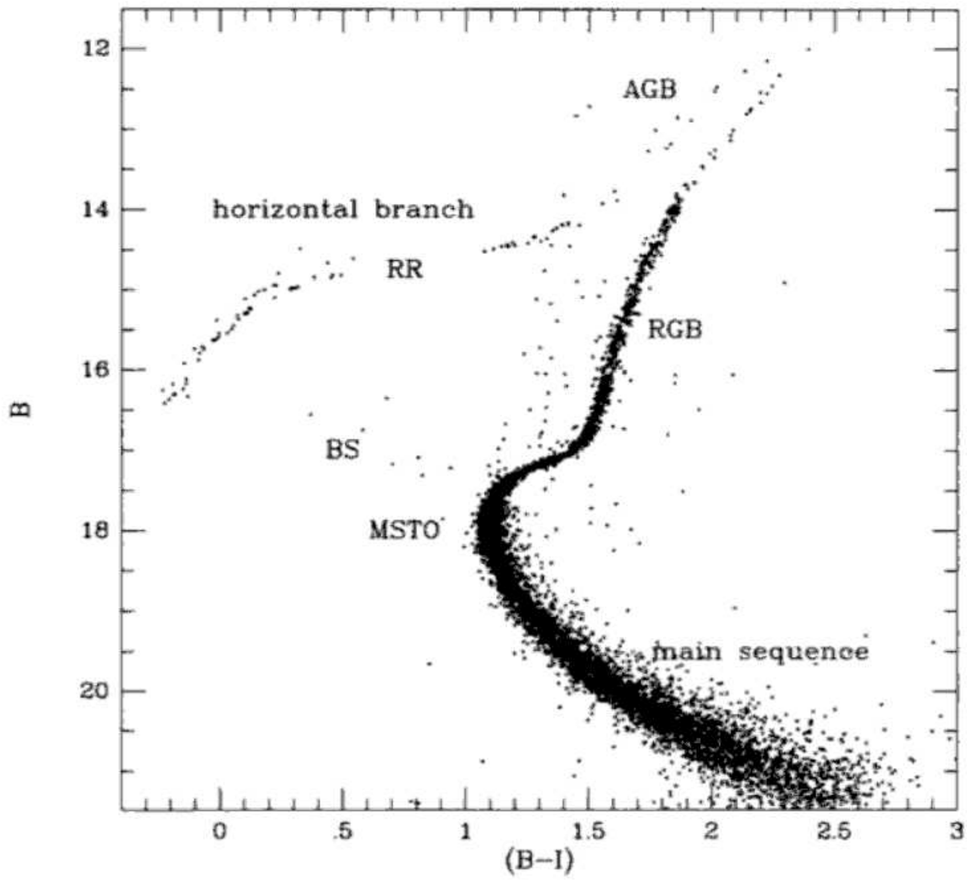

Figure 1.2: *The colour-magnitude diagram of* M5. *Various branches are labelled (see text). Reproduced from Ashman & Zepf (1998).*

yrs or more. However, in Magellanic Clouds (LMC & SMC), GCs with a wide range of age can be found (10^6–10^{10} yr), which make them very useful for studying dynamical evolution of GCs (Elson, Fall & Freeman, 1987; Mackey & Gilmore, 2003a,b). Dense star clusters with young stellar population can also be observed, particularly in galaxy mergers, *e.g.*, the Antennae, which are referred to as *young massive star clusters* (YMSC). These objects have recently received significant attention, as they may have promising clues for understanding the formation of GCs and open clusters.

In Fig. 1.2, the color-magnitude diagram (CMD) of the GC M5 is shown as an example. Well-defined main sequence (MS) and horizontal branch (HB) can be observed and the main-sequence turn-off (MSTO) is indicative of the age of the stellar population. Other stellar-evolutionary branches (Kippenhan & Weigert, 1990; Clayton, 1968), *viz.*, the red giant branch (RGB) and the asymptotic giant branch (AGB) can also be observed. The gap RR in the HB branch is the region where the instability strip (Kippenhan & Weigert, 1990) intersects the HB, called the RR Lyrae gap. The stars following the MS branch beyond the MSTO are called *blue stragglers* (BS) (Bailyn, 1995; Leonard, 1996). While several opinions exist regarding their formation (see (Ashman & Zepf, 1998) for a discussion), it is now generally accepted that these heavier main-sequence stars are formed through collisions (Hills & Day, 1976) between MS-MS or MS-red giant (RG) stars and subsequent mergers between them (Lombardi et.al., 1996).

1.3.2 Compact stars

Apart from normal stellar populations, GCs also host compact remnants of stars from their young age, when there were significant number of massive stars. X-ray and radio observations of GCs indicate the presence of a large number of low-mass X-ray binaries (LMXB) and cataclysmic variables (CV) in GCs and also recycled pulsars. However, there is no clear evidence for stellar-mass black-hole candidates in GCs, the reason for which is still unclear. While for neutron stars (NS) natal kick is evident from observations of pulsar velocities (Paczyński, 1990; Lyne & Lorimer, 1995), which may eject a significant number of NSs from the GCs (Davies & Hansen, 1998), there is no convincing evidence for natal kicks for black-holes (BH) (White & van Paradijs, 1996; Dewi et.al, 2006). N-body simulations (see Sec. 1.6.3) have been performed to understand the dynamics of a GC in presence of a population of BHs (Merritt et.al, 2006) and recent simulations indicate agreement with observations of GCs in LMC (Mackey et.al, 2007). N-body simulations also indicate the possibility of formation of one or more *intermediate-mass black holes* (IMBH) in YMSCs (Portegies Zwart et.al., 2004; Gürkan et.al, 2004), which will of course be retained in the cluster because of their large masses ($10^2 M_\odot - 10^4 M_\odot$). There is also indirect observational evidence of the presence of an IMBH in a GC in the Virgo Cluster giant elliptical galaxy NGC 4472 (Maccarone et.al, 2007).

The compact remnants, being generally significantly heavier than the low-mass stars, rapidly sink into the core of the GC on a two-body relaxation timescale, due to *mass segregation* (Spitzer, 1987). The latter effect refers to the process in which the heavier stars slow down on an average, due to their tendency towards equipartition with lower mass stars, and move towards the center of the cluster. In general, a group of stars with larger mass will tend to be more concentrated towards the center, because of mass-segregation. Therefore, the NSs and WDs in a GC are contained almost solely in the core, where they form a dynamically significant population density, making the dynamical formation of compact binaries highly probable exclusively in this region.

1.3.3 Binaries

Binary stars constitute a very important class of members in a GC, not only in their own right, but also in relation to the physics of GCs. Both normal-star-normal-star binaries and compact-binaries, consisting of at least one compact star (NS or WD) as a member, are of interest to us. Although, this thesis is essentially entirely dedicated to the dynamics of compact binaries, a general introductory discussion on GC binaries and their role is in order. Unlike the field, it is much more difficult to observationally identify binaries in a GC, as GC binaries are much narrower compared to those in the field. Wide visual binaries are not expected in a GC, as they are easily destroyed by encounters with the dense stellar background. As in the case of compact objects, the binaries, being generally heavier than the GC stars, tend to sink to the GC core, where only tight binaries can survive.

GC binaries were first identified from X-ray observations (Verbunt & Hut, 1987; Grindlay, 1988), when X-ray binaries have been identified in GCs. While earlier observations have inferred X-ray sources in the Galactic GCs, they have been resolved in unprecedented details by the ~ 0.5 arcsecond resolution images by observatories like *Chandra*. Fig. 1.3 shows an example for the case of the GC 47 Tuc. Such observations have discovered a large population of X-ray binaries (LMXBs and CVs) in GCs not only in our Galaxy (Pooley et al., 2003), but also in M31 and massive elliptical galaxies (Angelini et.al., 2001). Such rich population

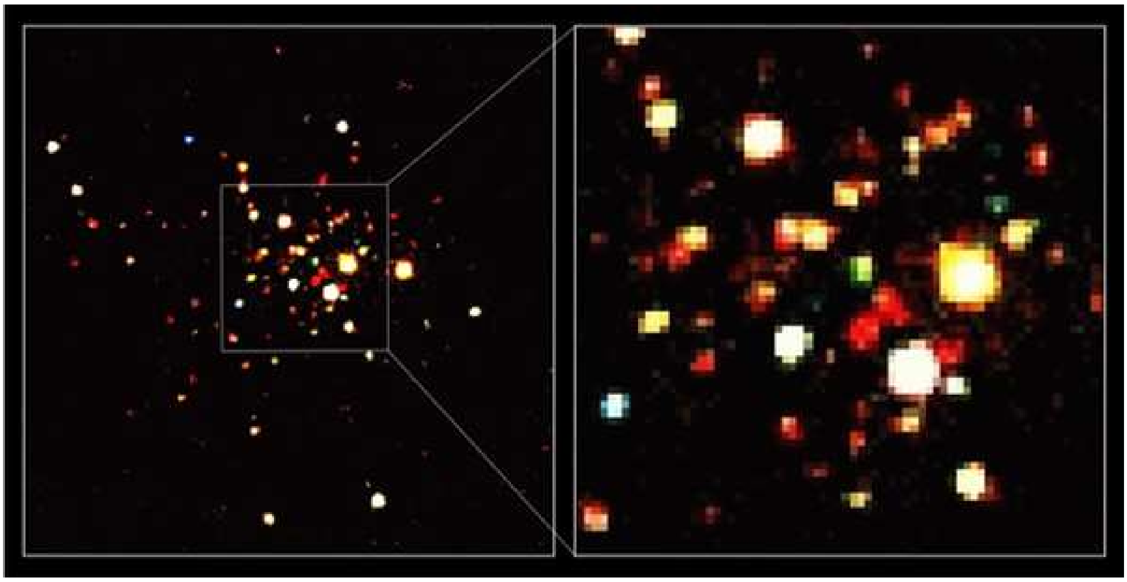

Figure 1.3: Chandra *image of the globular cluster* 47 Tuc. *The zoomed-in central part of the image in the left panel is shown in the right panel.* [NASA/CfA/Grindlay et.al]

of X-ray binaries is what turned astrophysicists' attention to GCs. We shall discuss more about X-ray binaries in GCs in Sec. 1.4.

Detection of normal stellar binaries in GCs have been more difficult due to their small size, crowding towards the center due to segregation and observational biases. However, with the development of newer observational techniques, they were also eventually detected, the first few of them being detected by measurements of radial velocities of GC stars (Gunn & Griffin, 1979). The radial velocity binaries are usually biased towards the RG members because of their brightness and a binary fraction of only about 1.5% were initially detected by surveying GC RGs (Latham et.al, 1985; Pryor et.al, 1989). However, in view of the severe selection effects, Pryor et.al (1989) estimate that it is consistent with $\sim 10\%$ main-sequence cluster members being the primary of a binary. HST observations has made it possible to search for stellar binaries in highly dense GCs (Gilliland et.al, 1995; Edmonds et.al, 1996). Short-period GC stellar binaries have also been detected by observations of eclipses (Kaluzny et.al., 1998). Unresolved binaries can also be identified in colour-magnitude diagrams, where they show up as stars which are considerably brighter for their colours (Rubenstein & Bailyn, 1997). While initial observations were mostly biased towards binaries with RG members because of their large brightness, radial velocity MS-MS binaries have also been identified in recent years (Côté & Fischer, 1996). While the question of fraction of stellar binaries in GCs is not yet completely settled, which in fact appears to vary considerably between GCs (Meylan & Heggie, 1996), the binary fraction is found to be similar to that of the field for several GCs (Côté et.al, 1994).

While the discovery of a significant number of binaries appears satisfying for astrophysicists in general, because of the similarity with field stellar population in this respect, it imposed new challenge to stellar dynamics (Hut et.al., 1992). Apart from interesting evolutionary properties, all kinds of (*i.e.*, both stellar and compact binaries) tight binaries significantly influence the dynamical evolution of a dense star cluster. Tight or *hard* (see Sec. 1.4.2) binaries can have binding energy of the order of the total K.E. of a GC core and so even the presence of a few hard binaries can influence the evolution of a whole GC (Spitzer, 1987; Heggie & Hut, 2003)! A binary does so by releasing its binding energy to its surrounding stars because of its *negative specific heat* (Heggie & Hut, 2003). Binary-single and binary-binary encounters have been studied in details both theoretically (Heggie, 1975) and through extensive numerical experiments (Hills, 1975a,b; Sigurdsson & Phinney, 1993; McMillan & Hut, 1996). We shall discuss such encounters in more details in Sec. 1.5 and in the following chapters, which is the backbone of the work reported in this thesis. Physical implications kept aside, inclusion of binaries in a GC makes the numerical simulation of its dynamical evolution much more challenging compared to if they have been absent. Various specialized numerical techniques have been developed to handle binaries in simulations, since their importance have been realized from 70's, which is still an evolving topic. We shall discuss about them briefly in Sec. 1.6.

1.4 Compact binaries in globular clusters: X-ray binaries

Compact binaries are among the most interesting members of GCs, which make the astrophysics of GCs so interesting and diverse. The presence of binaries and diverse classes of stellar members in a densely packed environment of a GC core is what makes it a fertile breeding ground for various kinds of dynamically formed compact binaries. The most well-observed among them are the X-ray binaries which we briefly discuss in the following subsection. GCs also host a significant number of recycled pulsars which are widely believed to be the end-products of LMXBs (van den Heuvel, 1991, 1992), which are recently being observed. Among the other kinds of compact binaries that can be expected in GCs, double NS (DNS) systems have perhaps received the highest attention as very promising sources gravitational wave (GW) bursts and short-period gamma-ray bursts (GRB). Unlike the galactic field, the GC compact binaries are very efficiently produced through dynamical means like *tidal capture* and *exchange*. We shall deal with the different dynamical encounters in a GC in details throughout this thesis, beginning with a general introduction to this subject in Sec. 1.5 of the present chapter.

1.4.1 X-ray binaries

X-ray binaries consist of a compact star, *viz.*, a NS or WD (the *primary*) accreting matter from a low-mass ordinary *companion*, and are called LMXBs and CVs respectively. Such accretion of mass takes place when the binary is close enough that the companion's radius exceeds its Roche-lobe (Ghosh, 2007), which can be thought of as the last closed equipotential surface around it, so that matter flows out of the companion's surface due to gravitational pull of the primary, and is accreted onto it. The dissipation of K.E. of the accreted matter on the surface of the compact star gives rise to the X-ray emission (Shapiro & Teukolsky, 2004). Since the accreting material carries angular momentum arising due to the relative orbital rotation of the binary members, the accretion takes place through the formation of an accretion disk. The interesting physics of accretion disks is one of the most fascinating topics in astrophysics (Shakura & Sunyaev, 1973; Frank et.al., 2002; Ghosh, 2007), which are believed to be responsible for the wide variety of properties that can be observed in X-ray binaries (Frank et.al., 2002). Fig. 1.4 depicts the situation for an LMXB. A significant fraction of the X-ray flux is also contributed by the accretion disk for the case of LMXBs, *i.e.*, accretion onto NS. In that case, the inner radius of the accretion disk is small and the material there is hot enough to emit in soft X-rays (Shakura & Sunyaev, 1973). The thermal X-ray flux generated due to matter falling on the NS surface is of course much harder.

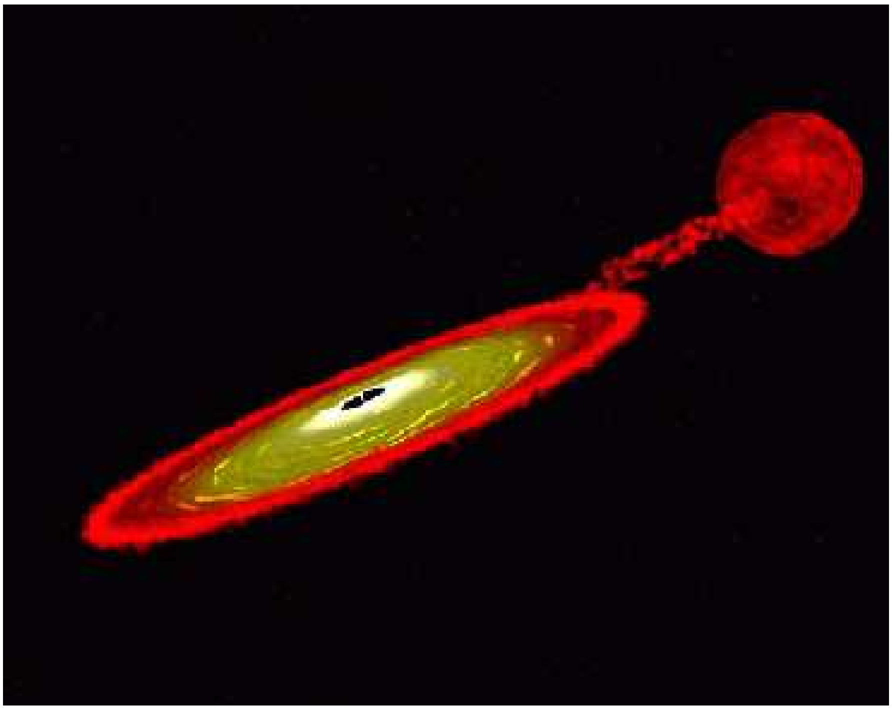

Figure 1.4: *Cartoon depiction of a typical (wide) LMXB.* [Courtesy: NASA HEASARC]

Evolution of X-ray binaries depends largely on the nature and evolutionary state of the companion and also its orbital separation. For CVs, the companion is on the main sequence, and the system evolves in a dynamical timescale due to loss of orbital angular momentum due to *gravitational radiation* (Landau & Lifshitz, 1962; d'Inverno, 1992) and *magnetic braking* (Verbunt & Zwaan, 1981), which continues to shrink the orbit and keeps the companion in Roche-lobe contact (van den Heuvel, 1992). In the former process, a compact binary emits gravitational radiation and so loses energy and angular momentum, which makes its orbit shrink. The latter mechanism is envisaged as follows. The low-mass companion has a significant magnetic field, and also has its rotation tidally coupled or "locked" to that of orbital revolution. The companion drives a wind, which carries away angular momentum at an enhanced rate because the magnetic field enforces corotation of the wind out to a radius considerably larger than that of the star, and this angular momentum ultimately comes from the orbit because of the above tidal locking, thus making the orbit shrink. We shall discuss the mechanisms of orbit-shrinkage in details in Chap. 2. The same scenario is also applicable to an LMXB for which the initial orbital period is smaller than $P_i \approx 18$ hr (Podsiadlowski et.al., 2002). On the other hand, if the orbit is wide enough ($P_i > 3$ days), the loss of orbital angular momentum is negligible. In that case, the Roche-lobe overflow can take place only when the companion evolves off its main sequence and continues to expand along the red giant branch (Kippenhan & Weigert, 1990). In this case, the orbit expands during mass transfer on the nuclear evolution timescale of the companion (van den Heuvel, 1992; Tauris & van den Heuvel, 2006). For 18 hr $< P_i <$ 3 dy, the semi-major-axis of the LMXB does not evolve appreciably, the orbit shrinkage due to angular momentum loss being compensated by the tendency of expansion due to nuclear evolution. The physics of evolution of CVs and LMXBs has been discussed in the excellent reviews by van den Heuvel (1992); Tauris & van den Heuvel (2006). In Chap. 3 and Chap. 4 we shall discuss quantitative results regarding orbital evolution of X-ray binaries, derived earlier by several authors (Tauris & van den Heuvel (2006) and references therein), which we adopt for our computations with relevant modifications.

The deposition of orbital angular momentum of the accretion disk onto the NS spins it up significantly and results in a highly spun-up NS after the conclusion of the accretion phase, with its spin-period of the order of milliseconds (van den Heuvel, 1991, 1992). Such millisecond pulsars or *recycled pulsars*, as they are called, are usually accompanied by a low-mass He WD, which is the remnant of the donor star. However, in several cases, the donor may be evaporated away during the accretion phase, due to X-ray irradiation from the primary, giving rise to an isolated recycled pulsar (van den Heuvel, 1991; Tauris & van den Heuvel, 2006).

1.4.2 Observed properties of GC X-ray binaries

Observing compact binaries in GCs poses extra challenges, because, being generally heavier than the isolated stars, they are all segregated within the GC core and hence require very high spatial resolution for observation. Till the present time, GC compact binaries have best been observed in X-rays. X-ray binary populations in GCs in our Galaxy and external galaxies have been unveiled through observations by high-resolution X-ray observatories like *Chandra*, which has discovered a large number of X-ray sources in several GCs in our Galaxy (Pooley et al., 2003), in others spirals like M31, and in many elliptical galaxies (Angelini et.al., 2001). These observations indicate that the Milky Way and M31 GCs contain about 100 times more X-ray binaries (per stellar mass) compared to the field and the enhancement is much higher for elliptical galaxies. It has been realized for about 30 years now that compact binaries are produced efficiently in GCs through dynamical encounters like tidal capture and exchange, which proceeds at a significant rate in the densely packed core of a GC unlike outside it, which is responsible for the observed overabundance of X-ray sources in GCs (see Hut et.al. (1992) for a review). The dynamical formation is of course generally applicable to all kinds of compact binaries although the details of the scenario and dynamical rates can be different for different kinds of binaries. A GC is therefore a "factory" of all kinds of compact binaries and presents us opportunities to study their populations in detail.

The compact binaries that are formed dynamically can be *hard* in the sense that their binding energy is larger than the mean kinetic energy of the single stars. Such hard binaries can in turn influence the overall dynamical evolution of GC significantly through dynamical processes like mass segregation and "binary-heating" (Spitzer, 1987; Heggie & Hut, 2003). As the X-ray binaries are the most well-accounted type of compact binaries in a GC and at the same time play important role in the dynamics of the GC, it is important to study GC X-ray binaries in detail. In this thesis, we study the formation and evolution of X-ray binaries in GCs.

X-ray binaries have been observed in most detail in the GCs of the Milky Way (Pooley et al., 2003) and massive elliptical galaxies (Angelini et.al., 2001; Sarazin et al., 2003). These observations show that the fraction of X-ray binaries associated with GCs is much higher (by factors of 10^2-10^3) than that for the optical light, indicating the high efficiency of dynamical encounters in GCs in producing compact binaries. Pooley et al. (2003) deduced the number of X-ray sources N_{XB} (above 4×10^{30} erg S^{-1} threshold flux in the 0.5-6 Kev spectral range) in Galactic GCs from the high-resolution *Chandra* images of these GCs (see Fig. 1.3 as an example, though not by these authors). They found a strong positive correlation between N_{XB} and the estimated two-body encounter rate of the GCs Γ (see Chaps. 2 & 3), *viz.*, $N_{XB} \propto \Gamma^{0.74\pm0.36}$. The X-ray sources included are mostly CVs and LMXBs, although a few of them are other types of soft X-ray sources, *e.g.*, recycled pulsars and coronally active stellar binaries (Pooley et al., 2003). This result strongly indicates that the majority of the X-ray binaries in the GCs are formed dynamically. The plot of N_{XB} vs. Γ from Pooley et al. (2003) is reproduced in Fig. 1.5, where it can be seen that apart from NGC 6397 and ω Centauri, all GCs lie very close to the fitting line. We utilize this data throughout this thesis for purposes of comparing our results with observations.

Observations of massive elliptical galaxies has also provided us many interesting inferences regarding properties of X-ray binaries in GCs. Such observations indicate that the probability of finding a bright LMXB among all the GCs is about 4% and remains approximately same for different Galaxy types (Kundu et.al., 2002). Interestingly, it has also been observed that the redder/younger GCs (Ashman & Zepf, 1998) are more likely to host a X-ray binary than the blue/older GCs indicating that the formation and evolution of X-ray binary population may be affected either by age or by metallicity of the cluster (Sarazin et al., 2003). It is suggested that metallicity might enhance the X-ray binary formation rate, as a star with higher metallicity has larger opacity and emits more stellar wind, as its envelope experiences stronger radiation pressure. Such stellar wind can increase the K.E. dissipation during close passage between a normal and a compact star, thus increasing the tidal capture rate, forming more compact binaries.

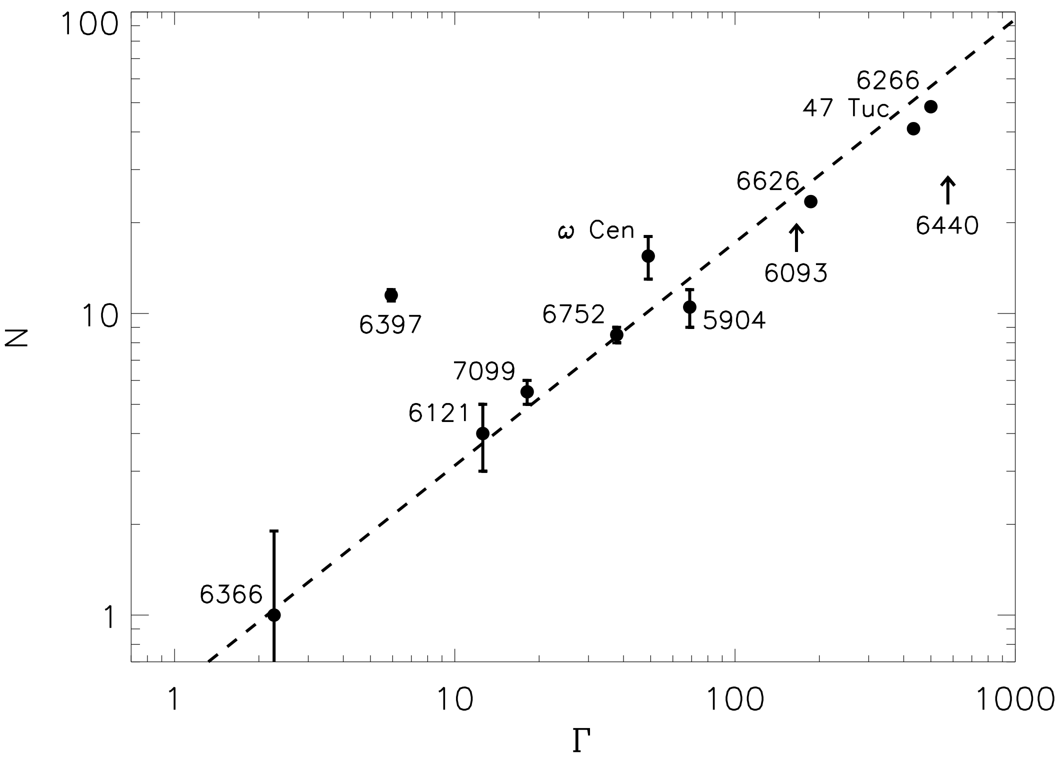

Figure 1.5: N_{XB} *vs.* Γ *reproduced from Pooley et al. (2003). A remarkable correlation can be observed between the two quantities, with most of the GCs lying very close to the fitting straight line of slope* 0.74($\pm$0.36). *The normalization has been chosen such that* $\Gamma/100$ *is approximately the number of LMXBs in a cluster or, for the cases* $\Gamma < 100$*, the percent probability of the cluster hosting an LMXB. An arrow indicates a GC for which the* Chandra *observation did not attain the required sensitivity.*

It is also observed that the total number of X-ray binaries in different galaxies increase in proportion with the total number of GCs hosted by them rather than the optical luminosity of the galaxies, suggesting that most or all of the X-ray binaries may have been formed in the GCs (White et.al., 2002). In that case, the X-ray binaries that are located outside GCs are either ejected from their host clusters due to recoils in close encounters or are remnants of their hosts that dissolved in the galactic tidal field, as suggested by several authors (White et.al., 2002; Sarazin et al., 2003). This is further supported by the lack of evidence of any significant difference between GC and non-GC X-ray binary population

(Sarazin et al., 2003). However, it is important to note that the observed X-ray binaries are generally inferred to be LMXBs or CVs (for our Galaxy), and there is no clear indication that GCs host BH binaries.

Apart from the classical X-ray binaries, *i.e.*, LMXBs and CVs, a population of very bright ($L_X \sim 10^{36} - 10^{39}$ erg s^{-1}) and short orbital period ($P <$ 1hr) X-ray binaries have been observed in Galactic GCs and massive elliptical galaxies. These are called ultra-compact X-ray binaries (UCXB). A significant number of UCXBs is found in the massive elliptical galaxies, and for our Galaxy, the $(4 - 7) \times 10^{37}$ erg s^{-1} source 4U 1820-30 in NGC 6624 is the best known example. Such an object is usually thought to be a tight binary between a very low-mass C/O or He white dwarf donor ($< 0.1 M_\odot$) and a neutron star (Verbunt, 1987; Bildsten & Deloye, 2004). Such binaries are predicted to be formed due to a physical collision between a red giant (RG) and a neutron star, which results in a common envelope (CE) inspiral of the latter and subsequent ejection of the envelope, forming a narrow binary between the NS and the degenerate core (Verbunt, 1987; Ivanova et.al., 2005). Dense GC cores are therefore believed to be exclusive locations for forming them. UCXBs may well dominate the bright end of the LMXB luminosity function of massive elliptical galaxies, as argued by Bildsten & Deloye (2004), although they may be minor in actual number (Ivanova et.al., 2005; Banerjee & Ghosh, 2007).

1.5 Dynamical formation, destruction and evolution of compact binaries

In this section, we introduce the dynamical encounters that occur in a dense stellar system, with particular attention to the formation, destruction and evolution of compact binaries, which is the primary focus of this thesis. Compact binaries, consisting of an ordinary star and a compact star (NS/WD), are formed in GC cores efficiently through dynamical processes like tidal capture and exchange mechanisms, as we discuss below. Such a dynamically formed compact-binary may in general be detached, *i.e.*, not in Roche-lobe contact (see Sec. 1.4.1) and become a X-ray binary after the non-degenerate companion fills its Roche-lobe through evolution of the binary. Evolution of such *pre X-ray binaries* or PXBs (Banerjee & Ghosh, 2006), as we shall refer to them throughout this thesis, are not only governed by “natural” mechanisms, namely, orbital angular momentum loss and evolution of the companion, but as well by repeated encounters with the surrounding stars in the GC core.

Encounter between hard binaries and single stars is a subject of interest in its own and has a long history of investigation (Marchal, 1990). However, serious quantitative study of this old three-body problem has begun since 1970s. A major breakthrough in this subject is in fact the realization that exchange between the incoming star and one of the binary members can occur in such a dynamical encounter, although the possibility of exchange has been suggested much earlier (Becker, 1920). Cross sections of such dynamical processes have been determined by the pioneering theoretical study by Heggie (1975) and pioneering numerical studies by Hills (1975a,b). More detailed and systematic study of binary-single-star encounters followed, primarily through numerical scattering experiments and a clear classification of the various types of encounters were possible (Hut & Bahcall, 1983; Hut, 1993).

In the following subsections, we discuss the different dynamical processes that form, destroy and affect the evolution of compact binaries, or more precisely, the PXBs. More detailed and quantitative discussions follow in the subsequent chapters.

1.5.1 Dynamical formation of compact binaries

One of the important channel for formation of compact binaries is *tidal capture*. A compact star, during a close passage by an ordinary star, raises tidal deformation on the latter and sets non-radial oscillations in it. The energy dissipated in the process is taken from that of relative motion of the two stars, and can be large enough to make them bound, provided their first periastron separation r_p is smaller than a critical value r_p^{max} (Fabian et.al., 1975). After getting bound, the binary is usually highly eccentric, and circularizes within several periastrion passages to the binary radius $a \approx 2r_p$ (Spitzer, 1987), assuming no mass loss from the system. The value of r_p^{max} depends on the amount of energy dissipation in tidal heating which has been estimated by several authors, starting from the simplest *impulsive approximation* (Spitzer, 1987) to more detailed analysis which computes the contributions of individual modes of oscillation (Press & Teukolsky, 1977; Lee & Ostriker, 1986). It depends on the the mass ratio of the two stars and their relative speed, as discussed in details in Chap. 3.

Compact binaries can also be formed by *exchange encounter* between a compact star and a non-compact stellar binary. The stellar binary can either be primordial or may itself have formed dynamically through tidal capture. During a close encounter between the compact star and the stellar binary, the compact star, being generally heavier, preferentially replaces one of the binary members to form a PXB. The three stars may initially form an unstable triple-system if the relative speed of approach v between the binary and the compact star is less than a critical value $v_{\rm crit}$, defined to be the relative speed that gives the incoming star just enough K.E. to dissociate the binary (Spitzer, 1987). Such a temporary phase is called a *resonance*, which breaks up into the exchanged binary and single star after $\sim 10 - 100$ orbits (Spitzer, 1987; Heggie & Hut, 2003). The trajectories of the stars in the triple system can be complex — Fig. 1.6 shows an example which is reproduced from Hut & Bahcall (1983). On the other hand, if $v > v_{\rm crit}$, only direct exchange is possible. The cross-section for binary-single-star exchange encounters for arbitrary mass ratios has been determined in a seminal work by Heggie, Hut & McMillan (1996). These authors performed detailed numerical scattering experiments involving exchange encounters with various mass ratios using the STARLAB software package (Portegies Zwart et.al. (2001), also see Sec. 1.6) for stellar-dynamics tools. Using analytical asymptotic cross-sections for extreme mass ratios and those obtained from the numerical experiments for the intermediate masses, these authors obtained a semi-analytical fit for the exchange cross-section as a function of the particle masses. We utilize the Heggie, Hut & McMillan (1996) exchange cross-section to estimate the formation (and also destruction, see below) rate of PXBs through exchange, as discussed in Chap. 3.

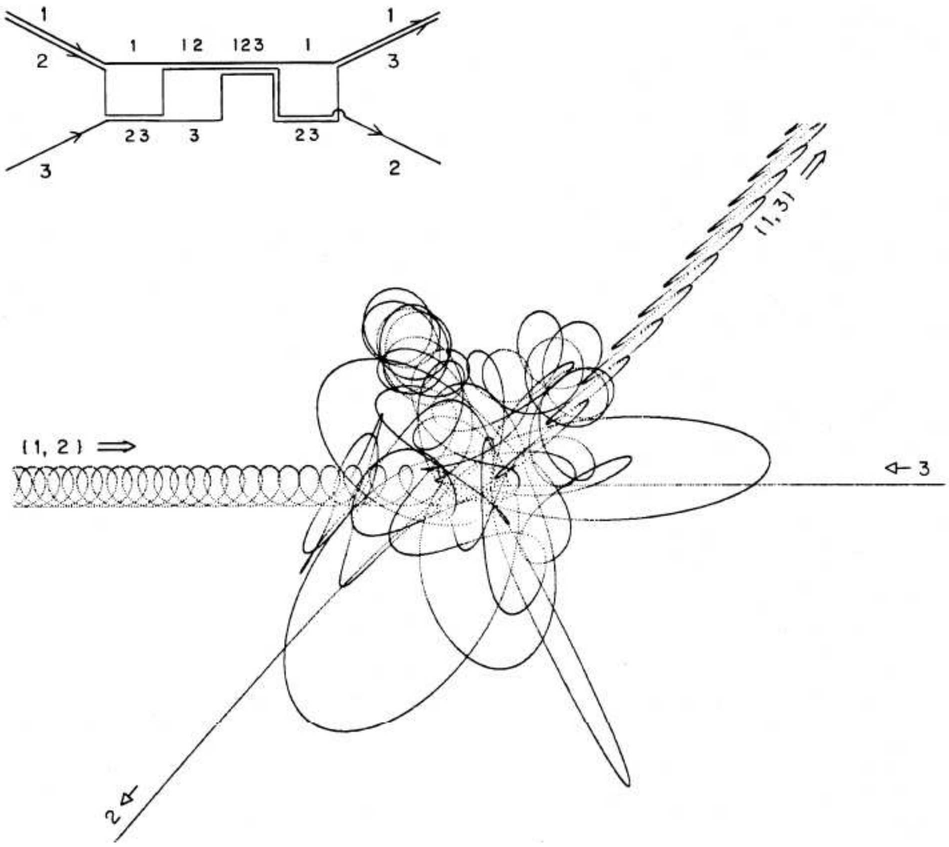

Figure 1.6: *An example of resonant exchange between equal-mass stars reproduced from Hut & Bahcall (1983), where the two-dimensional projection of the trajectories of the three stars are drawn. In the upper-left corner, the degree mutual gravitational binding of the three stars is represented schematically.*

1.5.2 Dynamical destruction of PXBs

PXBs are destroyed by exchange encounters also. This occurs when the non-compact companion of a PXB is exchanged by an (heavier) incoming compact star, resulting in a double-compact binary. Such compact binaries do not become X-ray binaries in general, since both of the stars are degenerate. As in the case of exchange formation, such destruction mechanism is efficient only for wider PXBs.

Double-NS systems, though not X-ray sources, are possible sources of gravitational waves and short GRBs upon merger. Grindlay et.al. (2006) performed numerical scattering experiments to determine the cross-section of formation of double-NS systems by exchange interaction of a NS with a NS-companion system (*i.e.*, a PXB) that are capable of merging within a Hubble time. They estimated that $\sim 30\%-40\%$ of the off-Galactic-plane short GRBs may occur through NS-NS mergers in GCs.

A PXB can also be destroyed by dissociation in a close encounter with a fast-moving star with $v > v_{\rm crit}$. Since the PXBs are significantly hard, $v_{\rm crit}$ is very high and only a few stars in the high-speed tail of the Maxwellian velocity distribution are able to dissociate the binary (Spitzer, 1987). Thus the destruction by dissociation is negligible for hard binaries in general. Dissociation cross-section as a function of binary binding energy for both hard and soft binary limits has been determined by Hut & Bahcall (1983) through detailed numerical scattering study.

1.5.3 Dynamical evolution of PXBs

Once formed, PXBs evolve due to (a) orbital angular momentum loss, (b) evolution of the companion star and (c) encounter with surrounding stars. A PXB becomes an X-ray binary when the companion fills its Roche-lobe (see Sec. 1.4.1) and starts mass transfer to the compact primary. The mechanisms of orbital angular momentum loss, *viz.*, gravitational radiation and magnetic braking has been introduced in Sec. 1.4.1. These mechanisms shrink the PXB orbit until it comes to Roche-lobe contact.

The above two mechanisms affect the binary evolution irrespective of whether it is inside a GC. However, inside a dense GC core, the binaries are subjected to repeated scatterings with the densely-packed background stars, unlike when it is outside the GC. According to Heggie's law (Heggie, 1975), hard binaries *preferentially* shrink or harden as a result of dynamical encounters, while soft binaries soften, *i.e.*, widen. This implies the existence of a "watershed" binding energy, so that on two sides of it the statistical behaviors of binaries are opposite. This explains, in the first place, why there can only be hard binaries in a dense stellar environment like the core of a GC. The above result has been predicted theoretically by Heggie (1975) and verified in many subsequent numerical scattering experiments (Hills, 1975a; Hut, 1983). Heggie & Hut (2003) provides a very stimulating discussion on the above Heggie rule. It is important to appreciate that while a *single* scattering may result in expansion or shrinkage of the binary orbit, *statistically* hard binaries become harder, and soft binaries softer, as a result of many scatterings. Fig. 1.7 is an excellent demonstration of the Heggie rule from Hut (1983), where the average change in binary binding energy is shown as a function of the incoming star's speed (scaled by the critical speed).

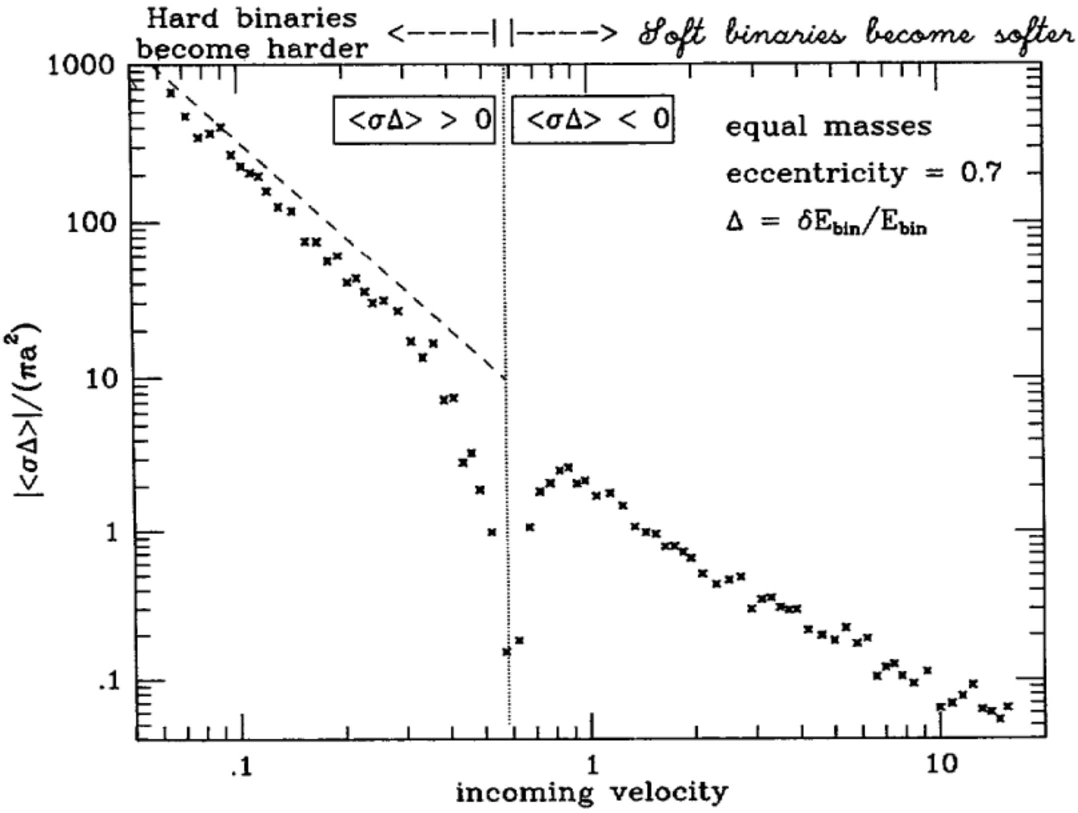

Figure 1.7: *Average of change Δ in binary binding energy from Hut (1983). Hard binaries at the left side of the watershed will on average gain binding energy, thus moving to the left and becoming harder. Soft binaries, on the right, lose binding energy on the average, move to the right, and become softer.*

Detached and hard PXBs in a GC core which undergo very frequent encounters with its surrounding stars will shrink as a result of these encounters. It has been shown by Banerjee & Ghosh (2006) that it is this *collisional hardening* which shrinks a wider PXB (say, $a > 20R_\odot$) upto a point where further hardening upto Roche-lobe overflow can be taken over by gravitational radiation and magnetic braking. Without collisional hardening, these wide PXBs could never shrink as their angular momentum loss rate is initially negligible due to much smaller orbital angular speed (see Chap. 2). Approximate analytical mean rate of collisional hardening rate has been obtained by Shull (1979), by fitting theoretically determined encounter rates to data obtained from numerical scattering experiments, which we discuss in Chap. 2.

1.6 Numerical methods

In this section, we provide an introductory discussion on techniques for simulating the evolution of a GC and the dynamical encounters inside it, as described above. The subject of computing the dynamics of a gravitationally interacting system of masses is about 50 years old, beginning with the first direct integration of a 10-body system by von Hoerner (1960). In that time, neither the computer hardware was fast enough, nor the numerical codes were sufficiently sophisticated, so that these pioneering calculations had to be halted when the first binary was formed. Rapid development of the computer hardware and as well the development of new algorithms for integrating gravitationally bound N-body systems (Aarseth, 2003) improved the situation rapidly, so that by the early 1970s direct integration of 500-body systems with binaries was possible. In parallel to the method of direct integration, the semi-analytic Fokker-Planck method (Spitzer & Härm, 1958; Cohn, 1979, 1980) and Monte-Carlo methods (Spitzer & Thuan, 1972; Hénon, 1971a,b) for evolving dense stellar systems were also developed, which are of course computationally much less demanding compared to direct integration, while also being less accurate in several aspects (see below). All these techniques, *viz.*, direct integration, Fokker-Planck methods and Monte-Carlo methods are now widely used for simulating GCs with realistic numbers of stars and binaries and incorporating physical processes stellar collisions and mergers, and also stellar evolution in more recent times (albeit still through semi-analytic prescriptions in most cases). In the following subsections we briefly discuss about each of these methods.

1.6.1 Fokker-Planck method

In the Fokker-Planck description of a dynamical system, the particles are collectively represented by a smooth distribution function $f(\mathbf{r}, \mathbf{v}, t)$ of particle position $\mathbf{r} = \{x_i\}$, particle velocity $\mathbf{v} = \{v_i\}$ and time t. This distribution function evolves with time due to the numerous encounters between the particles. If the particles undergo only weak encounters, so that their relative change of speed $\Delta v/v$ is small, then the evolution of $f(\mathbf{r}, \mathbf{v}, t)$ can be looked upon as a diffusion in the phase-space, describing dynamical relaxation of the system.

The evolution of $f(\mathbf{r}, \mathbf{v}, t)$ in presence of encounters is given by the *collisional Boltzmann equation*,

$$\frac{Df}{Dt} = \frac{\partial f}{\partial t} + \sum_i a_i \frac{\partial f}{\partial v_i} + \sum_i v_i \frac{\partial f}{\partial x_i} = \left(\frac{\partial f}{\partial t}\right)_{\mathrm{enc}}, \tag{1.6}$$

where, the effect of encounters between particles is included in $(\partial f/\partial t)_{\mathrm{enc}}$. $a_i = \dot{v}_i$s are the acceleration components of the particles. For gravitationally interacting systems, it is the acceleration produced by the gravitational potential of the whole system.

If $\Psi(\mathbf{v}, \Delta\mathbf{v})\mathbf{d}\Delta\mathbf{v}$ denotes the probability that the velocity of a particle $\mathbf{v}$ changes by $\Delta\mathbf{v}$ in a unit time, then the first and second order diffusion coefficients are defined as,

$$\langle \Delta v_i \rangle \equiv \int \Psi(\mathbf{v}, \Delta\mathbf{v}) \Delta v_i \mathbf{d}\Delta\mathbf{v}.$$

$$\langle \Delta v_i \Delta v_j \rangle \equiv \int \Psi(\mathbf{v}, \Delta\mathbf{v}) \Delta v_i \Delta v_j \mathbf{d}\Delta\mathbf{v}. \tag{1.7}$$

In the case of gravitationally interacting particles, the probability function Ψ can be determined from the analytic theory of two-body encounters (Spitzer, 1987). Ignoring for the moment the dependence of f on position $\mathbf{r}$, we have,

$$f(\mathbf{v}, t + \Delta t) = \int f(\mathbf{v} - \Delta\mathbf{v}, t) \Psi(\mathbf{v} - \Delta\mathbf{v}, \Delta\mathbf{v}) \mathbf{d}\Delta\mathbf{v}. \tag{1.8}$$

From the second order Taylor expansion of Eqn. (1.8) it can be shown that (see Spitzer (1987)),

$$\left(\frac{\partial f}{\partial t}\right)_{\mathrm{enc}} = -\sum_{i=1}^{3} \frac{\partial}{\partial v_i}(f\langle \Delta v_i \rangle) + \frac{1}{2} \sum_{i,j=1}^{3} \frac{\partial^2}{\partial v_i \partial v_j}(f\langle \Delta v_i \Delta v_j \rangle) \tag{1.9}$$

Eqn. (1.6) with the encounter term expressed in terms of the diffusion coefficients (upto second order) as in Eqn. (1.9), is known as the Fokker-Planck equation. Ignoring the higher order terms in Eqn. (1.9) is valid provided $\Psi(\mathbf{v}, \Delta\mathbf{v})$ becomes small when $\Delta v/v$ is appreciable, since under this condition the higher-order diffusion coefficients are negligible compared to $\langle \Delta v_i \rangle$ and $\langle \Delta v_i \Delta v_j \rangle$. In other words, the Fokker-Planck equation incorporates only the effect of weak, distant encounters which are responsible for the relaxation of the system. Close, strong encounters, *e.g.*, binary formation by three-body encounters (Hut, 1985; Goodman & Hut, 1993), binary-star and binary-binary scattering, although much rarer compared to distant two-body encounters, influence the dynamics of dense star clusters significantly. Such effects are not incorporated in the Fokker-Planck equation itself and have to be included separately in a Fokker-Planck scheme, as discussed below.

The most convenient way to describe a star cluster however is to express the distribution function in terms of the energy E and angular momentum J per unit mass of the particles. The general procedures for coordinate transformation in Fokker-Planck equation have been developed (Rosenbluth et.al, 1957). The Fokker-Planck scheme for evolving GCs have been developed in 1980s mainly by Cohn and collaborators (Cohn, 1979, 1980; Statler, Ostriker & Cohn, 1987; Murphy & Cohn, 1988). The original formulation by Cohn (1979) was in a two-dimensional phase space of E and J, which was later reduced to an one-dimensional form (Cohn, 1980). Although the one-dimensional Fokker-Planck formulation ignores anisotropy in the velocity distribution unlike the two-dimensional formulation, it is significantly faster. Also, the possibility of using the Chang & Cooper (1970) differencing scheme provided much better energy conservation compared to the original two-dimensional formulation. The one-dimensional method has been notably successful for isolated clusters, where it has been especially used for studying the late stages of cluster evolution (Cohn, 1980), post-collapse evolution (Statler, Ostriker & Cohn, 1987; Lee, 1987a,b), effect of a central massive black hole (Shapiro, 1985) and the role of primordial binaries (Gao et.al., 1991). In all these studies, one also have to account for the strong encounters, capture and mass-loss due to stellar wind, depending on the details of the modelling of the dynamical system (see Gao et.al. (1991) for a discussion). Such physical processes, *i.e.*, those other than the two-body relaxation have been introduced separately in the above schemes by estimating the rates of these processes obtained from their detailed studies. For example, Gao et.al. (1991) have utilized the encounter cross-sections obtained from detailed numerical binary-single (Heggie & Hut, 1993) and binary-binary (Mikkola, 1984a,b) scattering experiments, to determine the occurrences of these close encounters (or "collisions") in a Monte-Carlo fashion, in conjunction with relaxing the system using the Fokker-Planck equation.

However, the one-dimensional method does overestimate the evaporation rate significantly from that obtained from direct N-body integrations for the case of tidally truncated clusters (Portegies Zwart et.al., 1998), for which the velocity anisotropy significantly affects the evaporation rate. Recent extensions of the Fokker-Planck method (Drukier et.al., 1999; Takahashi, 1995, 1996) allow for two-dimensional distribution functions and as well possess much improved energy conservation. These newer implementations provide much better agreement with the N-body results (Takahashi & Portegies Zwart, 1998) and take into account the mass loss due to stellar evolution (Takahashi & Portegies Zwart, 1999) and binary encounters (Drukier et.al., 1999).

1.6.2 Monte-Carlo method

The Monte-Carlo method provides perhaps the most straightforward technique for computing the evolution of the velocity distribution function as a result of encounters. In this method, each of the particles in the system or in a representative sample is followed in time and is subjected to encounters at known rates, the effects of which are chosen at random in accordance with known probabilities. In the case of a star cluster, the probability for the change in velocity $\Delta \mathbf{v}$ can be obtained from the theory of two-body encounters (Spitzer, 1987; Heggie & Hut, 2003).

There are two different implementations of the Monte-Carlo approach for computing the dynamical evolution of star clusters, *viz.*, the *dynamical Monte-Carlo method* or "Princeton method" (Spitzer & Thuan, 1972) and the *orbit-averaged Monte-Carlo method* (Hénon, 1971a,b; Shapiro & Marchant, 1978; Marchant & Shapiro, 1979). In the dynamical Monte-Carlo method, the positions of the stars are numerically integrated during the interval Δt_p between velocity perturbations, using a simplified equation of motion for each star and assuming spherical symmetry (see Spitzer (1987) for details). The time-step Δt_p is taken to be an appropriate fraction of the half-mass relaxation time, so that the perturbations $\Delta\mathbf{v}$ represent averages over many (distant) two-body encounters. They can therefore be directly obtained from the diffusion coefficients. An isotropic, Maxwellian velocity distribution is assumed in the Princeton method for analytically calculating the diffusion coefficients for $\Delta\mathbf{v}$ and $(\Delta v)^2$. At the time when this method was developed, the available computing resources were not enough to evolve a cluster with realistic number of stars, which is of the order of $N = 10^5 - 10^6$. Typically, $N_t \approx 1000$ "test stars" were considered to represent the velocity distribution function. To estimate the correct gravitational potential of the cluster during the dynamical integrations, each test star was considered as representative of several stars (typically 100), all with same values of r, v_r and v_t and uniformly distributed over a spherical surface, so that these "superstars" add up to the intended number of stars N of the cluster. Also, to keep track of the superstars, each of the shells were ranked according to their increasing radius r_j. However, with the computing resources that are available at the present time, the assumption of superstars is no more necessary, and a typical GC can be evolved directly with realistic number of stars (Joshi et.al., 2000). The dynamical Monte-Carlo method does not conserve energy very well, and the energy conservation has to be enforced by adjusting the velocity perturbations over several (typically 40) consecutive shells. Also, to avoid the singularity arising as a shell approaches very small r_j, a reflecting sphere of small radius (typically a percent of the half-mass radius) is usually assumed in the Princeton models.

One of the major advantages of the above Monte-Carlo method is that the use of direct dynamical integration makes it possible to follow the violent relaxation phase of the cluster. More importantly, the correct treatment of velocity perturbations produced in a single orbit makes it possible to study the escape rate from an isolated cluster. The major disadvantage of the dynamical Monte-Carlo method is that it requires significantly more computing resources than other Monte-Carlo implementations (see below), due to the use of dynamical integrations.

The orbit-averaged Monte-Carlo method (Hénon, 1971a,b) involves direct analytic computation of the perturbations of energy E and angular momentum J (per unit mass) for each star so that the time-consuming dynamical integration of their orbits can be avoided. Instead, the new position of each star after the change of its E and J are chosen from the potential of the cluster (from previous cycle). Specifically, the position of the star is determined randomly between pericenter r_p and apocenter r_a of the orbit appropriate for its new E and J, weighing each position by the time it spends around that position. In the case of a sample distribution, as discussed above, the actual potential of the cluster have to be recalculated after this reallocation of the superstars. In computing the perturbations, neighboring pairs of stars are allowed to interact. ΔE and ΔJ for each star are calculated analytically as an average over all possible (distant) two-body encounters during the time-step Δt_p. These perturbations depend on its position, velocity and the density of stars in its neighborhood. The density is usually determined using a sampling procedure. After the perturbations, the positions of the stars are reallocated as described above and the procedure is repeated over many time-steps. This method is also known as the "Hénon method". A variant of the Hénon method has been developed at Cornell (Shapiro & Marchant, 1978; Marchant & Shapiro, 1979), which provides information on the dynamical processes that occur in an orbital timescale, *e.g.*, escape of stars or their capture by a central black hole. In this approach, also known as the "Cornell method", ΔE and ΔJ are computed for encounters during a few number of orbits, particularly for stars nearing the escape energy. The Hénon method does not provide such results directly since the averaging is performed over many orbits to yield statistically accurate results.

Among earlier uses of the Monte-Carlo method, are the study of gravothermal instability (Spitzer & Hart, 1971a,b; Hénon, 1971a,b) and the effect of a central massive black-hole in a GC (Lightman & Shapiro, 1977). With the computing resources presently available, and the development of sophisticated Monte-Carlo codes, this method has proven to be a promising alternative to direct N-body integration, with the aid of which realistic star clusters can be evolved using much less computing resources. Another attractive feature of the Monte-Carlo method is that it is much easier to implement more complexity and realism into an existing code in comparison to the direct N-body integration schemes. Fregeau, Joshi, Rasio and collaborators has recently utilized a modified version of the Hénon's original algorithm (Joshi et.al., 2000) to evolve astrophysically realistic GCs, which allows for the time-step to be made much smaller to resolve the dynamics more accurately. Mass-spectrum and stellar evolution of the stars has been introduced by Joshi et.al. (2001). Fregeau et.al. (2003) incorporated close binary-single and binary-binary encounters (with equal, point masses) using known cross-sections of these processes. Fregeau & Rasio (2007) implemented direct numerical integrations of binary-single and binary-binary encounters by incorporating the few-body integration tool “Fewbody” (Fregeau et.al., 2004) into their Monte-Carlo code. They have also taken into account stellar collisions in this Monte-Carlo code.

Monte-Carlo methods have also been used to study specific types of dynamical interactions in a GC, *e.g.*, tidal capture (Di Stefano & Rappaport, 1992; Portegies Zwart et.al., 1997b), interactions involving primordial binaries (Hut, McMillan & Romani, 1992), stellar evolution and mergers (Portegies Zwart et.al., 1997a,b). All these studies however assumed a dynamically unevolving stellar background and uniformly used what is known as the “rejection method”. In such a method, the occurance a particular event during each time-step , *e.g.*, tidal capture, binary-single or binary-binary close encounters, is decided on the basis of pre-determined probability of that event (see Portegies Zwart et.al. (1997a)). The new configuration of the system is then determined from the outcome of the event. While the assumption of a dynamically unevolving background is definitely an over-simplification, these studies provide important insights on the statistics of these dynamical events.

1.6.3 N-body integration

Direct integration of the equation of motions of the constituent particles is the most straightforward way for evolving a cluster. While direct N-body integration is till date the most accurate way of studying dynamical evolution of star clusters, it is much more expensive compared to Fokker-Planck or Monte-Carlo method in terms of computational cost. The cpu-cost for integrating a N-body system increases with the number of particles N as N^3, so that it becomes prohibitive for directly integrating a GC with realistic number of stars, even in a present-day workstation. Pioneering improvements have been achieved in both the hardware and the software front, before we can reliably integrate about $10^4 - 10^5$ stars at the present time.

Evolving a star cluster is among the most computer-intensive and delicate problems in computational astrophysics. For systems like a dense GC, where the interchange of energy between binaries and single stars plays key role in the evolution of the cluster, one has to deal with a span of time scales $\sim 10^{14}$ (Heggie & Hut, 2003), the smallest timescale being that of a close passage between two (normal) stars ($\sim$ hrs) and the largest being that on which the cluster relaxes as a whole ($\sim$ Gyr). If we consider compact stars, this discrepancy is $\sim 10^{20}$. Such large timescale-difference implies that the close passage between two (or more) stars, *e.g.*, as in the case of tight binaries, would behave as a singularity and stall the whole calculation. Also, a GC typically have a large density gradient — the density-contrast between the center and the half-mass radius can be as large as 10^4, implying that the central relaxation time t_c to be smaller than the half-mass relaxation time t_{rh} by a similar factor. As the cluster evolves as a whole in the time-scale of t_{rh}, the central part will remain approximately in thermal equilibrium throughout the evolution. Since it is the small deviations from thermal equilibrium that drives the evolution of the cluster, one have to compute the forces and the motion of the stars to a very high degree of accuracy, especially those for the close encounters.

These challenges have been overcome by the development of ingenious numerical techniques and simultaneous development of highly efficient, organized, production-level numerical codes which materialize them. Several N-body simulation packages have been developed, the most widely used being the STARLAB (Portegies Zwart et.al., 2001) and the NBODYx family (Aarseth, 1999). These codes rely on numerical integration of the particles using the well-known *predictor-corrector schemes* (Makino & Aarseth, (1992)), in conjunction with the *individual time-step* (ITS) method (Aarseth, 1963), where each particle i has its own time-step δt_i for updating its dynamics. This ensures accurate integration for each of the particles in the system irrespective of the timescale of its motion. A variant of the ITS scheme is the *block time-step* scheme (Aarseth, 2003), where all particles in the system are allowed to have time-steps only in powers of two, so that several particles are simultaneously assigned the same time step for updating their dynamics. This presents extra advantages over the purely individual time-steps, for integration with the GRAPE hardware and parallelized systems (see below). To achieve numerical efficiency further, the NBODYx family of codes also allow to use the *neighbor scheme* or *Ahmad-Cohen scheme* (Ahmad & Cohen, 1973) in which the force on each particle is contributed only from a list of its neighboring particles in all time steps, and the force due to all the particles in the system is considered only at larger time-steps. To avoid the singularity caused by close approach between two stars, say, when they are in a binary, the NBODYx codes use various *regularization* techniques. For a two-body system, the *KS regularization* (Kustaanheimo & Stiefel, 1965) is used and for 3-body and few-body systems, *Chain regularization* (Mikkola & Aarseth, 1996) is employed. An alternative to the rigorous regularization methods is to use *softening* in which the separation between two particles is not allowed to vanish as they come close, but approach a chosen small non-zero value instead. Such method is also successfully used in many N-body codes, *e.g.*, STARLAB.

To study the evolution of a realistic star cluster however, one needs to incorporate the nuclear evolution of individual stars and the hydrodynamical encounters between them, which are not only important in their own rights, but also may play key roles in the dynamical evolution of the cluster itself. Therefore, to simulate a cluster of real stars, stellar evolution and hydrodynamics models have to be coupled with the point-mass N-body integrator. STARLAB and NBODYx codes incorporate stellar evolution using simple and automated stellar and binary evolution codes like "SeBa" (Portegies Zwart et.al., 2001) or "BSE" (Hurley et.al., 2002) and toy hydrodynamical models which prescribe different schemes for different kinds of merger events (Portegies Zwart et.al., 2001). More recently, the effect of tidal encounters has been adapted in the NBODY4 code by Baumgardt et.al. (2006). These authors computed the energy dissipation of a star due to its nearest neighbor using the analytic prescription by Portegies Zwart & Meinen (1993) during each close passage.

The present state-of-art achievement of the N-body simulation not only relies on the remarkable development from the software side, but also equally dependent on the tantalizing progress in computer hardware development. A breakthrough in this direction is the development of the special-purpose hardware GRAPE-4 for calculating the gravitational forces between particles at Tokyo University in 1995 (Makino & Taiji, 1998). The GRAPE-x (GRAvity PipE) family of processors greatly accelerate the main time-consuming $\sim N^2$ force calculations by directly computing them through hardware, leaving the host workstation with only the remaining $\sim N$ calculation (energy transport). With a typical workstation of ~ 100 Mflops, a complete GRAPE-4 configuration can perform with an effective speed over 1 Tflops, and its next version GRAPE-6 is about 100 times faster! N-body codes (NBODY6++ and STARLAB) are also parallelized for running in parallel supercomputers (without GRAPE) with similar efficiency as GRAPE workstations, and the development of codes to perform in parallel GRAPE systems is also in progress (Portegies Zwart et.al., 2007b). More interestingly, N-body integrations are recently being performed in Graphic Processing Units (GPU) instead of GRAPE processors (Portegies Zwart et.al., 2007a; Belleman et.al., 2008), which is a very promising alternative to the less-available and expensive GRAPE hardware.

1.7 Our Boltzmann scheme

In this thesis, we introduce a new formalism of studying the evolution of compact-binary populations in globular clusters, *viz.*, a Boltzmann scheme for following the time-evolution of such populations (Banerjee & Ghosh, 2007, 2008a,b). We use the (collisional) Boltzmann equation in its original form to evolve the orbital-radius (a) distribution $n(a, t)$ of a GC compact binary population in time t, keeping track of their dynamical formation, destruction and hardening. One virtue of this approach is that, unlike the Fokker-Planck approximation to the Boltzmann equation, the original Boltzmann prescription automatically includes on the same footing both weak, frequent *and* strong, rare encounters. A second virtue of such a Boltzmann scheme is that it is quite generic in the sense that it does not assume any particular dynamical model, so that any suitable model for formation, destruction and orbital evolution of compact binaries can be inserted into it to study its effect on the evolution of the above distribution function. In our approach, we take into account the dynamical processes through cross-sections of the relevant processes, as determined earlier through extensive work on numerical experiments with two-body and three-body encounters (Spitzer, 1987; Hut & Bahcall, 1983; Heggie, Hut & McMillan, 1996; Portegies Zwart et.al., 1997b). A third virtue of this approach is that it is computationally much less expensive and faster than direct N-body integration and less expensive then even Monte-Carlo/Fokker-Planck methods.

We develop our Boltzmann formalism in a step-by-step manner. In the first step, we explore the *continuous limit* of the above dynamical processes, representing them as smooth rate functions in the Boltzmann formalism (Chap. 3). In the next stage, we incorporate the stochastic nature of the dynamical processes by considering the corresponding rates fluctuating randomly about their mean value (Chap. 4). We model these fluctuations through the formalism of the Wiener process, the mathematical description of Brownian motion, as detailed in Chap. 4. The resulting Boltzmann equation becomes a *stochastic partial differential equation* (SPDE), the study of which is itself a subject of considerable interest , both from the point of view of its mathematical properties (Øksendal, 2004) and as a challenging numerical problem (Kloeden et.al., 1994; Gaines, 1995). We apply the existing methods of stochastic calculus, also known as the *Itô calculus* (see Appendix C), to compute the (stochastic) evolution of the binary distribution function. By this method, we model the simultaneous effect of all dynamical processes operating on the compact-binary population, and study the evolution of (a) the total number of X-ray binaries as the formation and destruction processes continue to operate and (b) the orbital-period distribution of the population.

In the above parts of this thesis work, we consider the stellar background to be unevolving, *i.e.*, ignore the effect of the evolution of the host GC, which has widely been done in the literature (Hut, McMillan & Romani, 1992; Sigurdsson & Phinney, 1993; Portegies Zwart et.al., 1997b) as a first simplifying assumption. However, GCs do undergo dynamical evolution driven by two-body relaxation, which has been studied through Fokker-Planck (Gao et.al., 1991), Monte-Carlo (Joshi et.al., 2000; Fregeau et.al., 2003) and N-body simulations (Makino, 1996). We discuss the nature of GC evolution in Chap. 5. In the subsequent part of this thesis, we study the effects of Gc evolution on that of the compact binary population. We do so through our Boltzmann scheme again, mimicking numerical results for GC evolution with the aid of simple, analytical model, and following the evolution of compact-binary population (Chap. 5) that occurs in this situation.

Our results from the Boltzmann scheme show that the total number N_{XB} of X-ray binaries expected in a globular cluster exhibit characteristic scaling with well-known globular cluster parameters, *viz.*, the total star-star encounter rate Γ and star-binary encounter rate γ (Verbunt, 2003), for which we coin the name "Verbunt parameters" (see Chap. 3). The computed theoretical trends compare very well with the observed trends in recent data on X-ray binaries in Galactic GCs from the *Chandra* observatory (Pooley et al., 2003). In the subsequent chapters, we present a detailed exposition of our Boltzmann scheme. But before doing so, we describe in the next chapter an interesting scaling of the collisional hardening process with the Verbunt parameter γ that we found (Banerjee & Ghosh, 2006) while beginning this thesis work, and a related, simple "toy" scheme that we explored at that time for obtaining first qualitative insights into the scaling of N_{XB} with Verbunt parameters.

Chapter 2

Collisional Hardening of Compact Binaries in Globular Clusters

2.1 Introduction

It is well-known that globular clusters contain far more than their fair share of compact X-ray binaries per unit stellar mass, compared to their host galaxies (Verbunt & Hut 1987, Verbunt & Lewin 2004). The enhancement factor is ~ 100 in the Milky Way and M31 (Verbunt & Lewin 2004, Pooley et al. 2003), and possibly much higher in elliptical galaxies, as recent *Chandra* observations have suggested (Angelini et.al. 2001, Pooley et al. 2003). The origin of this overabundance of close binaries has been realized for some thirty years now to be the dynamical formation of such binaries — through tidal capture and/or exchange interactions — which can proceed at a very significant rate in dense cores of globular clusters (henceforth GCs) because of the high stellar-encounter rates there (Hut 1985, Hut & Verbunt 1983, Hut et.al. 1992), but whose rate is negligible over the rest of the galaxy, where the stellar density is low by comparison. The GC X-ray binaries that we shall be mainly concerned with in this work are those which are powered by accretion onto compact stars. These can be either (a) low-mass X-ray binaries (henceforth LMXBs), containing neutron stars accreting from low-mass companions, or, (b) cataclysmic variables (henceforth CVs), containing white dwarfs accreting from low-mass companions. Accordingly, we shall not explicitly consider here binaries which contain either (a) two "normal" solar-mass stars, one or both of which are coronally active, or, (b) recycled neutron stars operating as rotation-powered millisecond pulsars, with a white-dwarf or a low-mass normal companion, although such binaries can be low-luminosity X-ray sources. However, general considerations on the dynamical formation of close binaries do apply to these as well; indeed, the latter binaries are now widely accepted as evolutionary products of LMXBs (van den Heuvel 1991, 1992).

In tidal-capture formation of a compact-star binary, a compact star (neutron star/white dwarf) passing close to a normal star dissipates its kinetic energy significantly by creating tidal deformation in the latter star, and so becomes bound to it. In the exchange process of formation, a compact star replaces one of the stars of an existing binary system of two normal stars during a dynamical encounter (Hut 1985, Hut & Verbunt 1983, Spitzer 1987). These dynamical processes have been introduced in Sec. 1.5 and we shall discuss them quantitatively in Chap. 3.

After formation in such an encounter, the compact-star binary continues to undergo stellar encounters in the dense cores of GCs, and it is on one particular effect of the continuing encounters that we focus in the present chapter. In the mid-1970s, it was realized that a major effect of the binary-single star encounters would be to extract energy from a given binary, making it more tightly bound or *harder*, and giving this energy to the motion of the single stars in the GC, thus "heating" the cluster (Heggie 1975, Spitzer 1987, Hut et.al. 1992). We can call this effect *collisional hardening* of the compact-star binary, which makes the binary's orbit shrink at a rate higher than that which would obtain if it were not subject to the above stellar encounters, *i.e.*, if it were not in a GC. The latter rate is believed to be determined by a combination of two processes, *viz.*, (a) emission of gravitational radiation and (b) magnetic braking. In gravitational radiation, a compact binary emits gravitational radiation and so loses energy and angular momentum, which makes its orbit shrink (d'Inverno, 1992). Magnetic braking occurs as follows. The low-mass companion to the compact star has a significant magnetic field, and also has its rotation tidally coupled or "locked" to that of orbital revolution. A dynamo operates in such low-mass stars, which have a convective envelope, and is indicated by the observed chromospheric (CaII, H and K) and coronal emissions from the rapidly rotating low-mass stars (Zwaan, 1981). Such activity drives a wind from the companion, which carries away angular momentum at a significantly enhanced rate because the magnetic field enforces co-rotation of the wind out to a radius considerably larger than that of the star. This angular momentum ultimately comes from the orbit because of the above tidal locking, thus making the orbit shrink (Verbunt & Zwaan, 1981). We discuss in this chapter the relative roles of the above mechanisms for binary hardening, particularly the role of collisional hardening *vis-á-vis* that due to gravitational radiation, indicate and clarify a scaling that naturally emerges from this interplay, and briefly suggest possible observational signatures of this scaling.

In Sec. 2.2, we discuss the hardening of compact binaries by the three mechanisms discussed above, bringing out the particular role of collisional hardening. We show that a characteristic scaling of the orbit-shrinkage time of such binaries with an essential GC parameter emerges because of the interplay between collisional hardening and that due to gravitational radiation. In Sec. 2.3, we explore possible observational signatures of this scaling. We sketch a very simple "toy" scheme for describing the evolution of compact X-ray binaries in GCs, and indicate a possible signature of the above scaling within the bounds of this toy model. We show that current data on X-ray binaries in GCs are consistent with this signature. We discuss our results in Sec. 2.4, exploring possible lines of future enquiry.

2.2 Hardening of Compact Binaries

We consider the shrinking of the orbital radius of a compact binary by the three mechanisms introduced above. Consider gravitational radiation first. The rate at which the radius a of a binary decreases due to this process is given by (see, *e.g.*, d'Inverno (1992); Landau & Lifshitz (1962)):

$$\dot{a}_{\rm GW} \equiv \alpha_{GW} a^{-3}, \qquad \alpha_{GW} \approx -12.2 M m_X m_c \, R_\odot/{\rm Gyr} \tag{2.1}$$

In this equation, m_X and m_c are respectively the masses of the compact star and its companion in solar masses, $M \equiv m_X + m_c$ is the total mass in the same units, and the orbital radius a is expressed in units of solar radius. We shall use these units throughout this thesis.

Now consider magnetic braking. The orbit shrinkage rate due to this process is given in the original Verbunt-Zwaan prescription (Verbunt & Zwaan, 1981) as:

$$\dot{a}_{\rm MB} \equiv \alpha_{MB} a^{-4}, \quad \alpha_{MB} \approx -190 \frac{M^2}{m_X} \left(\frac{R_c}{a} \right)^4 \, R_\odot/\text{Gyr} \tag{2.2}$$

where R_c is the radius of the companion. The above formula has been obtained by applying the observed age-dependence of equatorial rotation velocity of main-sequence G stars (Skumanich, 1972) to the case of compact binaries (Verbunt & Zwaan, 1981). We give below further discussion on this mechanism.

Finally consider the rate of orbit shrinkage due to collisional hardening, which is given by (Shull, 1979),

$$\dot{a}_{\rm C} \equiv \alpha_C \gamma a^2, \qquad \alpha_C \approx -2.36 \times 10^{-7} \frac{m_{GC}^3}{m_X m_c} \, R_\odot/\text{Gyr} \tag{2.3}$$

Here, m_{GC} is the mass of the normal stars in the GC core which are undergoing encounters with the binary. In this introductory work, we assume m_{GC} to be a constant, representing a suitable average value for a GC core, which we take to be $m_{GC} \approx 0.6 M_\odot$. The above expression for shrinkage rate includes both the fly-by and exchange encounters. It is derived by fitting analytical cross-sections with those from numerical scattering experiments as discussed in Heggie (1975).

The parameter γ is a measure of the encounter rate between a given binary and the background of single stars in the core of the GC: it is a crucial property of the GC for our purposes, so that we shall use it constantly here and in the following chapters. It is one of the *Verbunt parameters* that we define in Chap. 3. It scales as $\gamma \propto \rho/v_c$ with the (average) core density ρ of the GC, and the velocity dispersion v_c of the stars in the core. Following the convention often employed in the GC literature (Verbunt 2003, Hut 1985), we can, in fact, *define* this parameter as:

$$\gamma \equiv \frac{\rho}{v_c}. \tag{2.4}$$

Then the unit of γ is $\approx 6.96 \times 10^5 M_\odot R_\odot^{-4}$ sec, corresponding to the units of ρ and v_c commonly used in the GC literature, namely, $M_\odot \text{pc}^{-3}$ and km sec^{-1}

respectively. In these units, values of γ generally run in the range $\sim 10^3 - 10^6$ (see below).

In this work, we take the mass of the compact star to be $m_X = 1.4M_\odot$ and that of the companion to be $m_c = m_{GC} \approx 0.6M_\odot$, the latter corresponding to a typical average mass of normal stars in a GC core (see above). According to the mass-radius relation for low-mass main-sequence stars, the radius of such a main-sequence companion will then be $R_c \approx 0.6R_\odot$. Furthermore, we consider only circular orbits in this work, returning to this point in Sec. 2.4.

The total rate of orbit shrinkage due to the combination of the above mechanisms is given by:

$$\dot{a} = \dot{a}_{\rm GW} + \dot{a}_{\rm MB} + \dot{a}_{\rm C} \tag{2.5}$$

We emphasize that the first two terms in Eq. (2.5) are always operational, irrespective of whether the binary is in a GC or not, and it is the relative effect of the third term, which represents the effects of the encounters in a GC core, that we wish to study here. The interplay between the first and the third term was investigated in a pioneering study by Shull (1979), before the magnetic braking mechanism was postulated (Verbunt & Zwaan, 1981).

Note first that the three terms have different regions of dominance, as shown in Fig. 2.1. Collisional hardening dominates at large values of the orbital separation a, *i.e.*, for wide binaries, while hardening by gravitational radiation and magnetic braking dominates at small a, *i.e.*, for narrow binaries. Between the latter two, magnetic braking dominates at the smallest orbital separations, if we adopt the original Verbunt-Zwaan (henceforth VZ) scaling for it (see below). The relative orbit shrinkage rate $\dot{a}/a$ thus scales as a at large orbit separations, passes through a minimum at a critical separation a_c where the gravitational radiation shrinkage rate, scaling as $\dot{a}/a \sim a^{-4}$, takes over from collisional hardening, and finally rises at very small separations as $\dot{a}/a \sim a^{-5}$ due to VZ magnetic braking. The changeover from gravitational radiation shrinkage to that due to magnetic braking occurs at a radius $a_m < a_c$. These two critical radii are easily obtained from Eqs. (2.1), (2.2), and (2.3), and are given by

$$a_c = \alpha_{\rm GW}^{1/5} \alpha_{\rm C}^{-1/5} \gamma^{-1/5}, \qquad a_m = \frac{\alpha_{\rm MB}}{\alpha_{\rm GW}} \tag{2.6}$$

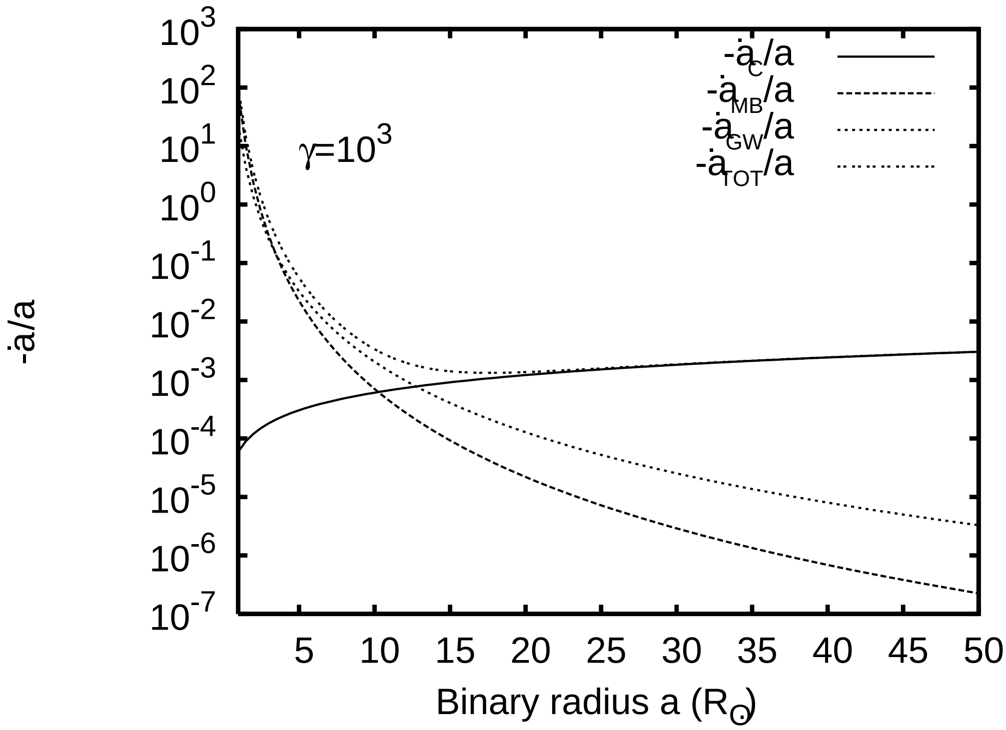

Figure 2.1: *Relative orbit shrinkage rates -ȧ/a due to gravitational radiation, magnetic braking and collisional hardening, shown as functions of the binary separation a. Also shown is the total shrinkage rate. Value of γ as indicated.*

Note the scaling $a_c \propto \gamma^{-1/5}$, which is crucial for much of our discussion here, as we shall see below. The critical orbital separation a_c varies in the range $\sim (5-12)R_\odot$ for the canonical range of values of the above GC parameter (Verbunt, 2003) $\gamma \sim 10^3 - 10^5$ in the above units (Shull, 1979).

The relevance of this to close compact-star binaries in GCs is as follows. When such a binary is formed, its orbital separation in most cases is such that the low-mass companion is not in Roche lobe contact, since the Roche-lobe radius has to be $R_L \sim 0.6R_\odot$ or less for this to happen for a typical low-mass main sequence or subgiant companion of mass $\sim 0.6M_\odot$ (see above). Mass transfer does not occur under such circumstances, so that such binaries are pre-LMXBs or pre-CVs, and we can call them by the general name *pre-X-ray binaries*, or PXBs for short. It is the above orbit-shrinkage or hardening process that brings the companion into Roche-lobe contact, so that mass transfer begins, and the PXB turns on as an

X-ray binary (LMXB or CV), or XB for short (see Sec. 1.4 for a discussion on X-ray binaries).

Depending on the initial separation a_i of the binary, some or all of the above processes can thus play significant roles in shrinking it to the point where mass transfer begins. Recent numerical simulations suggest that tidal-capture binaries are born with orbital radii (or semi-major axes) in the range $1 < a_i/R_\odot < 15$ for main-sequence (henceforth ms) or early subgiant companions, and in the range $40 < a_i/R_\odot < 100$ for horizontal-branch companions (Portegies Zwart et.al. 1997b). For binaries formed by exchange encounters, the orbital radii are generally expected to be somewhat larger than those for corresponding tidal binaries with identical members. Thus, both collisional hardening and gravitational radiation are expected to play major roles in the orbital shrinkage to Roche-lobe contact for most of the PXBs in GCs, whether dynamically formed or primordial.

Although we have included magnetic braking as above for completeness, its role in hardening of PXBs into XBs appears to be rather insignificant, at least for the VZ scaling adopted above. This is evident from the fact that there is little change in any of the results described here whether magnetic braking is included or not. For the VZ scaling, this is easy to understand. With a steep increase at small a, this effect is significant only at very small orbital separation, when the PXB has already come into Roche-lobe contact and become an XB. Thus, this process may well be significant in the further orbital evolution of the XB as mass-transfer proceeds (van den Heuvel 1991, 1992), but not in the PXB-hardening process under study here.

Actually, further study of magnetic braking since the original VZ formulation has revealed many interesting points. The nature and strength of this effect very likely depends on the mass and evolutionary state of the companion star. For example, magnetic braking may become totally ineffective for very low-mass companions with $m_c \sim 0.3M_\odot$ or less, as these stars are fully convective. Whereas a significant convective envelope is necessary for strong magnetic braking, "anchoring" of the magnetic field in a radiative core is also believed to be essential for it, and it is argued that the effect would basically vanish when the star becomes fully convective (Spruit & Ritter 1983, Podsiadlowski et.al. 2002). Indeed, this forms the basis for the standard explanation for the *period gap* in CVs (van den Heuvel

1992 and references therein). Further, studies of the rotation periods of stars in open clusters have suggested that magnetic braking may be less effective than that given by the VZ prescription: this has been modelled in recent literature by either (a) the VZ scaling as above, but a smaller numerical constant than that given above, or, (b) a "saturation" effect below a critical value of a, wherein the scaling changes from the VZ $\sim a^{-4}$ scaling of Eq. (2.2) to a much slower $\sim a^{-1}$ scaling below this critical a-value (van der Sluys et.al. 2005). While these modifications are of relevance to XB evolution, it does not appear that they can alter the PXB-hardening results described here in any significant way. Accordingly, we shall not discuss magnetic braking any further here, and keep this term in the complete equations only to remind ourselves that it is operational, in principle, for companions with $m_c \geq 0.3M_\odot$.

2.2.1 An Interesting Scaling

Interplay between collisional hardening and gravitational-radiation hardening near the above critical orbital separation a_c produces a characteristic scaling, which we now describe. Consider the shrinkage time τ_{PXB} of a PXB from an initial orbital separation a_i to the final separation a_f corresponding to Roche-lobe contact and the onset of mass transfer, given by:

$$\tau_{PXB}(a_i, \gamma) \equiv \int_{a_i}^{a_f} \frac{da}{\dot{a}_{\rm GW} + \dot{a}_{\rm MB} + \dot{a}_{\rm C}} \tag{2.7}$$

For given values of stellar masses, τ_{PXB} scales with the GC parameter γ introduced above as

$$\tau_{PXB} \sim \gamma^{-4/5}. \tag{2.8}$$

The scaling is almost exact at high values of γ, *i.e.*, $\gamma > 10^4$, say, there being a slight fall-off from this scaling at low γ's.

How does this scaling arise? To see this, consider first the qualitative features of the integrand on the right-hand side of Eq. (2.7), *i.e.*, the reciprocal of the total shrinkage rate at an orbital separation a, which we denote by $\zeta(a)$, and which is displayed in Fig. 2.2. It is sharply peaked at $a \sim a_c$: indeed, the peak would be *exactly* at the above critical separation a_c but for the effects of magnetic braking, as can be readily verified. Since the latter effects are not important in

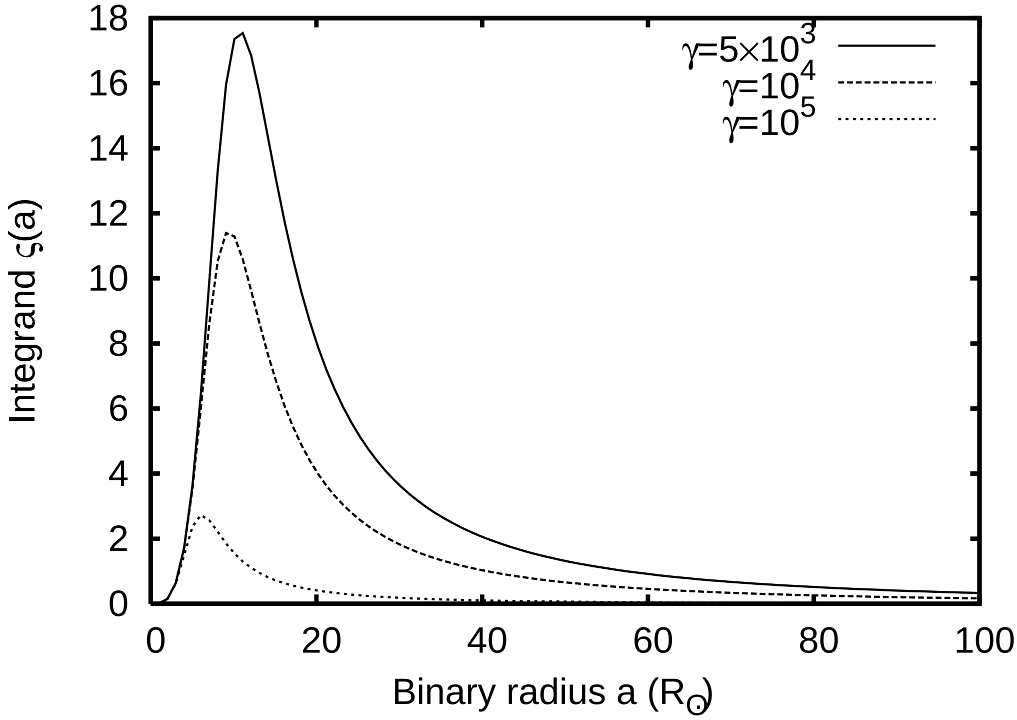

Figure 2.2: *Integrand $\zeta(a)$ in Eq.* (2.7) *shown as function of orbital separation a, with values of γ as indicated.*

the range of a-values relevant for this problem, as explained above, we can get a good estimate of the actual result by considering only gravitational radiation and collisional hardening. Because of this dominant, sharp peak in $\zeta(a)$, most of the contribution to the integral, *i.e.*, to τ_{PXB}, comes from there, provided that the integration limits (a_i, a_f) are such that *all or most of the peak is included.* We assume for the moment that this is so, and return to a discussion in the next subsection of what happens when this condition fails.

Under the above circumstances, we can immediately give a rough estimate of τ_{PXB}, which is the area under the curve in Fig. 2.2, as $\tau_{PXB} \sim 2a_c \times$(maximum value of the above integrand). This maximum value is simply $1/(2\alpha_{GW}a^{-3})$ if we neglect magnetic braking, since the gravitational radiation term equals the collisional hardening term there, as explained above. This gives $\tau_{PXB} \sim \alpha_{GW}^{-1} a_c^4$, which, with the aid of Eq. (2.6), yields $\tau_{PXB} \sim \alpha_{GW}^{-1/5} \alpha_C^{-4/5} \gamma^{-4/5}$. This is the basic reason for the scaling given by Eq. (2.8).

An exact evaluation of the integral in Eq. (2.7), with the magnetic braking term neglected, confirms this, as expected and as detailed in Appendix A. The exact result is:

$$\tau_{PXB} = \alpha_{GW}^{-1/5} \alpha_{C}^{-4/5} \gamma^{-4/5} [I(b_f) - I(b_i)]. \tag{2.9}$$

Here, b is a dimensionless orbital separation defined by $b \equiv a/a_c$, and the integral $I(x)$ is given in Appendix A. As $I(x)$ has only a logarithmic dependence on x under these circumstances, the basic scaling is $\tau_{PXB} \sim \gamma^{-4/5}$, as above. It is this basic scaling that leads to the essential behavior of the shrinkage time τ_{PXB} discussed in this chapter.

2.2.2 Breakdown of Scaling?

When would the above scaling break down, and why? A simple answer is clear from Fig. 2.2: this would happen when the integration limits (a_i, a_f) are such that all or most of the above peak in $\zeta(a)$ is *not* included. For the present problem, this basically reduces to an upper bound on a_f, since a_i is normally large enough to ensure that the region of integration in Fig. 2.2 extends well into considerably larger values of a beyond the peak. When a_f becomes so large as to exceed a_c, the region of integration is severely curtailed from the left in Fig. 2.2, so that most of the peak's contribution is missed, and the above scaling breaks down. We might think that such a situation would arise when the low-mass companion in the PXB is an evolved, horizontal-branch star, which has a much larger radius than a ms/subgiant companion of the same mass, and so would be expected to come into Roche-lobe contact at a much larger value of R_L, say $5 - 10R_{\odot}$, and correspondingly larger values of a_f. But such binaries are not relevant to our discussion here, since the lifetimes ($\approx 10^7$ y) of such horizontal-branch stars are too short to be of significance to the long binary-hardening timescales under consideration here. Thus, this possibility is not of practical importance here.

However, there *is* a situation in which this scaling is not relevant, not because it breaks down, but, rather because we move into a region of γ-values where τ_{PXB} computed in the above way exceeds the expected main-sequence lifetime τ_c of the low-mass ms/early-subgiant companion. Under these circumstances, the companion starts evolving into a giant and rapidly fills its Roche lobe, for essentially any value that a is likely to have at that stage. This is formally equivalent to saying that τ_{PXB} saturates at a value τ_c in this range of γ. We return to this point below.

2.2.3 Shrinkage Time

We now calculate the exact variation of the shrinkage time τ_{PXB} with the encounter-rate parameter γ introduced earlier, keeping all terms in Eq. (2.7). For this, we need to specify the initial and final values, a_i and a_f, of the orbital separation. We adopt $a_f \approx 1.94R_\odot$ for ms/subgiant companions corresponding to Roche-lobe contact, when the radius of the Roche-lobe R_L of the companion becomes equal to the radius of the companion itself. This translates into the above value of the orbital separation a_f by the well-known Paczyński (1971) relation:

$$R_L = 0.46a \left(\frac{m_c}{M}\right)^{1/3} \tag{2.10}$$

corresponding to R_L being equal to companion radius $\approx 0.6R_\odot$ for a companion mass $\approx 0.6M_\odot$.

In general, a_i will have a value which is within a possible range (a_i^{min}, a_i^{max}), which is indicated in Table 2.1. This range depends on the formation-mode of the binary, and also on the evolutionary status of the companion. The former has two possibilities, namely, (a) the binary is primordial, *i.e.*, it was already a binary when the globular cluster formed, or, (b) it formed by tidal capture or exchange interactions in the dense core of the globular cluster. The latter has also two basic possibilities, namely that the companion is either (a) a ms/subgiant, or, (b) a horizontal-branch star, as explained earlier. As explained above, however, the short lifetimes of horizontal-branch (Kippenhan & Weigert 1990, Clayton 1968) stars compared to the timescales of hardening processes under study here make it clear that they are of little importance in this problem, and we shall not consider them any further in this work. The ranges of a_i adopted in various cases are detailed in Table 2.1, and are taken from current literature (Portegies Zwart et.al. 1997b).

Since a GC has a distribution of a_is, we wish to study how $\tau_{PXB}(\gamma, a_i)$ averaged over such a distribution scales with γ, since both of these represent overall

Table 2.1: *Distribution functions $f(a_i)$ and range of initial orbital separations a_i of compact-star binaries in globular clusters*

Type of compact binary	*Range of initial radius a_i*	*Form of distribution function $f(a_i)$*
Dynamically formed compact star binary with ms or subgiant companion	$2R_\odot$ - $50R_\odot$	$f(a_i) \sim \frac{1}{a_i}$, $f(a_i) =$ constant, $f(a_i) \sim a_i$, Gaussian in a_i with $\mu = 6.0R_\odot$ and $\sigma = 12.7R_\odot$
Primordial compact binaries	$2R_\odot$ - $500R_\odot$	$f(a_i) \sim \frac{1}{a_i}$

properties of the cluster. To this end, we define a suitable average shrinkage time as:

$$\tau(\gamma) \equiv \langle \tau_{PXB} \rangle \equiv \int_{a_i^{min}}^{a_i^{max}} \tau_{PXB}(\gamma, a_i) f(a_i) da_i, \tag{2.11}$$

where $f(a_i)$ is the normalized distribution of a_i in the range (a_i^{min}, a_i^{max}). For this distribution, some indications and constraints are available, as follows. For primordial binaries, the distribution $f(a) \propto 1/a$ (corresponding to a flat cumulative distribution in $\ln a$) is well-established (Kraicheva et.al., 1978). For tidal capture/exchange binaries, results from numerical simulations like those of Portegies Zwart et.al. (1997b) generally suggest a bell-shaped distribution over the relevant ranges for both ms/subgiant companions and horizontal-branch companions, although other distributions are not ruled out. To explore a plausible range of possibilities, we have studied the following distributions, as detailed in Table 2.1: (a) the above reciprocal distribution $f(a) \propto 1/a$, (b) a uniform distribution $f(a) = $ const, (c) a linear distribution $f(a) \propto a$, and (d) a gaussian distribution $f(a) \propto \exp[-(a-a_0)^2/\sigma^2]$ with appropriately chosen central value a_0 and spread σ given in Table 2.1. The ultimate purpose is to assess the sensitivity (or lack thereof) of the final results on this distribution, as we shall see.

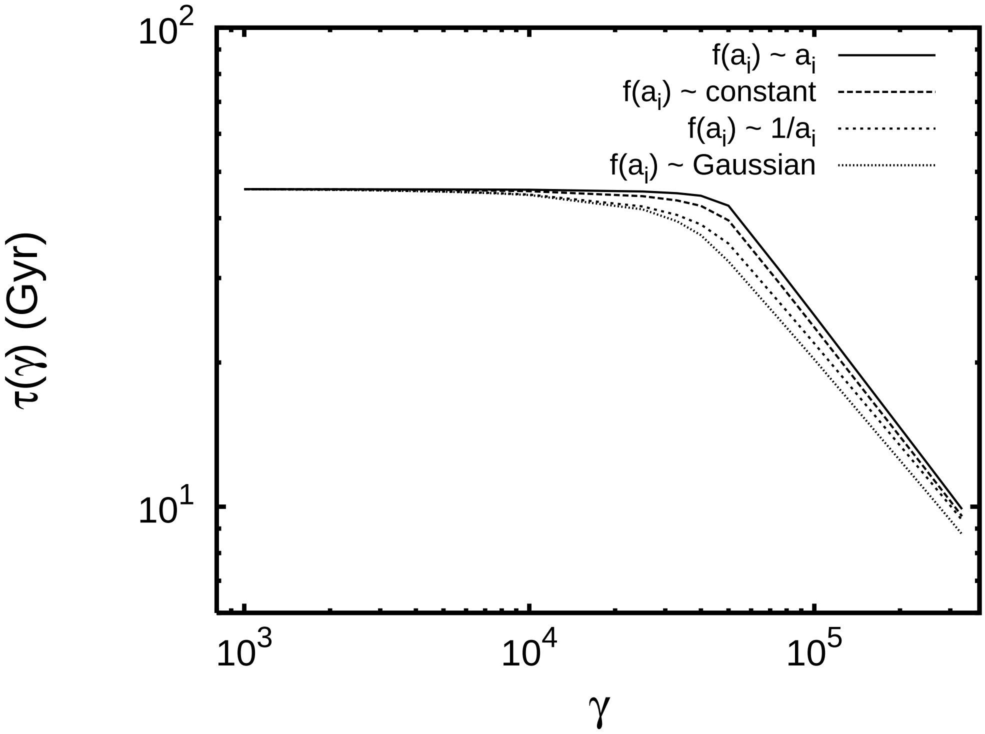

Figure 2.3: $\tau(\gamma)$ *vs.* γ *for* PXB*s: see text. Curves so normalized as to have the same "saturation value"* $\tau_c = 45$ Gyr *at low values of* γ*.*

Calculation of $\tau(\gamma)$ clarifies the following points. Primordial binaries have a range of a_is whose upper limit is considerably larger than that for ms/early-subgiant binaries, but most of those binaries which lie between these two upper limits are too wide to be of any practical importance in this problem. Thus, it appears that we need consider in detail only PXBs with ms/early-subgiant companions for our purposes here, and Fig. 2.3 shows the distribution-averaged shrinkage time $\tau(\gamma)$ as a function of the encounter-rate measure γ for such binaries. As can be seen, the above $\gamma^{-4/5}$-scaling is almost exact at high values of γ, say for $\gamma > 10^4$, there being a fall-off from this scaling at intermediate γs, the extent of which depends on the case, as shown. We find that the above behavior

Table 2.2: *Values of* γ_0 *obtained by fitting Eqn.* 2.12 *to computed* $\tau(\gamma)$ *vs.* γ *curves in Fig.* 2.3.

Type of initial distribution function	Value of γ_0
$f(a_i) \sim a_i$	8.49×10^3
$f(a_i) \sim$ constant	8.74×10^3
$f(a_i) \sim 1/a_i$	1.21×10^4
$f(a_i) \sim$ gaussian	1.06×10^4

can be well-represented by the analytic approximation

$$\tau(\gamma) \approx \frac{A_0}{\gamma_0^{4/5} + \gamma^{4/5}}, \tag{2.12}$$

where A_0 is a constant which depends on the range (a_i^{min}, a_i^{max}) (and also on the stellar masses, as explained above), and γ_0 depends on the above and also on the distribution $f(a_i)$. To illustrate the latter effect, we have given in Table 2.2 the inferred values of γ_0, where the curves begin to deviate from the asymptote, for various distributions in the case of tidal capture/exchange binaries.

We can see the trend that, as the distribution of a_i tends to emphasize larger and larger values of a_i over the permissible range (as happens in going from a $f(a_i) \sim a_i^{-1}$ to a uniform distribution $f(a_i) \sim$ const., and further to a linear distribution $f(a_i) \sim a_i$), γ_0 decreases. The physical reason for this is straightforward. Collisional hardening, whose rate scales with γ, is dominant at large a (scaling as a^2, as shown by Eqn. (2.3)). Hence, larger values of a_i increase the relative contribution of collisional hardening to τ, making it dominant over a larger range of γ, so that the asymptote $\tau \approx A_0\gamma^{-4/5}$ corresponding to pure collisional hardening is followed over a larger range of γ, and so γ_0 becomes smaller. It follows that those distributions which emphasize larger values of a_i will lead to smaller values of γ_0.

Finally, at low values of γ (about 10^3 - 3×10^4), the following aspect of the low-mass companion's evolutionary characteristics enters the picture. The value of $\tau(\gamma)$ calculated in the above manner then exceeds the main-sequence lifetime τ_c of the companion, a simple, widely-used estimate for which is

$$\tau_c \approx 13 \times 10^9 \, (m_c/M_\odot)^{-2.5} \text{ yr.} \tag{2.13}$$

For a typical low-mass companion with $M_c \approx 0.6M_\odot$, therefore, $\tau_c \approx 45$ Gyr. When $\tau(\gamma)$ calculated as above exceeds this value of τ_c, what happens is that the companion evolves into a giant, and so comes into Roche-lobe contact at a time $\approx \tau_c$ for essentially all plausible values of a at this point, irrespective of the calculated value of $\tau(\gamma)$. This is formally equivalent to the statement that $\tau(\gamma)$ reaches a saturation value of τ_c at low values of γ, the change-over occurring at $\gamma = \gamma_c$ such that $\tau(\gamma_c) = \tau_c$. Thus, the computed values can be analytically approximated by the prescription that $\tau(\gamma)$ is given by Eq. (2.12) for $\gamma > \gamma_c$, and by $\tau(\gamma) = \tau_c$ for $\gamma < \gamma_c$. This is shown in Fig. 2.3, where we normalize all the curves to the above, common "saturation value" $\tau_c = 45$ Gyr. Note that the lifetimes of GCs are typically $\sim 10 - 14$ Gyrs, so that, in a given GC, only those PXBs which reach Roche-lobe contact within its lifetime would be relevant for our purposes. What we have shown in Fig. 2.3 is the *formal* behavior of the distribution-averaged $\tau(\gamma)$ for plausible distributions of a_i. For a given GC, only that range of values of a_i which corresponds to Roche-lobe contact within its lifetime will go into the specific calculation for it.

2.3 Evolution of Compact-Star Binaries in Globular Clusters

How can we test the above scaling? Since τ is not directly observable, are there possible signatures that its scaling with γ might leave in the observed behavior of the populations of compact X-ray binaries in globular clusters? We briefly consider this question now and suggest possible answers.

As remarked earlier, PXBs are formed in GCs primarily by tidal capture and exchange interactions in the GC core. The rate of the former process is proportional to the encounter rate between single stars in the GC core. The latter rate is commonly denoted by Γ in the literature, and it scales as $\Gamma \propto \rho^2 r_c^3 / v_c$ with the average core density ρ, the velocity dispersion v_c of the stars in the core, and the core radius r_c. We can describe this as a rate of increase of the number N_{PXB} of PXBs in the GC which is $\alpha_1\Gamma$, where α_1 is a constant. In an exchange interaction, one of the members of a binary consisting of two normal stars is replaced by a heavier compact star. The rate of this process is proportional to the encounter rate between the above two populations. Assuming the population of compact stars in a GC to scale with the entire stellar population in the GC, and also the population of normal-star binaries in a GC to scale with its total population, both of which are normally done, the rate of the exchange process also scales with the square of the stellar density, and therefore with the above Γ parameter, and we can express it in a similar vein as $\alpha_2\Gamma$, where α_2 is another constant. Thus, we can write the entire formation rate phenomenologically as $\alpha\Gamma$, where $\alpha \equiv \alpha_1 + \alpha_2$.

After formation, two main processes affect the fate of the PXBs. The first is the process of the hardening of the PXB to the point of Roche-lobe overflow and conversion into an XB. This proceeds on a timescale τ_{PXB}, which means that the PXB population decreases on a timescale τ_{PXB}, which we can describe phenomenologically by a rate of decrease of N_{PXB} which is N_{PXB}/τ_{PXB}. This process may be slightly modified by second-order ones, which are normally ignored. For example, during the above hardening, an exchange encounter of the PXB with a single normal GC star heavier than the companion in the PXB can replace the latter.

The second process is the destruction of a PXB by its encounter with single stars in the GC core. This can happen in the two following ways. First, a fraction of the star-PXB encounters leads to a disruption or *ionization* of the PXB. This leads to a reduction in N_{PXB}, whose rate is proportional to γ, the star-binary encounter rate introduced earlier, and also to N_{PXB}. We can thus express this rate of decrease in N_{PXB} phenomenologically as $\beta_1\gamma N_{PXB}$, where β_1 is a constant. Secondly, in a smaller fraction of such encounters, a compact star can replace the normal low-mass companion in an exchange encounter, resulting in the formation of a double compact-star binary. This is equivalent to destroying the PXB, since such a binary will not evolve into an XB. The rate of this process scales with both N_{PXB} and the rate of encounter between a given PXB and compact stars. If we again argue that the population of compact stars in a GC scales with the entire stellar population in it, this rate is $\propto \gamma$, and the rate of reduction of N_{PXB} can be written phenomenologically as $\beta_2 \gamma N_{PXB}$, where β_2 is a constant. The total PXB destruction rate can thus be written as $\beta\gamma N_{PXB}$, with $\beta \equiv \beta_1 + \beta_2$.

2.3.1 A Simple "Toy" Evolutionary Scheme

We now combine the above points into a simple "toy" description of PXB and XB evolution in GCs, which we can use in an attempt to extract possible signatures of the scaling described in this work. In this "toy" scheme, which is similar in spirit to that of White & Ghosh (1998) and Ghosh & White (2001) for following the evolution of X-ray binary populations of galaxies outside GCs, the evolution of the PXB population is given by:

$$\frac{\partial N_{PXB}}{\partial t} = \alpha\Gamma - \beta\gamma N_{PXB} - \frac{N_{PXB}}{\tau_{PXB}}. \tag{2.14}$$

wherein the above rates of increase and decrease of N_{PXB} have simply been collected together.

The evolution of the XB population N_{XB} resulting from the above PXBs is described in a similar manner:

$$\frac{\partial N_{XB}}{\partial t} = \frac{N_{PXB}}{\tau_{PXB}} - \frac{N_{XB}}{\tau_{XB}}. \tag{2.15}$$

Here, τ_{XB} is the evolutionary timescale for XBs. The idea here is that XBs are created from PXBs at the rate N_{PXB}/τ_{PXB}, and conclude their mass-transfer phase, and so their lifetime as XBs, on a timescale τ_{XB}.

In the spirit of the "toy" model, all timescales in equations (2.14) and (2.15) can be considered constants, as can α and β, while in reality they depend on orbital parameters and stellar properties, as also on other parameters. These equations can then be solved readily, and of interest to us here is the asymptotic behavior, obtained by setting the time-derivatives to zero in these, which yields an XB population:

$$N_{XB} = \frac{\alpha\Gamma\tau_{XB}}{1 + \beta\gamma\tau(\gamma)}. \tag{2.16}$$

The effect of collisional hardening is immediately seen on the right-hand side of Eqn. (2.16), in the second term in the denominator. Since collisional hardening always decreases τ, it increases N_{XB}, other things being equal. This enhancement in N_{XB} is as expected, as collisional hardening makes a larger number PXBs reach Roche-lobe contact. Thus, in a GC with given properties, the number of X-ray sources is expected to be enhanced by collisional hardening compared to what it would be if this effect were negligible.

2.3.2 Signature of Collisional Hardening?

Can we look for observational evidence of the above enhancement in XB populations of GCs expected from collisional hardening? We discuss briefly an attempt to use *Chandra* observations of GCs to this end, with the cautionary remark that our evolutionary model, as given in the previous subsection, is still too simple-minded to apply quantitatively to actual GC data. What we are looking for, therefore, is a possible *qualitative* trend that is consistent with the ideas of collisional hardening introduced in this chapter, which will encourage us to perform a more detailed study.

The trend given by Eqn. (2.15) readily translates into one of the form

$$\frac{\Gamma}{N_{XB}} = A + B\gamma\tau(\gamma), \tag{2.17}$$

where $A \equiv 1/\alpha\tau_{XB}$ and $B \equiv \beta A$ are constants, independent of the cluster parameters. We can compare this with data obtained from *Chandra* observations of GCs, as given in Pooley et al. (2003) (see Sec 1.4.2). This is shown in Fig. 2.4.

It is clear that the trend suggested by Eq. (2.17) is consistent with the data, while that expected when collisional hardening is entirely neglected is not. The flattening of the trend on inclusion of collisional hardening is precisely due to the scaling discussed above. However, we stress again that ours is only a “toy” model at this stage, relevant only for exploring feasibility. To study the effect of a_i distributions, we have normalized the constants A and B for each distribution by having the curve pass through two chosen points at the lowest and highest values of γ for which data is available. The results show clearly that varying the distribution has almost no effect on the trend.

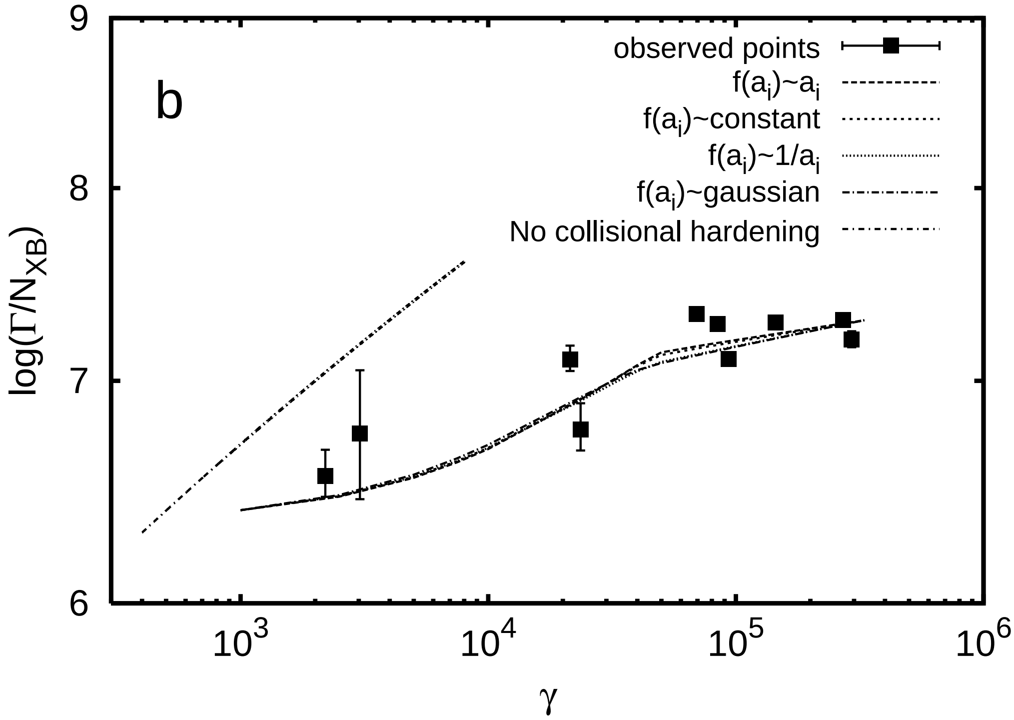

Figure 2.4: Γ/N_{XB} *vs.* γ *for Galactic globular clusters. Observational points with error bars from Pooley et al. (2003). Trend suggested by Eq. (2.17) shown for various distributions as indicated. Also shown is the trend expected in absence of collisional hardening.*

2.4 Discussions

In this chapter, we point out an essential effect in the hardening of PXBs in GCs, *viz.*, that collisional hardening *increases* with increasing a and orbital period, while that due to gravitational radiation has the opposite trend, so that their interplay leads to a characteristic scaling of the total hardening rate with GC parameters. In our introductory treatment of this effect here, we have given a very simple formulations of many physical processes. First, collisional hardening is an inherently stochastic process, wherein individual events of varying sizes accumulate to yield a final state, and the Shull (1979) rate we have used is a continuous approximation to it. Secondly, the essential two- and three-body interactions that determine the evolution and fate of a PXB in a GC are also stochastic by nature. For example, approximating an ionization event — in which a binary is disrupted — by a continuous term is necessarily a great oversimplification. Thus, an improved treatment must include a proper formulation of these stochastic processes. We shall discuss a formulation of incorporating the stochasticity in dynamical encounters in Chap. 4.

Thirdly, we have confined ourselves to circular orbits here, while binaries created by tidal capture and/or exchange interactions often have quite eccentric orbits, in which tidal circularization must play a dominant role during initial phases of hardening. Fourthly, mass segregation is an essential effect in GCs, which reflects itself in the accumulation of the heaviest objects in the core of a GC, and so in a change in the effective mass-function in the core. Finally, the evolution of the GC must be taken into account in a realistic calculation: this would make the GC parameters time-dependent, while we have treated them as constants here, and may indeed have a significant effect if core collapse and bounce are modelled. We incorporate some of these processes as we develop our approach in the following chapters.

Chapter 3

Evolution of Compact-Binary Populations in Globular Clusters: A Boltzmann Study. The Continuous Limit

3.1 Introduction

In this era of high-resolution X-ray observations with *Chandra* and *XMM-Newton*, studies of compact binaries in globular clusters have reached an unprecedented level of richness and detail. The numbers of compact X-ray binaries detected in Galactic globular clusters with high central densities are now becoming large enough that diagnostic correlations with essential cluster parameters, such as the two-body encounter rate Γ, can be performed (Pooley et al., 2003) at a high level of statistical significance. The results of such observational studies are naturally to be compared with those obtained from theoretical modeling of binary dynamics in globular clusters, which has had a long history, from the pioneering semi-analytic work of the 1970s (Heggie, 1975), to the more detailed numerical scattering experiments of the 1980s (Hut & Bahcall, 1983), leading to the wealth of detailed numerical work of the early- to mid-1990s (Makino & Aarseth, (1992); Heggie & Hut, 2003) using a variety of techniques including Fokker-Planck and Monte Carlo approaches, as also N-body simulations, and finally to the extensive

N-body simulations in the latter half of the 1990s using special-purpose computers with ultrahigh speeds (Makino & Taiji, 1998; Hut, 2001).

The range of problems studied by the above modeling has also been extensive. From the study and classification of individual scattering events to the construction of comprehensive fitting formulas for the cross-sections of such events (Hut & Bahcall, 1983; Heggie, Hut & McMillan, 1996), from the development of Fokker-Planck codes to the use of Monte Carlo methods for following binary distributions in globular clusters (Gao et.al., 1991; Hut, McMillan & Romani, 1992), and from tracking the fate of a relatively modest population of test binaries against a fixed stellar background to being able to tackle similar projects for much larger binary populations with the aid of the above special-purpose machines (Hut et.al., 1992; Makino, 1996), efforts along various lines of approach have shed light on the overall phenomenon of binary dynamics and evolution in globular clusters from various angles. For example, evolutions of the distributions of both *external* and *internal* binding energies of the binaries under stellar encounters have been studied by several authors, the emphasis usually being on the former, and final results on the external binding energy being expressed almost universally in terms of their radial positions r inside the cluster, which provides an equivalent description (Hut, McMillan & Romani, 1992; Sigurdsson & Phinney, 1993, 1995). Sec. 1.6 provides a comprehensive discussion on the different methods developed for simulating star clusters until recently and the various astrophysical questions that have been addressed.

Throughout the rest of this thesis, we introduce an alternative method of studying the evolution of compact-binary populations in globular clusters, wherein we use a Boltzmann description to follow the time-evolution of such populations, subject to both (a) those processes which determine compact-binary evolution in isolation (*i.e.*, outside globular clusters, or, in the "field" of the host galaxy, so to speak), *e.g.*, angular momentum loss by gravitational radiation and magnetic braking, as also orbital evolution due to mass transfer, and, (b) those processes which arise from encounters of compact binaries with the dense stellar background in globular clusters, *e.g.*, collisional hardening (Heggie, 1975; Shull, 1979; Banerjee & Ghosh, 2006), binary formation through tidal capture and exchange processes, and binary destruction. An introductory discussion on these processes has been provided in Sec. 1.5. We treat all of the above processes simultaneously through a Boltzmann formalism, the aim being to see their combined effect on the compact-binary population as a whole, in particular on the evolution of (a) the total number of X-ray binaries as the formation and destruction processes continue to operate, and, (b) the orbital-period distribution of the population. We stress at the outset that ours is not a Fokker-Planck description (see Sec. 1.6.1) but the original Boltzmann one, which in principle is capable of handling both the *combined* small effects of a large number of frequent, weak, distant encounters *and* the *individual* large effects of a small number of rare, strong, close encounters. In our approach, both of the above two types of effects are taken into account through cross-sections for the relevant processes, as determined from extensive previous work on numerical experiments with two-body and three-body encounters (Heggie, Hut & McMillan, 1996; Portegies Zwart et.al., 1997b). As these processes are inherently stochastic, a natural question that arises is how they are to be handled simultaneously with those which govern the fate of isolated compact binaries, and which are inherently continuous. It is essential to appreciate the importance of this question, since a simultaneous action of the above continuous and stochastic processes is precisely what operates on binaries in globular clusters, and so produces the observed properties of compact-binary populations in them.

Our answer to the above question is a step-by-step one. As the first step, in this chapter, we explore the continuous limit of the above stochastic processes, wherein the probability or cross-section of a particular such process happening with a given set of input and output variables is treated as a continuous function of these variables. This is, of course, a simplification, but it serves as a clarification of the average, long-term trends expected in the evolution of the binary population. In Chap. 4, we treat the stochastic processes as stochastic terms in the Boltzmann equation with cross-sections as derived in this chapter, with the aid of relatively recently-developed methods for solving stochastic partial differential equations. The resulting evolutionary trends show stochastic behavior, as expected, with fluctuations that vary from one particular "realization" of the essential processes to another. However, the average trends follow the continuous limit computed in the present chapter, which is as expected, and which shows the relevance of extracting this limit.

In the present and the next chapter, we model the stellar background provided by the globular cluster as a fixed background with given properties, as has been widely done in previous works (Hut, McMillan & Romani, 1992; Portegies Zwart et.al., 1997b; Sigurdsson & Phinney, 1993, 1995): this amounts to neglecting the back reaction of binary evolution on the background, which is reasonable if the main aim is an investigation of essential features of binary evolution, as was the case in the above previous works, as also in this work. However, the globular-cluster background does evolve slowly, passes through the core-collapse phase and possible gravothermal oscillations (Sugimoto & Bettwieser, 1983; Gao et.al., 1991), so that it would be interesting to be able to follow the effects of these on the evolution of the compact-binary population. We do this in Chap. 5, wherein we adopt previous results on time-evolution of globular-cluster properties, and study their effects on the evolution of compact-binary populations, again under the approximation of neglecting the back reaction of binary evolution on the globular-cluster background, as above and as appropriate for a first look.

In our study, we focus primarily on two aspects of the compact-binary populations of globular clusters. First, we study how the total number N_{XB} of X-ray binaries (henceforth XBs, which are mass-transferring compact binaries where the donor is a low-mass "normal" star, and the accretor is a degenerate star — a neutron star or a heavy white dwarf) in a cluster evolves as the stellar encounter processes proceed. Second, we also follow the evolution of the orbital-period (P) distribution of the pre-X-ray binaries (henceforth PXBs; also see below) and XBs, (or, equivalently, the distribution of their orbital radii a) within the framework of our model. However, we have adopted here only a very simple model of orbital evolution of individual binaries in order to assess the feasibility of our basic approach to globular-cluster environments, as detailed later. Consequently, while the P-distribution found by us may be roughly applicable to cataclysmic variables (CVs) with white-dwarf accretors, it cannot be compared at this stage to that of low-mass X-ray binaries (LMXBs) with neutron-star accretors, without including the essential stellar evolutionary processes that occur during the PXB and XB phase. Thus, we record our computed P-distribution here only as a preliminary indication of the results that emerge naturally from this line of study at this stage, to be improved upon later.

The basic motivation for our study comes from recent advances in X-ray observations of globular clusters, as mentioned above: with sufficient numbers of X-ray binaries detected in globular clusters, an understanding of how N_{XB} is influenced by essential globular-cluster parameters is becoming a central question. With the above goal in mind, we therefore explicitly follow the evolution of binaries only in internal binding energy (or binary period, or binary separation, which are equivalent descriptions if the stellar masses are known) and time, but not of their external binding energy (or position inside the globular cluster; see above). We emphasize that we do not *neglect* changes in the latter in any way, as they are automatically taken care of in the detailed dynamics of encounters which are represented by the relevant cross-sections mentioned above and elaborated on in the following sections. It is only that we do not keep an explicit account of them, as we do not need them for our purposes. In other words, we consider a bivariate binary distribution function $n(E_{in}, t)$, which may be looked upon as the integral of the distribution $\rho(E_{ex}, E_{in}, t)$ over all admissible values of E_{ex}, or equivalently over all positions r inside the globular cluster (Hut, McMillan & Romani, 1992; Sigurdsson & Phinney, 1993, 1995). We also emphasize that, by doing so, we do *not* implicitly assume any particular correlation, nor a lack thereof, between E_{in} and E_{ex} (Hut, McMillan & Romani, 1992): whatever correlations result from the dynamics of the encounters will be automatically displayed if we follow the evolution in E_{ex} or r, which is not of interest to us in this particular study.

Our first results from the above evolutionary scheme show that the total number N_{XB} of XBs expected in a globular cluster scales in a characteristic way with well-known globular cluster parameters Γ and γ (which we call Verbunt parameters: see Sec. 3.2.1) whose qualitative nature is rather similar to that found in our earlier "toy" model (see Chap. 2), although some details are different. Basically, N_{XB} scales with Γ — a measure of the dynamical formation rate of compact binaries, and, at a given Γ, N_{XB} decreases with increasing γ at large values of γ — a measure of the rate of destruction of these binaries by dynamical processes. These expected theoretical trends with the Verbunt parameters compare very well with the observed trends in recent data, encouraging us to construct more detailed evolutionary schemes.

In Sec. 3.2, we detail our model of compact binary evolution in globular clusters, describing, in turn, our handling of globular clusters, binary formation, destruction, and hardening processes, our Boltzmann scheme for handling population-evolution, and our numerical method. In Sec. 3.3, we give our model results on (a) the expected number of X-ray binaries in globular clusters as a function of their Verbunt parameters, and (b) the evolution of compact-binary period distribution. In Sec. 3.4, we compare these model results with the current observational situation. Finally, we collect our conclusions and discuss future possibilities in Sec. 3.5.

3.2 Model of Compact Binary Evolution in Globular Clusters

We consider a binary population described by a number distribution $n(a,t)$, where a is the binary separation, interacting with a fixed background of stars representing the core of a globular cluster of stellar density ρ and core radius r_c. We now describe various ingredients of our model and the evolutionary scheme.

3.2.1 Globular clusters

Globular cluster cores are described by an average stellar density ρ, a velocity dispersion v_c, and a core radius r_c. In this work, we consider star-star and star-binary encounters of various kinds, but neglect binary-binary encounters. For characterizing the former two processes, two encounter rates are defined and used widely (Verbunt, 2003, 2006). The first is the two-body stellar encounter rate Γ, already introduced in Chap. 2, which scales with $\rho^2 r_c^3/v_c$, and occurs naturally in the rates of two-body processes like tidal capture, stellar collisions and merger. In fact, we can *define* it as

$$\Gamma \equiv \frac{\rho^2 r_c^3}{v_c} \propto \rho^{3/2} r_c^2, \tag{3.1}$$

for our purposes here. Note that the last scaling in the above equation holds only for virialized cores, where the scaling $v_c \propto \rho^{1/2} r_c$ can be applied. In this work, we shall use this assumption where necessary, but with the caveat that some observed globular clusters have clearly not virialized yet.

The second is a measure of the rate of encounter between binaries and single stars in the cluster, the rate normally used being the encounter rate γ of a *single* binary with the stellar background, with the understanding that the total rate of binary-single star encounter in the cluster will be $\propto n\gamma$. We can *define* γ for our purposes as we did in Chap. 2, namely,

$$\gamma \equiv \frac{\rho}{v_c} \propto \rho^{1/2} r_c^{-1}, \tag{3.2}$$

where the last scaling holds, again, only for virialized cores.

The importance of the above cluster parameters Γ and γ in this context has been extensively discussed by Verbunt (Verbunt, 2003, 2006), and we shall call them *Verbunt parameters* here. Note that, for virialized cores, we can invert Eqs. (3.1) and (3.2) to obtain the scaling of the core density and radius with the Verbunt parameters as:

$$\rho \propto \Gamma^{2/5} \gamma^{4/5}, \qquad r_c \propto \Gamma^{1/5} \gamma^{-3/5} \tag{3.3}$$

It is most instructive to display the observed globular clusters in the $\Gamma - \gamma$ plane, which we do[1] in Fig. 3.1. The point that immediately strikes one in the figure is that the observed globular clusters seem to occur in a preferred, diagonal, "allowed" band in the $\Gamma - \gamma$ plane, along which there is a strong, positive correlation between the two parameters. We shall return to the significance of this elsewhere.

In Fig. 3.1, we also overplot the positions of those clusters in which significant numbers of X-ray sources have been detected from Pooley et al. (2003) (see Sec. 1.4.2), color-coding them according to the number of X-ray sources in each of them, as indicated. It is clear that these clusters are all in the upper parts of the above "allowed" band, which is entirely consistent with the widely-accepted

[1]Alternatively, the display can be in the $\rho - r_c$ plane, as in Verbunt's original work. We find the cluster dynamics more transparent when shown directly in terms of the Verbunt parameters.

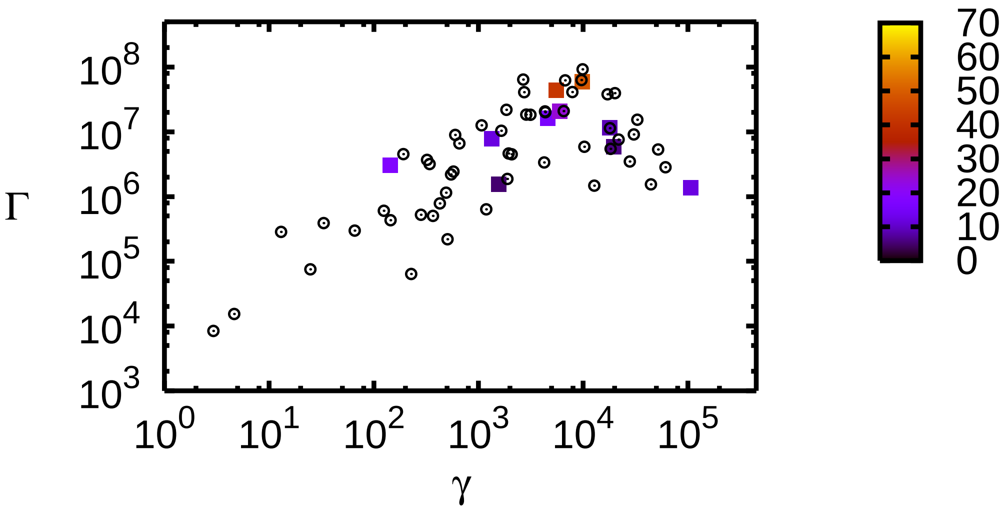

Figure 3.1: *Positions of Galactic globular clusters (open circles with dots) on the* $\Gamma-\gamma$ *(Verbunt parameters) plane. Overplotted are positions of those clusters with significant numbers of X-ray sources detected in them from Pooley et al. (2003) (filled squares), color-coded according to the number of X-ray sources in each, the color code being displayed on the right. Data from Harris (1996, revised in 1999).*

modern idea that the dominant mechanisms for forming these compact XBs in globular clusters are dynamical, *e.g.*, tidal capture, exchange encounters, and so on, since such mechanisms occur more efficiently at higher values of the Verbunt parameters Γ and γ, corresponding to higher stellar densities in the cluster core. Note that the probability of destruction of binaries by dynamical processes also increases with increasing γ, as we shall see below, so that, at first sight, we might have expected the highest incidence of XBs in those clusters which have high Γ and low γ. However, since Γ and γ are strongly correlated positively, as above, we cannot have arbitrarily high Γ and low γ for the same cluster. In reality, the highest number of XBs seem to occur, as Fig. 3.1 shows, in those clusters which have the highest values of Γ and high, but not the highest, values of γ. We return to this point later in this chapter, where we present our theoretical expectations for the scaling of the number of binary X-ray sources with the Verbunt parameters Γ and γ on the basis of the evolutionary scheme explored here.

In modeling the globular cluster core as a static background in this work, we assume that, initially, a fraction k_b of the stars is in primordial binaries, and that a fraction k_X of the stellar population is compact, degenerate stars with the canonical mass $m_X = 1.4M_\odot$ (representing neutron stars and heavy white dwarfs). The rest of the stellar background (including the primordial binaries) is taken to consist of low-mass stars of the canonical mass $m_f = 0.6M_\odot$, which is a reasonable estimate of the mean stellar mass of a mass-segregated core (Portegies Zwart et.al., 1997a). Naturally, the compact binaries formed from these ingredients consist of a degenerate star of mass $m_X = 1.4M_\odot$, and a low-mass companion of mass $m_c = m_f = 0.6M_\odot$. While this is clearly an oversimplification which must be improved upon in subsequent work, it appears to be adequate for a first look, which is our purpose here.

3.2.2 A Boltzmann evolutionary scheme

We explore in this work a Boltzmann evolutionary scheme, wherein the evolution of the number $n(a,t)$ of binaries per unit interval in the binary separation a (we choose to work here with a; equivalent descriptions in terms of the binary period P or the internal binding energy [see Sec. 3.1] E_{in} are possible, of course) is described by

$$\frac{Dn(a,t)}{Dt} = R(a) - nD(a). \tag{3.4}$$

Here, $Dn(a,t)/Dt \equiv \partial n/\partial t + (\partial n/\partial a)(da/dt)$ is the total derivative of bivariate $n(a,t)$: as explained in Sec. 3.1, this $n(a,t)$ is the result of an integration of a general, multivariate binary distribution over the variables we do not follow explicitly in this study, *e.g.*, the external binding energy or, equivalently, the position of the binary inside the globular cluster. Further, $R(a)$ is the total rate of binary formation per unit interval in a due to the various processes detailed below, and $D(a)$ is the total rate of binary destruction *per binary* per unit interval in a due to various processes, also detailed below. As our model stellar background representing the cluster core is taken as static for the present computation and also in the next chapter, the Verbunt parameters Γ and γ are time-independent, so that the formation and destruction rates R and D only depend on a and the stellar masses.

The above evolution equation can be re-written in the usual Boltzmann form

$$\frac{\partial n}{\partial t} = R(a) - nD(a) - \frac{\partial n}{\partial a} f(a), \tag{3.5}$$

where $f(a) \equiv da/dt$ represents the total rate of shrinkage or *hardening* of binaries (*i.e.*, $da/dt < 0$) due to several effects, which we introduced in Sec. 3.1, and which we elaborate on below. In the absence of all processes of formation and destruction, $R(a) = 0 = D(a)$, Eq. (3.5) becomes the usual collisionless Boltzmann equation

$$\frac{\partial n}{\partial t} = -\frac{\partial n}{\partial a} f(a), \tag{3.6}$$

representing a movement or "current" of binaries from larger to smaller values of a due to hardening. Equation (3.6) as akin to a wave equation with a formal "phase velocity" $f(a)$ of propagation. This analogy often proves useful for solving many problems, even with the more complicated formation and destruction terms present in Eq. (3.5). Note that, when $f(a)$ is constant (or roughly so, which can happen under certain circumstances, as we shall see later), the elementary wave-equation analogy is quite exact, and solutions of the form $n(a - f_0 t)$ should apply. We shall explore this point elsewhere.

Note further that the Boltzmann scheme outlined above does not have an explicit inclusion of the escape of those binaries from the globular cluster which receive a sufficiently large "kick". In principle, we can include this by suitably generalizing the above destruction term $D(a)$. However, in this introductory study, this did not appear crucial, as the main population affected by this process is that of primordial binaries, whereas our main concern here is with dynamically-formed compact binaries. The latter are, generally speaking, already so hard at formation that this process is much less effective in ejecting them from the cluster. Accordingly, we neglect this process here.

3.2.3 Binary hardening processes

In all of the dynamical encounter processes considered in this work, *viz.*, collisional hardening (described in this subsection), and dynamical formation and destruction processes (described in the next subsections), we shall assume the orbits to be circular, *i.e.*, neglect their eccentricity. This is, again, a simplification used for a first look. However, it is well-known from extensive numerical simulations that a large majority of the binaries formed by tidal capture are circular or nearly so (Portegies Zwart et.al., 1997b), due to the rapid circularization which follows capture. Since our main concern here is with dynamically-formed binaries, this approximation may well be a reasonable one for describing overall evolutionary properties of such binary populations.

3.2.3.1 Hardening in pre-X-ray binary (PXB) phase

As explained in detail in Chap. 2, the processes that harden binaries are of two types, *viz.*, (a) those which operate in isolated binaries, and are therefore always operational, and (b) those which operate only when the binary in a globular cluster. In the former category are the processes of gravitational radiation and magnetic braking, and in the latter category is that of collisional hardening. As discussed in detail in that chapter, collisional hardening, which increases with increasing a, dominates at larger orbital radii, while gravitational radiation and magnetic braking, which increase steeply with decreasing a, dominate at smaller orbital radii. It is these processes that harden a compact binary from its pre-X-ray binary (PXB) phase, during which its orbit is still not narrow enough for the companion (mass donor) star to come into Roche lobe contact, to the state where this Roche lobe contact does occur, at which point the companion starts transferring mass to the degenerate star, and the system turns on as an X-ray binary (XB) — either a CV or a LMXB, depending on the nature of the degenerate accretor (see Sec. 1.4.1 for a discussion).

Consider gravitational radiation first. Gravitational radiation from a binary system occurs due to the variation of the mass quadrapole moment of the system (Landau & Lifshitz, 1962). The energy and angular momentum flux carried by the gravitational wave from the system have been obtained by Peters

(1964) through detailed calculations using general relativity. We adapt the orbit-averaged angular momentum loss rate from the above work, which, for circular binaries, is given by,

$$j_{GW}(a) \equiv \left(\frac{\dot{J}}{J}\right)_{GW} = -\alpha_{GW} a^{-4}, \qquad \alpha_{GW} \equiv \frac{32G^3}{5c^5} m_c m_X (m_c + m_X). \tag{3.7}$$

Here, as before, m_X is the mass in solar units of the degenerate primary (neutron star or white dwarf) which emits X-rays when accretion on it occurs during the mass-transfer phase of the compact binary, m_c is the mass of its low-mass companion in solar units, and the unit of the binary orbital radius a is the solar radius. We shall use these units throughout the work.

Now consider magnetic braking. The pioneering Verbunt-Zwaan (Verbunt & Zwaan, 1981) prescription for this process has been reassessed and partly revised in recent years, in view of further observational evidence on short-period binaries available now (for further details, see discussions in Sec. 2.2 and references therein), and modern prescriptions are suggested in van der Sluys et.al. (2005). From these, we have chosen for this work the following one which preserves the original Verbunt-Zwaan scaling, but advocates an overall reduction in the strength of the magnetic braking process:

$$j_{MB}(a) \equiv \left(\frac{\dot{J}}{J}\right)_{MB} = -\alpha_{MB} a^{-5}, \quad \alpha_{MB} \equiv 9.5\times10^{-31} G R_c^4 \frac{M^3}{m_X m_c}, \quad M \equiv m_c + m_X \tag{3.8}$$

Here, R_c is the radius of the companion. Note that the strength of magnetic braking is still a matter of some controversy; while the evidence cited in the above reference argues for a reduction from the original value, it can also be argued that the presence of the well-known "period gap" in the period distribution of CVs requires a strength comparable to the original one. We have adopted here a recent prescription which is reasonably simple and adequate for our purposes: our final results do not depend significantly on the strength of this process.

Consider finally collisional hardening. As indicated earlier, it is a stochastic process, for whose continuous limit we use the prescription of Shull (1979), as has been done previously in the literature (see Sec. 2.4 for a discussion). According to this prescription, the rate of increase of orbital binding energy E of a compact binary due to collisional hardening is given in this limit by:

$$\left(\frac{\dot{E}}{E}\right)_C = A_C a\gamma, \qquad A_C \equiv 18G\frac{m_f^3}{m_c m_X} \tag{3.9}$$

Here, m_f is the mass of the stars in the static background representing the cluster. We shall use $M_\odot \mathrm{pc}^{-3}$ and km sec^{-1} as the units of ρ and v_c respectively. In the above units, the value of γ for Galactic globular clusters typically lie between $\sim 10^3$ and $\sim 10^6$ (see Chap. 2). The relation between $\dot{E}$ and $\dot{J}$ is:

$$\frac{\dot{J}}{J} = -\frac{1}{2}\frac{\dot{E}}{E} + \frac{3}{2}\left(\frac{\dot{m}_c}{m_c} + \frac{\dot{m}_X}{m_X}\right), \tag{3.10}$$

and the angular momentum loss rate is related to the shrinkage rate of the orbit $\dot{a}$, or hardening, as:

$$\frac{\dot{a}}{a} = 2\frac{\dot{J}}{J} - 2\frac{\dot{m}_c}{m_c} - 2\frac{\dot{m}_X}{m_X} \tag{3.11}$$

The $\dot{m}_c$ and $\dot{m}_X$ terms on the right-hand side of Eqn. (3.11) are nonzero during mass transfer in the XB phase. In the PXB phase, $\dot{m}_c = \dot{m}_X = 0$, so that $\dot{a}$ is simply related to $\dot{J}$ as:

$$\frac{\dot{a}}{a} = 2\frac{\dot{J}}{J} \tag{3.12}$$

Using Eqns. (3.10) and (3.9), we have in this case (cf. Eqn. (2.3) in Chap. 2),

$$j_C(a) \equiv \left(\frac{\dot{J}}{J}\right)_C = -\frac{1}{2}\left(\frac{\dot{E}}{E}\right)_C = \alpha_C a\gamma, \quad \alpha_C \equiv \frac{A_C}{2} = 9G\frac{m_f^3}{m_c m_X} \tag{3.13}$$

The total rate of loss of orbital angular momentum due to the above three processes is:

$$j_{TOT}(a) \equiv \left(\frac{\dot{J}}{J}\right)_{TOT} = j_{GW}(a) + j_{MB}(a) + j_C(a) \tag{3.14}$$

3.2.3.2 Hardening in X-ray binary (XB) phase

As mass transfer starts upon Roche lobe contact, its effect on the angular momentum balance in the XB must be taken into account, in the manner described

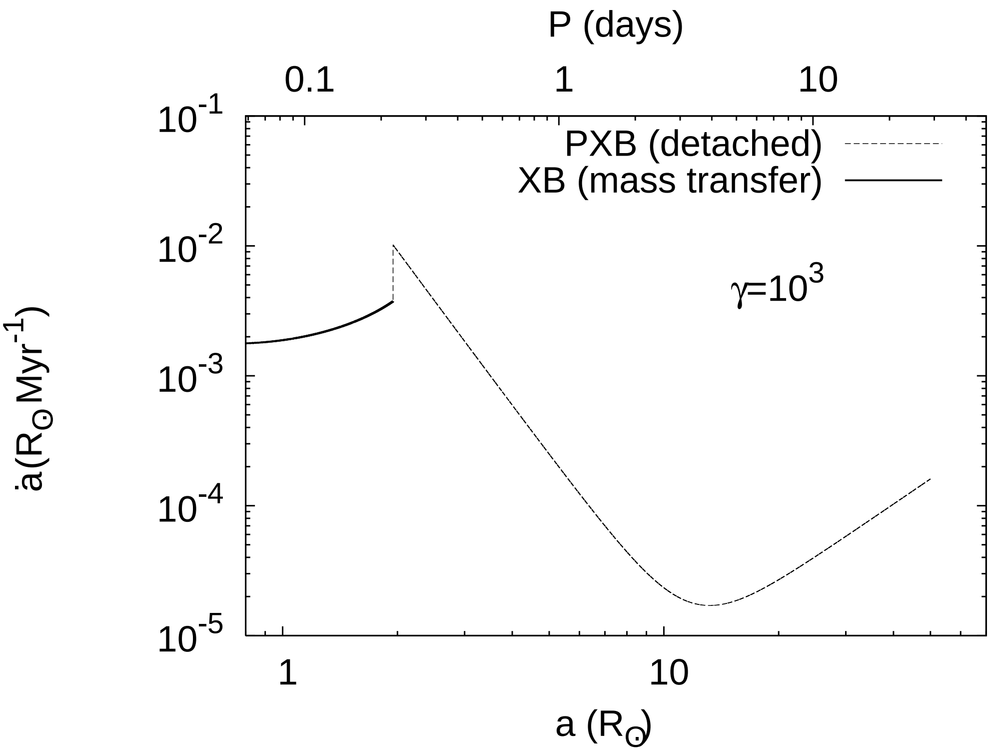

Figure 3.2: *Hardening rate $\dot{a}$ of a compact binary as a function of the orbital radius a, in a globular cluster with a Verbunt parameter of $\gamma = 10^3$. Collisional hardening dominates roughly at $a > 14R_\odot$, and gravitational radiation plus magnetic braking roughly in the range $2R_\odot < a < 14R_\odot$. These two regions, shown as dashed lines, are populated by pre-X-ray binaries (PXBs), which are detached. At $a \approx 2R_\odot$, Roche lobe contact occurs and mass transfer begins, so that the region shortward of this radius, shown as the solid line, is populated by X-ray binaries (XBs). This region is shown upto the orbital radius a_{pm} which corresponds to the period minimum of ≈ 80 min (see text). Along abscissa, both orbital radius a and orbital period P scales are shown for convenience.*

below. Note first that, for the radius of the Roche-lobe R_L of the companion, we can use either the Paczyński (1971) approximation:

$$R_L/a = 0.462 \left(\frac{m_c}{M}\right)^{1/3}, \tag{3.15}$$

which holds for $0 < m_c/m_X < 0.8$, or the Eggleton (1983) approximation:

$$R_L/a = \frac{0.49}{0.6 + q^{2/3}\ln(1 + q^{-1/3})}, \qquad q \equiv m_X/m_c, \tag{3.16}$$

which holds for the entire range of values of the mass ratio q. Both approximations have been widely used in the literature, and they give essentially identical results for the mass ratios of interest here. We have used the Paczyński approximation here for simplicity of calculation.

At the Roche-lobe contact point, R_L must be equal to the companion radius, the value of which is $R_c \approx 0.6 R_\odot$ for a companion of $m_c = 0.6 M_\odot$ (see above), according to the mass-radius relation for low mass stars. For $m_X = 1.4 M_\odot$, this translates into an orbital radius of $a_L = 1.94 R_\odot$ at Roche lobe contact, using Eqn. (3.15). After this, the companion continues to remain in Roche-lobe contact as the binary shrinks further, and continues to transfer mass (van den Heuvel, 1991, 1992). In other words, we have

$$R_c = 0.46 a \left(\frac{m_c}{M}\right)^{1/3}, \qquad (a < a_L) \tag{3.17}$$

throughout the XB phase. During this phase, the binary is already narrow enough that the collisional hardening rate is quite negligible compared to those due to gravitational radiation and magnetic braking.

Since no significant mass loss is expected from the XB in this phase, we have

$$\dot{m}_c = -\dot{m}_X. \tag{3.18}$$

Combining Eqns. (3.11), (3.17) and (3.18) with a mass-radius relation for the companion of the form

$$R_c \propto m_c^s, \tag{3.19}$$

we find:

$$\dot{a} = \frac{j_{tot}(a) a \left(s - \frac{1}{3}\right)}{\left[\frac{s}{2} + \frac{5}{6} - \left(\frac{m_c}{M - m_c}\right)\right]} \tag{3.20}$$

Here, $j_{tot}(a) = j_{GW}(a) + j_{MB}(a)$ is the effective total rate of loss of angular momentum, since the collisional-hardening contributions are negligible, as explained above.

For the low-mass main sequence companions that we consider here, $s \approx 1$. However, when the mass of the companion becomes less than about $0.03 M_\odot$, it becomes degenerate, so that $s \approx -1/3$. This results in a widening of the orbit ($\dot{a} > 0$) from this point onwards, which we do not follow here, since our study is not aimed at such systems, as explained in Sec. 3.4.1. This change-over point is, of course, that corresponding to the well-known period minimum of ≈ 80 minutes in the orbital evolution of CVs and LMXBs(van den Heuvel, 1992). Henceforth, we denote the value of a at the period minimum by a_{pm}, and we terminate the distributions of $\dot{a}$ and $n(a,t)$ in a at a minimum value of a_{pm} in the figures shown in this work. Thus, in Fig. 3.2, we display the hardening rate $\dot{a}$ against a, beginning from a wide PXB phase, going into Roche lobe contact, and continuing through the mass-transfer XB phase upto the above period minimum. Note that $\dot{a}$ has a very weak dependence on a during the XB phase, which may have interesting consequences, as we shall see later.

3.2.4 Binary formation processes

Compact binaries with degenerate primaries and low-mass companions are formed in globular cluster (henceforth GC) cores primarily by means of two dynamical processes, namely, (i) tidal capture (tc) of a degenerate, compact star (white dwarf or neutron star) by an ordinary star, and (ii) an exchange encounter (ex1) between such a compact star and a binary of two ordinary stars, wherein the compact star replaces one of the binary members (see Sec. 1.5). Accordingly, the total rate of formation of compact binaries per unit binary radius, $R(a)$, consists of the above tc rate $r_{tc}(a)$ and ex1 rate $r_{ex1}(a)$:

$$R(a) = r_{tc}(a) + r_{ex1}(a) \tag{3.21}$$

where a is the orbital radius of the compact binary so formed. We now consider the rates of formation by tidal capture and by exchange.

3.2.4.1 Tidal capture

In a close encounter between a compact star of mass m_X and an ordinary star of mass m_c with a distance of closest approach r_p, tidal capture can occur if their relative speed v is less than an appropriate critical speed $v_0(r_p)$, which we discuss below. The cross section for encounters within this distance r_p is given by the well-known form (Spitzer, 1987):

$$\sigma_g = \left(\pi r_p^2 + \frac{2\pi G M r_p}{v^2}\right) \tag{3.22}$$

which gives the *differential* cross section for tidal capture around r_p as:

$$\frac{d\sigma_{tc}}{dr_p} = \begin{cases} \left(2\pi r_p + \frac{2\pi GM}{v^2}\right) dr_p & v < v_0(r_p) \\ 0 & v \geq v_0(r_p) \end{cases} \tag{3.23}$$

The first terms in the right-hand sides of Eqs. (3.22) and (3.23) are the obvious geometrical cross sections and the second terms are due to gravitational focusing (also see below). It is clear that the latter terms dominate when r_p is small, as is the case for the range of values of r_p relevant to the problem we study here. We shall return later to the actual numerical values of r_p of interest to us in this study.

After being tidally formed, the binary is believed to circularize very rapidly to an orbital radius $a = 2r_p$, assuming conservation of angular momentum (Spitzer, 1987). Accordingly, the differential cross-section in terms of a is given by:

$$\frac{d\sigma_{tc}}{da} = \begin{cases} \left(\frac{\pi}{2} a + \frac{\pi GM}{v^2}\right) & v < v_0(a) \\ 0 & v \geq v_0(a) \end{cases} \tag{3.24}$$

Here, $v_0(a)$ is the critical velocity in terms of a, obtained by setting $r_p = a/2$ in Eq. (3.25) below.

In a sense, the whole cross-section as expressed above may be regarded as "geometrical", if we look upon pure considerations of Newtonian gravity as being geometrical. Details of the essential astrophysics enter only when we calculate the critical speed $v_0(r_p)$, and an inversion of this relation (together with other plausible requirements; see below) then readily gives us the range of r_p over which tidal capture is physically admissible. This is an interesting topic, with literature going back to the mid-1970s and earlier, and we summarize in this section those essential points which we need in this work. The basic physics of tidal capture is of course that, during a close encounter, the degenerate compact star excites non-radial oscillation modes in the normal companion star through tidal forcing (in an encounter between two normal stars, each excites oscillations in the other): the energy required to excite these oscillations comes from the kinetic energy of relative motion of the two stars, so that if enough energy is extracted from this source by exciting these modes, the stars become bound after the encounter. This energy condition readily translates into one between v_0 and r_p, giving an upper limit v_0 on velocity for a specified r_p as above, or, as expressed more commonly, an upper limit on the distance of closest approach r_p for a specified velocity (actually, often a *distribution* of velocities, *e.g.*, a Maxwellian, with a specified parameter in practical situations, as we shall see below).

The above relation between v_0 and r_p has been calculated in the literature at various levels of detail. The pioneering estimates given in Fabian et.al. (1975) or earlier works basically employ the impulse approximation for calculating the gain in the internal energy of the tidally-perturbed star, wherein the changes in the positions of the two stars during the tidal interaction are neglected. A clear account of the procedure is given in Spitzer (1987), where the final result is evaluated for two normal stars of equal masses. Upon generalizing this procedure appropriately to the problem we study, where we have (a) unequal stellar masses m_X and m_c, and (b) the fact that only the normal star of mass m_c undergoes tidally-induced oscillations, we obtain the following relation between v_0 and r_p:

$$v_0(r_p) = \left(\frac{4}{3}Gm_X R_m^2\right)^{\frac{1}{2}} r_p^{-\frac{3}{2}} \tag{3.25}$$

Here, R_m is the root-mean-square radius of the companion star, *i.e.*, its radius of gyration which is given in the polytropic approximation as $R_m^2/R_c^2 \approx 0.114$ in terms of the companion's radius R_c (Spitzer, 1987).

To obtain the overall rate of tidal capture in the GC core of volume $4\pi r_c^3/3$ per unit interval in a around a, we first consider this rate around a particular value v of the above relative velocity of encounter, *i.e.*, $r_{tc}(a,v) = (4\pi/3)r_c^3 k_X \rho^2 (d\sigma_{tc}/da)v$, in terms of the above differential cross-section, remembering that the rate of encounter scales with the product of the densities $k_X\rho$ and ρ of compact stars and normal stars respectively. We then average this rate over the distribution of v, obtaining the form:

$$r_{tc}(a) = \frac{4}{3}\pi r_c^3 k_X \rho^2 \langle \sigma_{tc}(a,v)v \rangle, \tag{3.26}$$

where the angular brackets indicate an average over the v-distribution.

For the actual averaging, we adopt in this work a Maxwellian distribution $f_{mx}(v)$, as has been widely done in the literature. A normalized Maxwellian is

$$f_{mx}(v) = Av^2 \exp(-\beta v^2), \quad \beta \equiv \frac{3}{2v_c^2}, \quad A \equiv \frac{4}{\sqrt{\pi}}\beta^{\frac{3}{2}}, \tag{3.27}$$

where v_c is the velocity dispersion introduced earlier, for which we adopt the canonical value 10 km s^{-1} in the numerical calculations (also see below).

With the aid of Eqns. (3.24), (3.25) and (3.27), we perform the averaging and obtain:

$$\begin{aligned} &\langle\sigma_{tc}(a,v)v\rangle = I_{geo} + I_{grav}, \\ &\text{where,} \\ &I_{geo} \equiv \sqrt{\tfrac{\pi}{\beta}}a\left[1 - \exp(-\beta v_0^2(a))(\beta v_0^2(a)+1)\right] \\ &I_{grav} \equiv 2\sqrt{\pi}GM\beta^{\frac{1}{2}}\left[1 - \exp(-\beta v_0^2(a))\right] \end{aligned} \tag{3.28}$$

The terms I_{geo} and I_{grav} above arise due to what we described respectively as the geometrical term and the gravitational focusing term in the discussion below Eq. (3.23). Eqns. (3.26) and (3.28) together give the total tidal capture rate as:

$$r_{tc}(a) = \sqrt{\frac{32\pi^3}{3}}k_X\Gamma GM\left[1 - \exp(-\beta v_0^2(a))\right], \tag{3.29}$$

where Γ is the Verbunt parameter describing the total two-body encounter rate in the cluster core, as introduced earlier, and we have ignored I_{geo} compared to I_{grav}, which is an excellent approximation for the range of r_p or a relevant here.

We show in Fig. 3.3 r_{tc} given by Eq. (3.29) as a function of a: this tidal capture cross-section is nearly constant for $a < 5R_\odot$, and decreases rapidly at larger a. At this point, we need to invoke additional physical arguments in order to estimate the range of values of a or r_p over which tidal capture is actually possible, and use the above cross-section only over this range for our calculations. The lower bound to the above range comes from the requirement that the two stars must form a binary and not merge into each other, and the upper bound comes from the requirement introduced earlier that enough energy of relative motion between the two stars must be absorbed by the tidally-excited oscillation modes that the stars become bound. Consider the lower bound on r_p first. Clearly, a minimum value of this bound must be the sum of the stellar radii, which in our case leads to the bound $r_p \geq R_c \approx 0.6R_\odot$. A more conservative bound comes from the requirement that the companion must underfill its Roche lobe after the binary has formed, *i.e.*, $R_c \leq R_L$, which, with the aid of Eq. (3.15) and $a = 2r_p$, yields $r_p \geq 1.6R_c \approx R_\odot$ for the masses $m_X = 1.4M_\odot$ and $m_c = 0.6M_\odot$ we have here. The idea behind the latter requirement is apparently that if the companion overfills its Roche lobe at this point, the ensuing mass transfer is likely to lead to a merger.

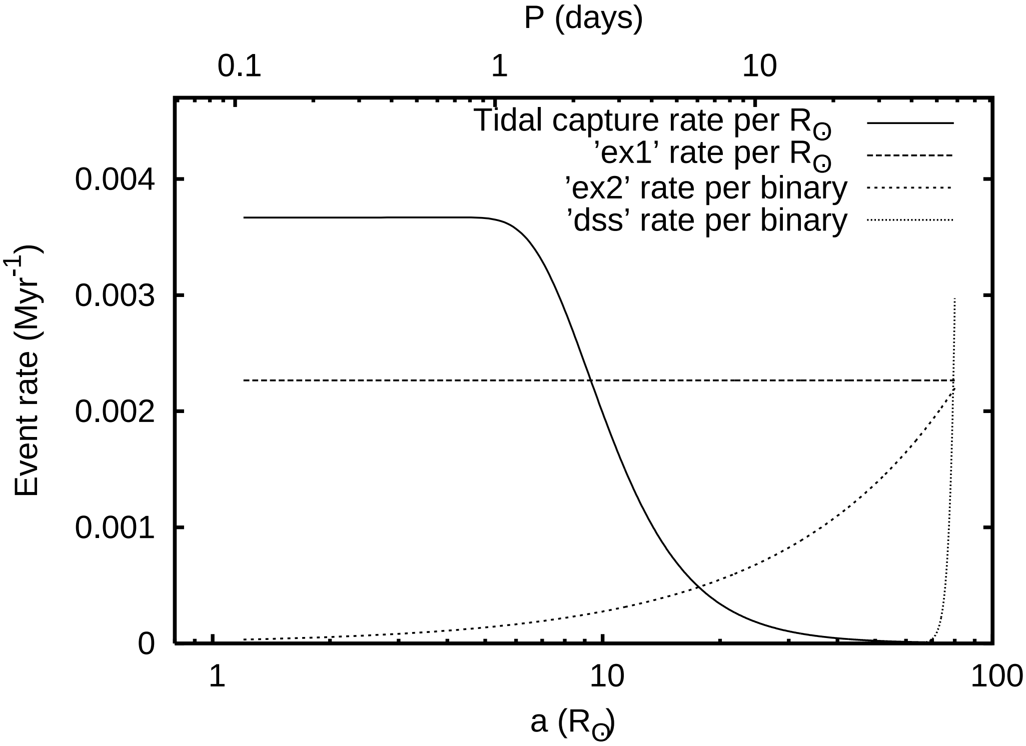

Figure 3.3: *Tidal capture (tc) rate, the exchange rates 'ex1' and 'ex2', and the dissociation (dss) rate, as described in text. Note that, compared to the tc rate, the ex1 rate has been magnified by a factor of 50, the ex2 rate rate by a of factor 60, and the dss rate by a factor of* 10^9*, so that all rates are clearly visible. Along abscissa, both orbital radius a and orbital period P scales are shown for convenience. Curves are terminated at a radius* $a_{min} = 1.2R_\odot$ *(see text).*

This seems reasonable at first, but detailed N-body simulations of recent years have suggested that this requirement may, in fact, be too restrictive. In the simulations of Portegies Zwart et.al. (1997b), which included stellar evolutionary effects according to the scheme of these authors, systems which violated the latter requirement but satisfied the former one were allowed to evolve, with the result that details of the evolution determined which systems merged and which did not. In fact, these authors found a lower limit on $a = 2r_p$ of approximately $a \geq R_\odot$ for tidal capture with an average companion mass very similar to ours, which is to be compared with the limits $a \geq 1.2R_\odot$ from the first requirement above, and $a \geq 2R_\odot$ from the latter. In view of this, we have adopted the lower bound of

$a^{min} \approx 1.2R_\odot$ for our calculations here, as shown in Fig. 3.3.

Consider now the upper bound on r_p. We have already given the relation between r_p and v_0 by Eq. (3.25) in the impulse approximation. Remembering that $v_0^2 = 1/\beta = 2v_c^2/3$ for a Maxwellian, the above relation yields, for a canonical value $v_c = 10$ km s^{-1} as given above, an upper limit of $r_p \leq 10.2R_c$ for a polytropic index $n = 3$ and one of $r_p \leq 14.1R_c$ for $n = 1.5$. Note that these bounds of r_p/R_c are larger than those given for two stars of equal mass (roughly 8 for $n = 3$ and 11 for $n = 1.5$) in Table 6.2 of Spitzer (1987) by a factor of $(m_X/m_c)^{1/3}$ since r_p^{max}/R_c scales with the mass-ratio in this manner in the impulse approximation, as can be seen readily from Eq. (3.25), remembering that $R_c \propto m_c$ for the companions we consider here. That r_p^{max}/R_c should increase with increasing (m_X/m_c) is qualitatively quite obvious, since, other things being equal, a higher value of the mass ratio excites tidally-forced oscillations of larger amplitude. We return below to the question of the exact scaling with this mass ratio.

As has been realized long ago, the impulse approximation is of limited validity, working best when the frequency of perturbation (*i.e.*, tidal forcing) is not very different from those of the stellar oscillation modes that are excited by this perturbation (Fabian et.al., 1975; Spitzer, 1987). Since this is not the case for the values of r_p^{max}/R_c estimated above, we need more accurate results, which come from detailed computations of the total energy dissipated by the above excited modes. Such numerical computations were pioneered by Press & Teukolsky (1977), and detailed results were established for various situations by several groups of authors in the mid-1980s, including Lee & Ostriker (1986) and McMillan et.al. (1987), which have been extensively used since. These results have shown that the exact upper bounds on r_p are considerably smaller than those given by the impulse approximation, as may have been expected, since the forcing frequency falls far below those of the oscillation modes at such large separations as are given by this approximation, and the efficiency of exciting these modes drops rapidly. Some exact results are given in Table 6.2 of Spitzer (1987) from the above references, but only for the equal-mass case, where the above upper bound r_p^{max}/R_c is 2.4 for $n = 3$ and 3.4 for $n = 1.5$.

For our purposes here, we need to obtain the above upper bounds for our mass ratio $m_X/m_c = 1.4/0.6 \approx 2.3$, which we do by doing a power-law fit of the form $r_p^{max} \propto (m_X/m_c)^\alpha$ to the results given for various values of the degenerate/normal star mass-ratios in Table 3 of Lee & Ostriker (1986). This yields $\alpha \approx 0.62$ (note that the quantity listed in Table 3 of Lee & Ostriker (1986) is the impact parameter R_0 defined by these authors; r_p^{max} scales as R_0^2, as shown in their paper). The interesting point about this scaling is that it is stronger than that given above by the impulse approximation, which corresponds to $\alpha = 1/3$. Clearly, then, the impulse approximation fails to extract the entire scaling with m_X/m_c. The reason for this appears to be related to nonlinear effects in exciting and dissipating tidally-induced oscillations, but needs to be investigated further[1]. With the above value of α, the upper bound r_p^{max}/R_c for our mass-ratio here is 4.1 for $n = 3$ and 5.7 for $n = 1.5$. As the latter value of the polytropic index is believed to give a better representation of a low-mass main-sequence companion of the kind we are considering here, we adopt $r_p^{max}/R_c \approx 5.7$ here. With $a = 2r_p$ and the value of R_c given earlier, this translates into an upper bound on a as $a^{max} \approx 6.8R_\odot$, which we can adopt for these calculations.

Thus we find a range of values $1.2R_\odot \leq a \leq 6.8R_\odot$ over which tidal capture is expected to be effective in the problem we study here. Consider now how the tidal-capture cross-section is expected to fall off at the bounds of this range. At the upper bound, the cut-off is not sharp, of course, as there is a distribution of velocities. In other words, the upper bound a^{max} as given above corresponds to a suitable average (actually, root-mean-square in this case) velocity, so that at any $a > a^{max}$, there will be some stars in the distribution whose velocities are sufficiently below this average that tidal capture will be possible for them. Of course, their number will decrease as a increases, producing a "tail" in the tidal capture cross-section whose shape is determined by that of the velocity distribution. We have used a Maxwellian distribution here, which gives the tail seen in Fig. 3.3, which falls off rapidly beyond $a^{max} = 6.8R_\odot$. We shall use this fall-off profile in our calculations: other profiles will not make a large difference.

[1]Note that this discrepancy is even stronger for the case where both stars are normal, main-sequence ones, since $\alpha \approx 1.6$ in that case, as can be shown readily from Table 2 in the above Lee-Ostriker reference. An obvious line of reasoning for this would be that larger nonlinear effects may be expected when two normal stars force tidal oscillations in each other, but we shall not speculate on this any further here.

At the lower bound, in view of the discussion given earlier, we expect the cross-section to actually fall off gradually from about $a = 2R_\odot$ to $a = a^{min} = 1.2R_\odot$, rather than being cut off sharply at a^{min}, but we shall ignore this complication here.

We close this discussion of tidal capture with some observations on the many investigations, conclusions, and points of view that the subject has now seen for more than three decades. From the pioneering suggestion and an essentially dimensional estimate of Fabian et.al. (1975), detailed calculations of the 1980s and '90s have reached interesting, and sometimes contradictory, conclusions. For example, concerns that energy dissipation by tidally-induced modes may lead to a large distention of the companion and so to a merger have been confronted with results from detailed computations of the nonlinear damping of the primary modes by coupling to other, high-degree modes, which suggested that the damping took place far more rapidly than thought before, and the energy dissipated was too small to have a significant effect on the companion's structure. We here have a adopted a somewhat moderate view that tidal capture is plausible, but efficient over only a restricted range of r_p or a. This view is supported by (a) recent observational demonstration that the number of X-ray sources in Galactic globular clusters scale with their Verbunt parameter Γ, *i.e.*, the two-body encounter rate (Pooley et al., 2003), as described earlier, and (b) recent N-body simulations of Portegies Zwart et.al. (1997b) showing tidal capture over a considerable range of a, admittedly under the algorithms adopted by these authors. Consider, finally, our suggested range of radii for efficient tidal capture, $a^{max}/a^{min} \approx 5.7$, as given above, in the context of other suggested ranges. Values in the range $a^{max}/a^{min} \approx 2 - 3$ have been thought plausible by Podsiadlowski et.al. (2002), while Portegies Zwart et.al. (1997b) have demonstrated tidal capture over a range $a^{max}/a^{min} \approx 10$. We here advocate a range $a^{max}/a^{min} \approx 4 - 6$ (depending on n), which is between the two, and still quite modest.

3.2.4.2 Formation by exchange

Exchange encounters between binaries and single stars with arbitrary mass ratios has been extensively studied by Heggie, Hut & McMillan (1996). They performed

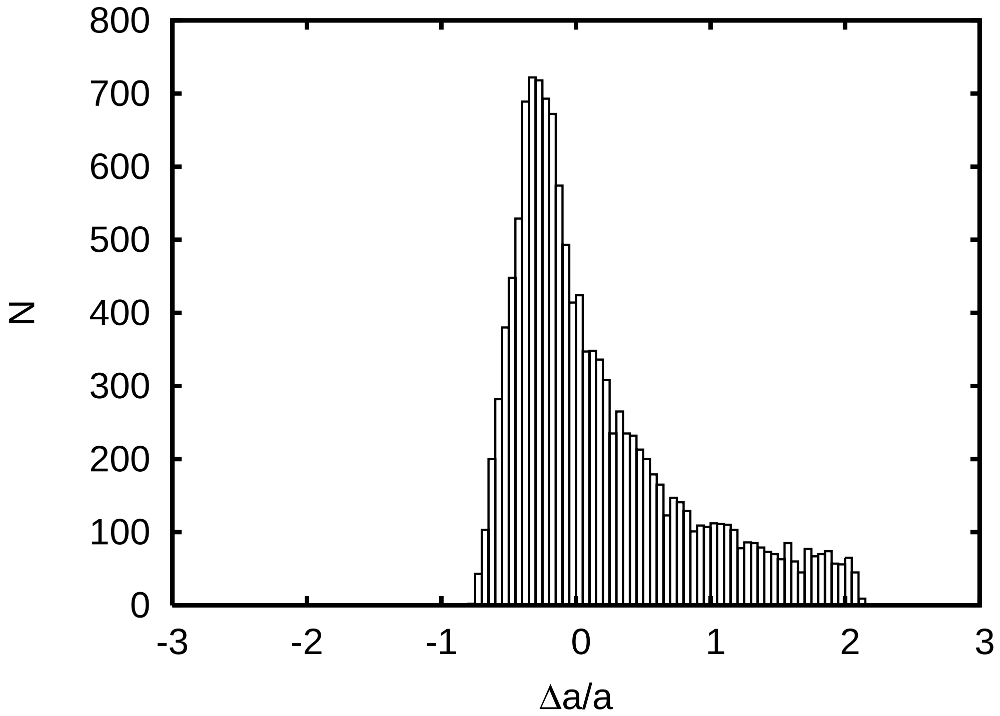

Figure 3.4: *Distribution of the fractional change in binary radius $\Delta a/a$ for $\sim$ 30000 scattering experiments with $v/v_{crit} = 0.5$ (see text) and random impact parameters. The distribution is highly asymmetric, with a peak at $\Delta a/a \approx -0.25$, and a long tail in the $\Delta a > 0$ direction.*

detailed numerical scattering experiments, using the automatic scattering tools of the STARLAB package. From the resulting exchange cross sections, they obtained a semi-analytic fit of the form:

$$\sigma_{ex}(R) = \frac{\pi G M_{tot} R}{2v^2}\overline{\sigma}(m_1, m_2, m_3). \tag{3.30}$$

Here, R is the orbital radius of the initial binary, m_1 is the mass of the escaping star, m_2 is the companion mass, m_3 is the mass of the incoming star, and $M_{tot} \equiv m_1+m_2+m_3$. $\overline{\sigma}(m_1, m_2, m_3)$ is the dimensionless cross section which is a function of these masses only and is given by the following expression (see Eqn. (17) of

Heggie, Hut & McMillan (1996)):

$$\overline{\sigma}(m1, m2, m3) = \left(\frac{M_{23}}{M_{tot}}\right)^{1/6} \left(\frac{m_3}{M_{13}}\right)^{7/2} \left(\frac{M_{tot}}{M_{12}}\right)^{1/3} \left(\frac{M_{13}}{M_{tot}}\right) \times \exp\left(\sum_{m,n;m+n=0}^{m+n=N} a_{mn}\mu_1^m \mu_2^n\right) \quad (3.31)$$

where, $M_{12} \equiv m_1 + m_2$ etc., $\mu_1 \equiv m_1/M_{12}$ and $\mu_2 \equiv m_3/M_{tot}$. The above expression is essentially a connecting formula between the analytically estimated cross-sections corresponding to extreme mass ratios (see Heggie, Hut & McMillan (1996) for details). The coefficients a_{mn} are determined by fitting Eqn. (3.31) with exchange cross-sections obtained from the numerical scattering experiments. We use Eqn. (3.30) to obtain the cross-section $\sigma_{ex1}(a)$ for the exchange process 'ex1' described above, but one essential point needs to be clarified first.

The radius a of the compact binary formed by exchange is not the same as the radius a' of the original binary undergoing exchange. Therefore, a relation between a' and a is required, since in Eqn. (3.30) R represents the radius a' of the initial binary, *not* the radius a of the compact binary formed by exchange. According to the binary-hardening rule of Heggie (Heggie, 1975), the final compact binary must, on an average, be harder, *i.e.*, have a larger binding energy. We performed illustrative scattering experiments with circular binaries and incoming stars with mass ratios of interest to us in this study, using the scattering tools of STARLAB. The resulting distribution of the change in orbital radius $\Delta a/a$ is shown in Fig. 3.4, and is seen to be highly asymmetric.

The long tail towards $\Delta a > 0$ implies that the binary radius *increases* in many scatterings. This does not of course contradict the above Heggie rule, since the increase of mass due to exchange (the mass of the incoming compact star, $1.4M_\odot$, is a factor ≈ 2.3 times the mass of the outgoing low-mass star, $0.6M_\odot$) increases the binding energy by itself by the above factor. From these experiments, we see that the peak of the distribution corresponds to a shrinkage of the binary by about 25 per cent. On the other hand, the *average* change in binary radius, calculated from the above distribution, is much closer to zero due to the above long tail of the distribution on the $\Delta a > 0$ side, so that we can take $a \approx a'$ for our purposes here without much error.

The total Maxwellian-averaged rate of formation of compact binary by this type of exchange (ex1) in the GC core is then:

$$r_{ex1}(a) = \frac{4}{3}\pi r_c^3 k_X \rho^2 f_b(a)\langle\sigma_{ex1}(a)v\rangle = \sqrt{\frac{8\pi^3}{3}} k_X f_b(a)\Gamma G M_{tot} a\overline{\sigma}(m_c, m_X) \quad (3.32)$$

Here, $f_b(a)$ is the distribution function of the orbital radii of the primordial stellar binaries in the cluster core. For primordial binaries, we can take the widely-used distribution $f_b(a) \propto 1/a$ (*i.e.*, a uniform distribution in $\ln a$) (Kraicheva et.al., 1978), with a lower bound at $a \approx 1.2R_\odot$, corresponding to the smallest possible radius for a binary of two $0.6M_\odot$ main-sequence stars. The ex1 rate is shown in Fig. 3.3.

3.2.5 Binary destruction processes

A compact binary can be destroyed by two major processes. First, an encounter with a star which has a relative speed higher than an appropriate critical speed (Hut & Bahcall, 1983) can lead to its dissociation (dss). Second, in an exchange encounter (ex2) of this binary with a compact star, the latter can replace the low-mass companion in the binary, forming a double compact-star binary consisting of two neutron stars, two white dwarfs, or a neutron star and a white dwarf, all with masses $m_X \approx 1.4M_\odot$. This, in effect, destroys the binary as an X-ray source (as accretion is not possible in such a system), and so takes it out of our reckoning in this study. This is so because such a system is not an X-ray source, and it is essentially impossible for one of the compact stars in such a system to be exchanged with an ordinary star in a subsequent exchange encounter, since $m_f = 0.6M_\odot$ is much lighter than $m_X = 1.4M_\odot$. The total destruction rate D(a) *per binary* is thus the sum of the above dissociation and exchange rates:

$$D(a) = r_{ex2}(a) + r_{dss}(a) \quad (3.33)$$

We now discuss the rates of these two processes.

3.2.5.1 Dissociation

To estimate the dissociation rate of compact binaries, we use the results of scattering experiments of Hut & Bahcall (1983). The Maxwellian-averaged dissociation rate (dss) *per compact binary* is then given by

$$r_{dss}(a) = k_X \rho \langle \sigma_{dss}(a) v \rangle \tag{3.34}$$

From Hut & Bahcall (1983), we adopt

$$\langle \sigma_{dss}(a) v \rangle = \frac{32\pi}{27} \sqrt{\frac{6}{\pi}} v_c a^2 \exp\left(-\frac{3}{2}\frac{v_{crit}^2}{v_c^2}\right). \tag{3.35}$$

a relation which was obtained by these authors by fitting the results of their scattering experiments with analytical models. Here, v_{crit} is the threshold relative velocity for ionization (see Sec. 3.2.5), given by:

$$v_{crit}^2 = \frac{Gm_X(2m_c + m_X)}{m_c + m_X}\frac{1}{a}. \tag{3.36}$$

As these authors pointed out, Eqn. (3.35) is an asymptotic form, which works well only for significantly hard binaries, *i.e.*, those with $v_c << v_{crit}$. This condition is of course satisfied for the compact binaries that we are interested in here.

We show in Fig. 3.3 the above dissociation rate, whose essential variation with a is seen by combining Eqs. (3.35) and (3.36), which yields the form $r_{dss}(a) \propto a^2 \exp(-a_c/a)$, where a_c is a constant. Thus, the dissociation rate is quite negligible for $a \ll a_c$, reflecting the fact that it is essentially impossible to dissociate very hard binaries. As a increases, the rate rises extremely sharply at first (the initial rise is determined by the exponential), and eventually scales as a^2 for $a \gg a_c$.

3.2.5.2 Destruction by exchange

By arguments similar to those given in Sec. 3.2.4.2, we arrive at a Maxwellian-averaged rate of this type of exchange (ex2) *per compact binary* which is:

$$r_{ex2}(a) = k_X \rho \langle \sigma_{ex2}(a) v \rangle = \sqrt{\frac{3\pi}{2}} k_X \gamma G M_{tot} a \overline{\sigma}(m_c, m_X), \tag{3.37}$$

and which is also shown in Fig. 3.3. This rate scales with a simply as $r_{ex2}(a) \propto a$. Note the different magnifications used for different curves in Fig. 3.3 in order to make all of them clearly visible. Of the two destruction processes, r_{ex2} dominates completely at all orbital radii of interest in our study (reflecting the fact that dynamically-formed binaries in GC cores are so hard that they cannot be dissociated or "ionized" by further encounters in that GC core), but the fast-rising r_{dss} eventually overtakes it at $a \approx 1000 R_\odot$, corresponding to very soft binaries.

3.2.6 The numerical method

Equation (3.5) for the evolution of compact binary populations is a partial differential equation (PDE) of hyperbolic type, with similarities to wave equations, as pointed out earlier. We solved this equation using a Lax-Wendorff scheme (Press et.al., 1992). This involves dividing the range of a and t in a discrete mesh (a_j, t_N) of constant space intervals (Δa) and time intervals (Δt). The PDE is then discretised into a set of linear difference equations over this mesh, which is solved numerically.

We denote by n_j^N the value of n at the Nth time step and the jth point in a. Discretisation of Eqn. (3.5) according to the Lax-Wendorff scheme is a two-step process:

$$\begin{aligned}
&\text{Half step :}\\
&n_{j+1/2}^{N+1/2} = \tfrac{1}{2}\left(n_{j+1}^N + n_j^N\right) + \left[R(a_{j+1/2}) - D(a_{j+1/2})\left(\tfrac{n_{j+1}^N + n_j^N}{2}\right)\right]\tfrac{\Delta t}{2}\\
&-\tfrac{f(a_{j+1/2})\Delta t}{2\Delta a}(n_{j+1}^N - n_j^N)\\
&\text{Full step :}\\
&n_j^{N+1} = n_j^N + \left(R(a_j) - D(a_j)n_j^N\right)\Delta t\\
&-\tfrac{f(a_j)\Delta t}{\Delta a}\left(n_{j+1/2}^{N+1/2} - n_{j-1/2}^{N+1/2}\right)
\end{aligned} \tag{3.38}$$

For a chosen mesh-interval Δa, Eqn. (3.38) will be numerically stable only if the time-step Δt is chosen to be small enough that it obeys the *Courant condition* (Press et.al., 1992) throughout the mesh:

$$\Delta t = \eta \frac{\Delta a}{f_{max}}, \qquad \eta < 1 \tag{3.39}$$

where f_{max} is the maximum value of $f(a)$ within the a-range of the mesh. The above condition can be rigorously proved by using the *von Neumann Stability Analysis* (Press et.al., 1992; Antia, 2002). It can also be looked upon physically as follows.

One of the primary source of instability at a particular point in a numerical solution scheme of a PDE is the lack of consideration of the behavior of its surrounding points which is crucial for the overall behavior of the solution (Antia, 2002). The effect of the surrounding points is usually taken into account by using centered values (Press et.al., 1992; Antia, 2002), which, in effect introduces a dissipative term (also called *numerical dissipation*) that suppresses the growth of spurious solutions that would otherwise dominate the solution (Press et.al., 1992; Antia, 2002). For a hyperbolic PDE, which has properties like that of a wave equation, the Courant condition essentially reflects the fact that for a given stepsize in the spatial direction, the time-step should be smaller than the time taken for the wave to travel the spatial stepsize. Otherwise, the chosen stepzsize would contain less information and render the solution scheme unstable.

We chose Lax-Wendorff scheme among the various existing schemes for solving hyperbolic PDEs primarily because it appears to be the only explicit method that does not have any significant numerical dissipation (Press et.al. 1992, and references therein) and is at the same time numerically stable, provided that the time step is chosen according to the Courant condition. This property can again be rigorously demonstrated using the von Neumann analysis (see, *e.g.*, Press et.al. (1992)) and can also be qualitatively addressed as follows. The key point is the use of two steps (see Eqn. (3.38)). In a differencing scheme of a hyperbolic PDE, numerical dissipation occurs because of the use of centered values, which is important to dissipate away the growth of spurious solutions. In the Lax-Wendorff scheme, as in Eqn. (3.38), the centering is done in the provisional half-step, which avoids numerical instability subject to Courant condition. The final values are however obtained only from the full step, which is not centered, so that the numerical dissipation does not show up significantly in the output. To have a very small numerical dissipation is important, since numerical dissipation can significantly affect the computed evolution of $n(a, t)$ and the X-ray binary population, as we observed while trying other methods, *e.g.*, the so-called staggered-leapfrog method. Other instabilities, *e.g.*, the mesh-drifting instability (Press et.al., 1992), also appeared to be insignificant in the method we chose.

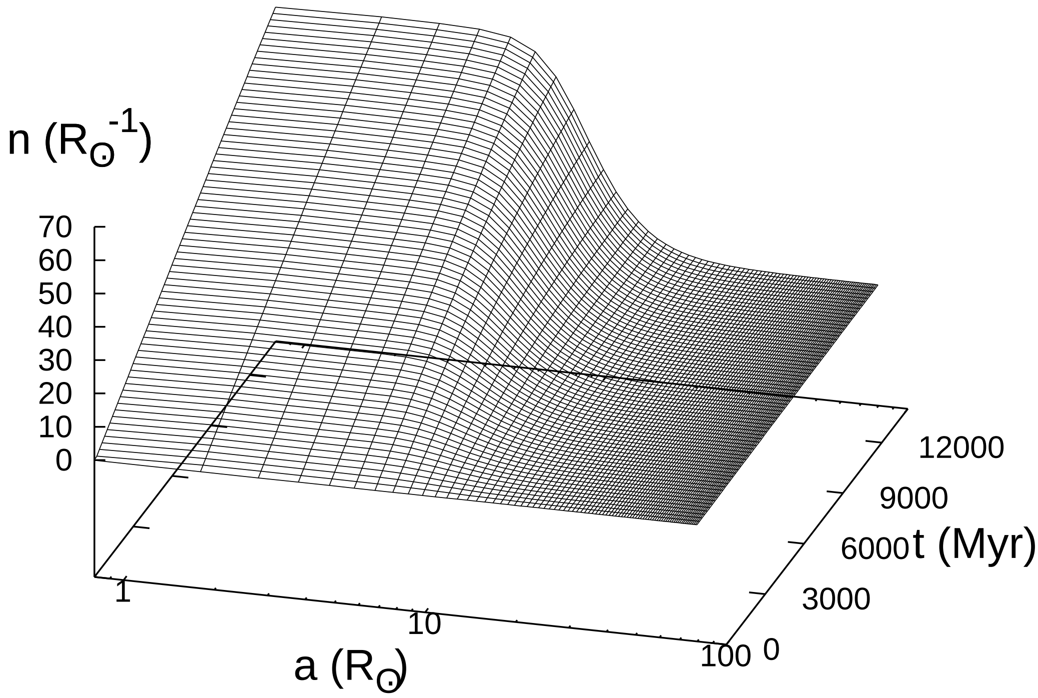

Figure 3.5: *Three-dimensional surface $n(a,t)$ describing the model evolution of population-distribution function of compact binaries for GC parameters* $\rho = 6.4 \times 10^4\ M_\odot\ \mathrm{pc}^{-3}$, $r_c = 0.5$ pc, $v_c = 11.6$ km sec^{-1} *(roughly corresponding to* 47 Tuc*). The lines on the surface represent only samples from the set of computed points, the computation having been done over a much finer grid.*

3.3 Results

3.3.1 Evolution of compact-binary distribution

A typical result from our computed evolution of the compact-binary distribution function $n(a,t)$ is shown in Fig. 3.5, wherein the surface $n(a,t)$ is explicitly displayed in three dimensions. The GC parameters chosen for this run were $\rho = 6.4 \times 10^4\ M_\odot\ \mathrm{pc}^{-3}$, $r_c = 0.5$ pc and $v_c = 11.6$ km sec^{-1}, similar to those of the well-known Galactic cluster 47 Tuc. The distribution function is seen to evolve as a smooth surface, with the compact binary population growing predominantly at shorter radii ($a < 10R_\odot$, say). We start with a small number of binaries at $t = 0$ following various distributions, and find that the distribution at large times $\sim$ Gyr is quite independent of these initial conditions, being determined entirely by the dynamical processes of formation and destruction, and by the various hardening processes detailed earlier. Note that, since the point of Roche lobe contact corresponds to $a \approx 2R_\odot$ in our study, as explained earlier, that part of the distribution which is shortward of this radius corresponds to XBs, while that part longward of it corresponds to PXBs.

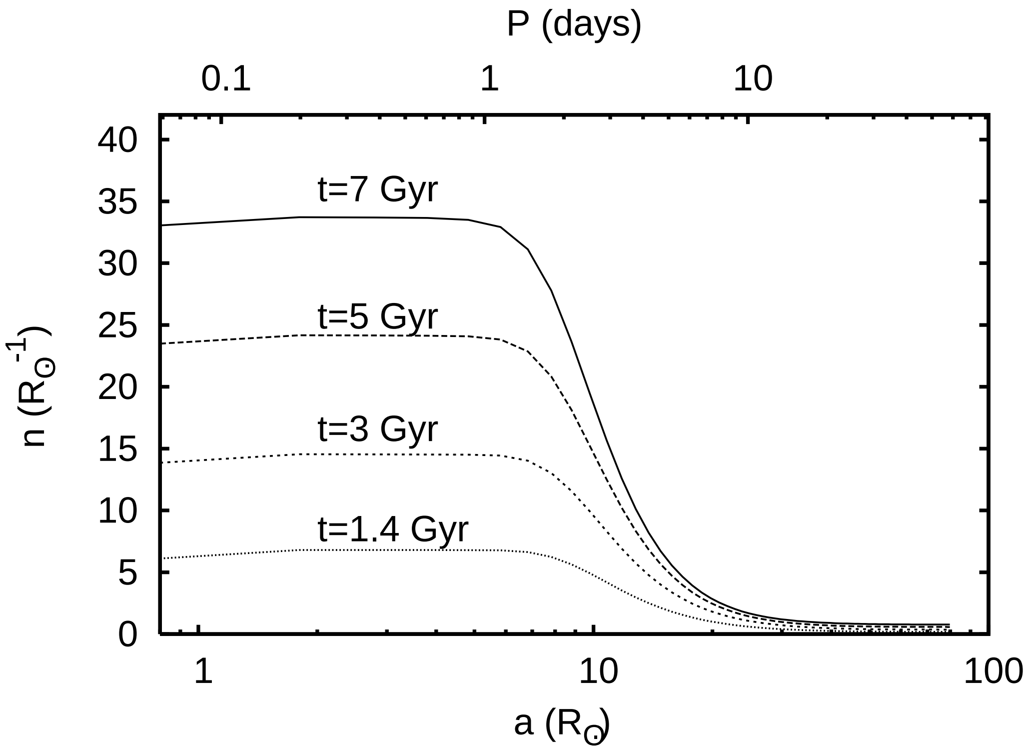

Figure 3.6: *Time slices, i.e., $n(a)$ at specified times t, for the evolution $n(a, t)$ shown in Fig. 3.5. Along abscissa, both orbital radius a and orbital period P scales are shown for convenience.*

To further clarify the nature of this evolution, slices through the above surface at various points along time axis and a-axis are shown in Figs. 3.6 and 3.7, in the former figure the abscissa being also marked in terms of the orbital period P, readily calculable in terms of a and the stellar masses with the aid of Kepler's third law, assuming conservative mass transfer during the XB phase. Figure 3.6 shows that $n(a)$ increases with time, roughly preserving its profile for $t > 1.5$ Gyr or so. This profile consists of a roughly uniform distribution in for short orbital radii, $a \leq 6R_{\odot}$, say, corresponding to $P \leq 1^d$ roughly, and a sharp fall-off at larger radii and orbital periods. Figure 3.7 shows that $n(a)$ at a given a increases with time and approaches saturation on a timescale $6 - 12$ Gyr or so, this timescale being longer at at smaller values of a.

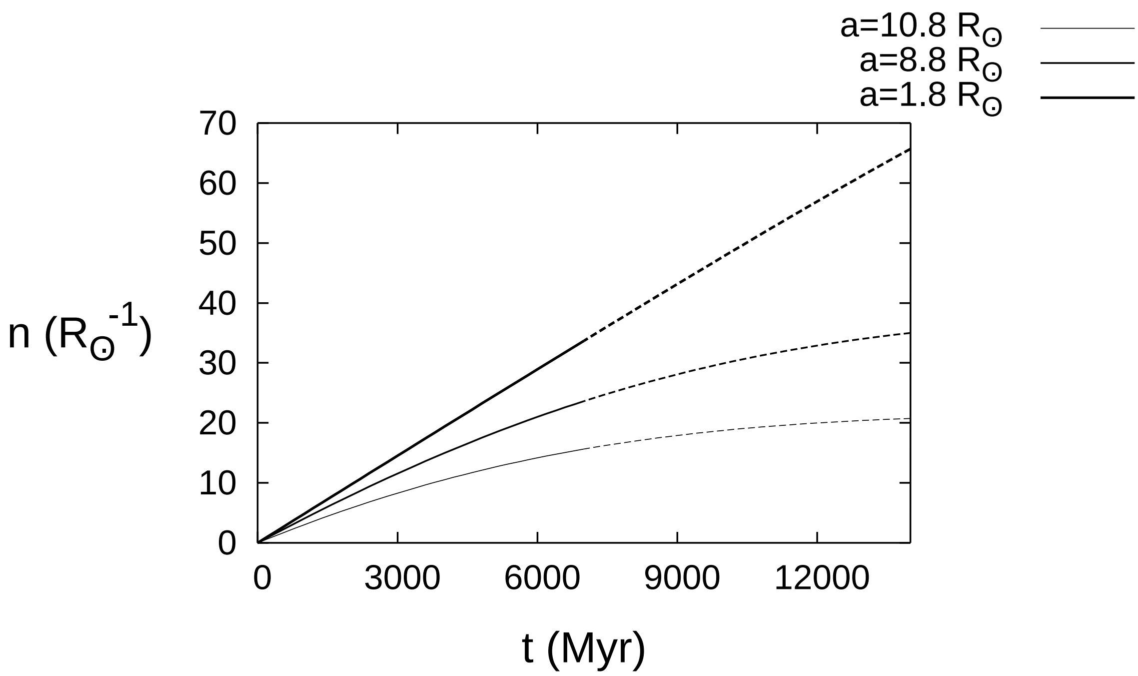

Figure 3.7: *Radial slices, i.e., $n(t)$ at specified orbital radii a, for the evolution $n(a,t)$ shown in Fig. 3.5.*

Figures 3.6 and 3.7 suggest that a regime of roughly self-similar evolution may be occurring in our model binary population at times beyond 1 Gyr or so, in the following way. An asymptotic profile of $n(a)$ is established on the timescale of a 1 Gyr or so, which thereafter evolves roughly self-similarly towards a saturation strength on a timescale $\sim 6-12$ Gyr or so. We shall discuss the origins of such behavior in detail elsewhere, since, as explained in Sec. 3.4.1, our model of orbital evolution requires additional ingredients before it can be compared with observations of X-ray binaries. However, the following qualitative remarks are appropriate here.

First, the origins of the establishment of the above self-similar profile in a Gyr or so (independent of the initial distribution we start from) clearly lie in the two terms that describe binary formation and hardening on the right-hand side of Eq. (3.5), namely, $R(a)$ and $\frac{\partial n}{\partial a} f(a)$ respectively. The latter term can be written qualitatively in the form n/τ_h, where τ_h is the overall hardening timescale, which is well-known to be of the order of a Gyr or so (see Chap. 2 and references therein). This timescale, which is also that on which a given binary passes from the large-a end of the distribution shown in Fig. 3.5 to the small-a end, is obviously the timescale that establishes the above profile. The shape of this profile, as detailed above, seems related to those of the tidal-capture rate (see Fig. 3.3) and the hardening rate (see Fig. 3.2). In particular, note that the former rate is roughly constant over $a_{min} \leq a \leq 5R_{\odot}$, and the latter roughly so for $a_{pm} \leq a \leq 2R_{\odot}$.

Second, the subsequent, roughly self-similar evolution of the above profile occurs on a (longer) timescale τ_s whose origins clearly lie in the binary destruction term on the right-hand side of Eq. (3.5), namely, $nD(a)$, since this term can be cast in the qualitative form n/τ_s, where τ_s is the saturation time $\sim 6-12$ Gyr. Whereas the earlier term n/τ_h describes the passage or "current" of binaries through the distribution, as described earlier, the term n/τ_s becomes important as n increases, preventing n from becoming arbitrarily large by enforcing saturation at the point where the rates of formation and destruction balance. As $D(a)$ scales with a, as shown above, and $\tau_s = 1/D(a)$, we expect saturation to occur at earlier times at larger radii, as seen in Fig. 3.7.

3.3.2 Number of X-ray binaries in globular clusters

The total number of X-ray binaries N_{XB} in a GC at any time can be computed directly from our approach by integrating $n(a,t)$ over the range of a relevant for XBs, *viz.*, $a_{pm} \leq a \leq a_L$, where a_{pm} is the value of a corresponding to the period

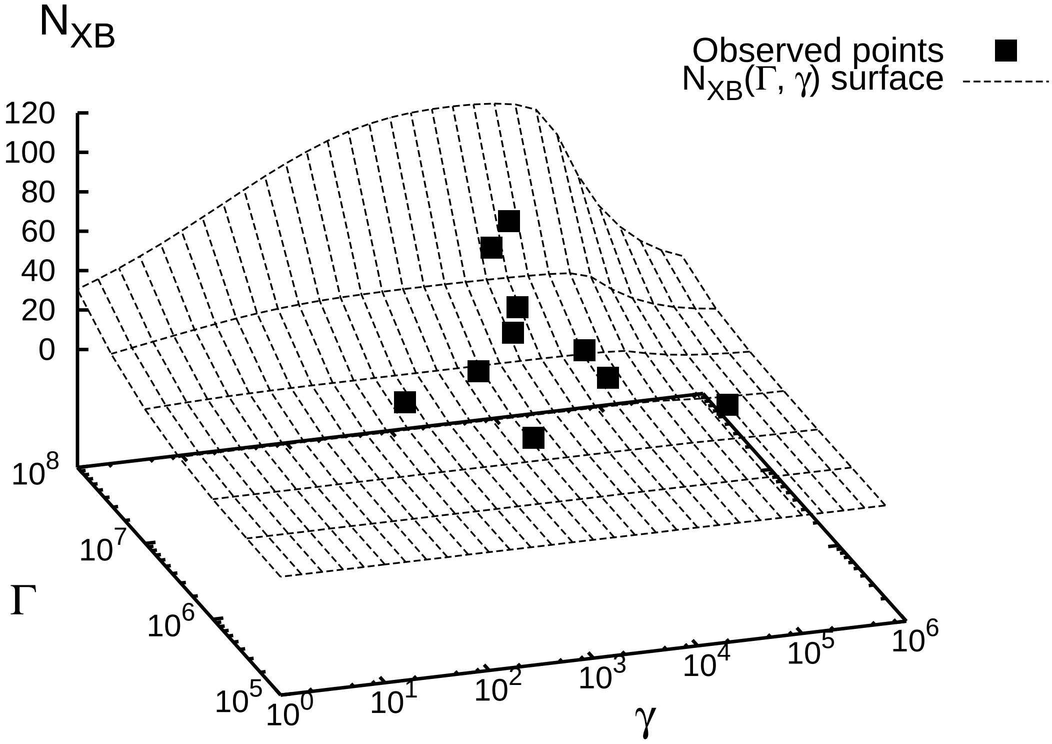

Figure 3.8: *Computed $N_{XB}(\Gamma, \gamma)$ surface. Overplotted are the positions of the globular clusters with significant numbers of X-ray sources (filled squares) from Fig. 3.1.*

minimum $P \approx 80$ minutes, and a_L is the value of a at the first Roche lobe contact and onset of mass transfer, as explained earlier. We have:

$$N_{XB}(t) = \int_{a_{pm}}^{a_L} n(a,t)da \tag{3.40}$$

Taking an evolutionary time $\sim$ 8 Gyr as representative, we can therefore determine N_{XB} at this point in time, and study its dependence on the Verbunt parameters Γ and γ that describe the essential dynamical properties of globular clusters in this context, as explained earlier. By doing so, we can attempt to make qualitative contact with the systematics of those recent observations of X-ray binaries in globular clusters which we have described earlier (Pooley et al., 2003). To this end, we computed values of N_{XB} over a rectangular grid spanning over $\gamma = 1 - 10^6$ and $\Gamma = 10^3 - 10^8$. (Of course, not all the points on the grid would be directly relevant for comparison with observation, since the observed globular clusters lie only along a diagonal patch on this grid, as shown in Fig. 3.1. However, in this introductory study, we wished to establish the theoretically expected trends of variation with Γ and γ, and so performed computations of N_{XB} over the entire rectangular grid)

For a specified grid point, *i.e.*, a pair of values of the Verbunt parameters, we obtained values of ρ, r_c and v_c with the aid of Eqs. (3.1), (3.2) and the virialization condition:

$$v_c \propto \rho^{1/2} r_c \tag{3.41}$$

which were used for the computation at this grid point. We chose this prescription for the sake of definiteness, because values of v_c are not known, in general, at a computational grid point, without which a pair of Verbunt parameters cannot specify all three variables ρ, r_c and v_c. This also introduced a certain uniformity of treatment of all grid points, which, we thought, would clarify the theoretically expected trends. On the other hand, this did lead to a feature at high values of Γ and low values of γ,*i.e.*, in that part of the grid which is completely devoid of observed globular clusters at this time (and which, in fact, may *actually* contain no clusters, because such combinations of Γ and γ may not be possible in nature), which appears unphysical, as we discuss below. Observationally, we know, of course, that some clusters appear fairly virialized and some do not, but any spread in v_c applied over the grid points would have been arbitrary, and would have led to a scatter, masking the systematic theoretical trends without purpose. Finally, throughout these computations, we used representative values for (a) the primordial binary fraction k_b, namely, 10 percent, and (b) compact star fraction k_X, namely, 5 percent (see Sec. 1.3).

Figure 3.8 shows the computed surface $N_{XB}(\gamma, \Gamma)$. There appears to be a "fold" in this surface, in a direction roughly parallel to the Γ axis, located around $\gamma = 3 \times 10^3$. From this fold, if we go towards higher values of γ, then, for any given value of Γ, N_{XB} decreases with increasing γ. This is a signature of the compact-binary destruction processes detailed in the previous section, whose strengths increase with increasing γ. Thus, the above value of γ corresponding to the fold seems to be a good estimate of the threshold above which these destruction processes dominate. At constant γ, the variation with Γ is quite straightforward: N_{XB} simply increases monotonically with increasing Γ, reflecting the fact that the formation rates of compact binaries, as described in the previous section, increase with increasing Γ.

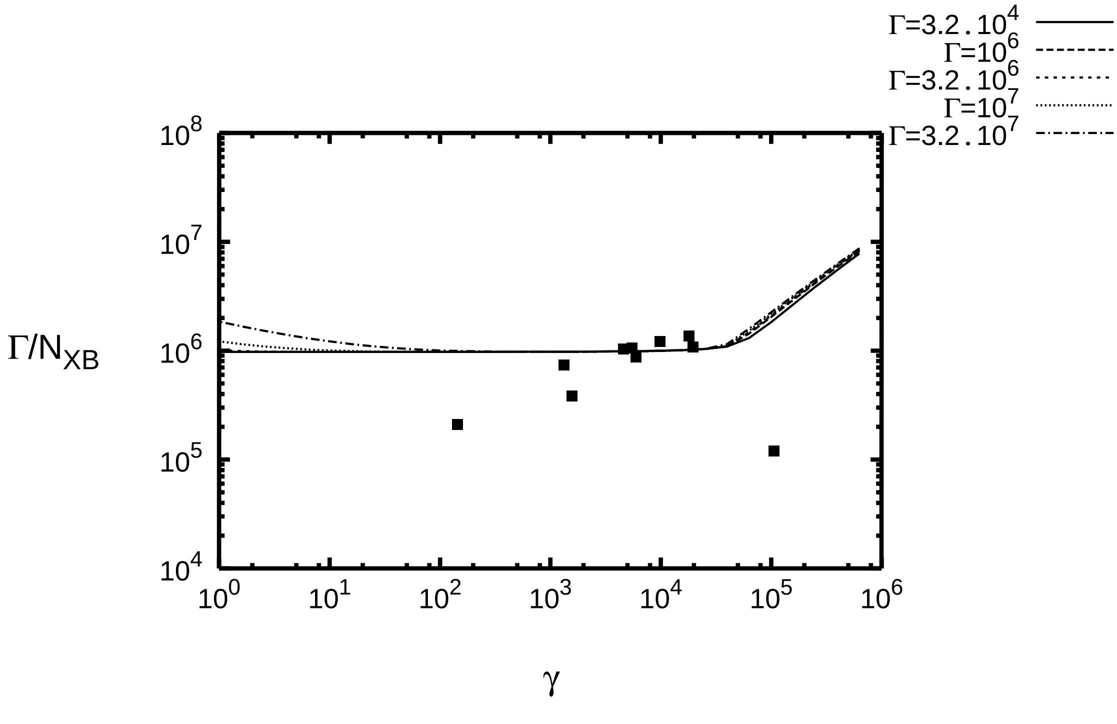

Figure 3.9: *Computed Γ/N_{XB} as a function of γ, showing scaling (see text). Computed curves for various values of Γ are closely bunched, as indicated. Overplotted are the positions of the globular clusters with significant numbers of X-ray sources (filled squares) from Fig. 3.1.*

To further clarify these trends, and to facilitate comparison with those obtained from the "toy" model discussed in Chap. 2, we display in Fig. 3.9 Γ/N_{XB} vs. γ, as was done there. The motivation is as follows. It was shown that this toy model leads to the scaling that Γ/N_{XB} was a function of γ alone, which was a monotonically increasing function of γ, for which the toy model gave a very simple, analytic form. Our purpose in Fig. 3.9 is to see how much of this scaling survives the scrutiny of a more detailed model, such as presented here. As the figure shows, this scaling does carry over approximately, although some details are different. Γ/N_{XB} is still almost a function of γ alone (except at the very highest values of Γ), showing that this scaling $N_{XB} \propto \Gamma g(\gamma)$ of the toy model carries over approximately to more detailed ones, thereby giving an indication of the basic ways in which dynamical binary formation and destruction processes work. The above "universal" function $g(\gamma)$ of γ is, except for a feature at low values of γ which we discuss below, still a monotonically increasing one, reflecting the increasing strength of dynamical binary-destruction processes with increasing γ. However, the shape of the function is different in detail now, as may have been expected.

We now discuss the low-γ feature referred to above: at the lowest values of γ, Γ/N_{XB} seems to rise again, reflecting an apparent drop in N_{XB}. This is difficult to understand, since binary-destruction effects are negligible at these values of γ. Actually, this is an artifact of the way in which we fixed the essential cluster parameters ρ, r_c and v_c from specified values of the Verbunt parameters for the computational grid (as explained above), which can be seen as follows. With the assumption of virialization, as done for this purpose, the velocity dispersion v_c can be expressed in terms of the Verbunt parameters in a manner analogous to that used in Eq. (3.3), the result being $v_c \propto \Gamma^{2/5}\gamma^{-1/5}$. This relates v_c to γ, so that the latter influences the Maxwellian-averaging process involved in the calculation of the tidal capture cross-section described in Sec. 3.2.4.1, since the parameter $\beta \equiv 3/(2v_c^2)$ of the Maxwellian then scales as $\beta \propto \Gamma^{-4/5}\gamma^{2/5}$. At small values of γ, β becomes small, which reduces the tidal-capture rate, as Eq. (3.29) readily shows. This is completely unphysical, of course, since γ has nothing to do physically with the tidal capture rate. Rather, it is an artifact produced by the way we (artificially) related v_c to γ for computational convenience. Accordingly, we ignore this low-γ feature in all further considerations.

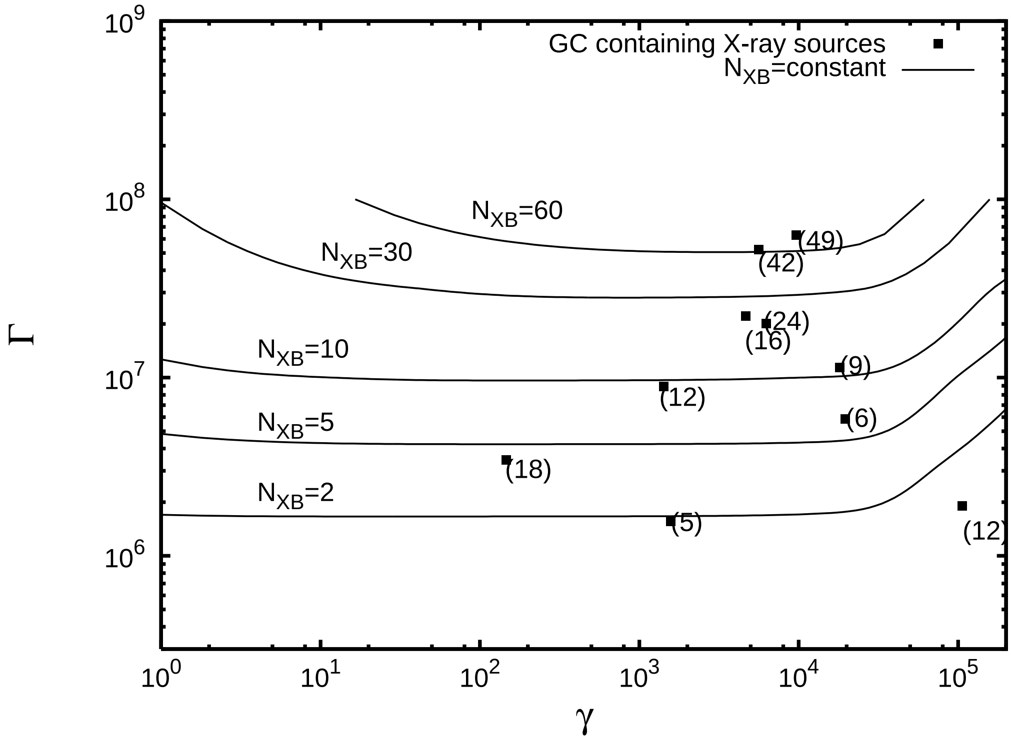

Figure 3.10: *Contours of constant N_{XB} in the $\Gamma - \gamma$ (Verbunt parameters) plane. Overplotted are positions of Galactic globular clusters with significant numbers of X-ray sources detected in them (filled squares) from Fig. 3.1. N_{XB} for each cluster is indicated by the number in parenthesis next to its marked position.*

3.4 Comparison with Observation

3.4.1 Applicability of our study

Before attempting to compare our results with observations, we review in brief some essential ingredients of our model study at this stage, so as to clarify which of our results can be so compared, and which need inclusion of further components before this can be meaningfully done. A major ingredient that is incomplete at this stage is our description of the orbital evolution of the binary, since it neglects nuclear evolution of the low-mass companion star altogether. While this may not be very unreasonable for CV systems, it is completely inadequate for LMXBs, where the stellar evolution of the companion plays a crucial role, which has been studied by many authors. In particular, recent studies by Podsiadlowski et.al.

(2002) and Pfahl et.al. (2003) have demonstrated the large range of possibilities covered by such evolution with realistic stellar evolutionary codes, performing a Monte Carlo binary population synthesis study in the latter reference with the aid of the library of evolutionary sequences described in the former. We plan to include stellar evolutionary effects in a subsequent work of the series and are assessing various methods of doing so. One possibility is to start with a semi-analytic scheme along the lines of the "SeBa" model (Portegies Zwart et.al., 2001), and to continue with a semi-analytic approximation to a more elaborate library of evolutionary sequences, such as described above.

Since most of the XBs in the Galactic GC data of Pooley et al. (2003) are CVs, our scheme should be able to describe the overall properties of these XB populations reasonably well. Even so, we shall make no attempt here to compare our results on orbital period distribution with the observed CV distribution, since the CVs in the latter distribution are almost exclusively from outside globular clusters, where dynamical formation is not relevant. We have here recorded the orbital-period distribution that comes from our computations (at this stage) only as a natural intermediate step. It can perhaps be compared with observation when the orbital-period distribution of CVs *in GCs* becomes observationally established. For LMXBs, where the observed orbital-period distribution at this time also consists overwhelmingly of those outside GCs, there is of course no question of comparison at this stage, for the reasons given above. Thus, our main aim here is to put in the observational context our results on the numerical properties of XB populations in GCs in relation to the GC parameters.

3.4.2 Ultracompact X-ray binaries

In recent years, a subset of LMXBs in GCs, in the Milky Way and possibly also in elliptical galaxies, have received much attention because of (a) their high, persistent brightness ($L_x \sim 10^{36} - 10^{39}$ erg s^{-1}), which would make them dominate the high end of the luminosity functions of X-ray binaries in ellipticals (Bildsten & Deloye, 2004) and (b) their very close orbits with $P < 1$ hr or so, sometimes as short as $P \sim 10$ minutes, the classic example being the 11 min binary 4U 1820-30 the Galactic cluster NGC 6624. These are the ultracompact

X-ray binaries (henceforth UCXBs), which are thought to consist of neutron stars in ultracompact orbits with very low-mass degenerate dwarf companions ($m_c \sim (0.06 - 0.2)M_\odot$) as mass donors. The evolutionary origin of UCXBs is of much current interest, and proposals for such origins include (a) direct collisions between red giants and neutron stars in GC cores, as a consequence of which the red-giant envelope can either be promptly disrupted (Ivanova et.al., 2005) or be expelled more slowly in a common-envelope phase, and (b) usual LMXB evolution with the initial orbital period below the "bifurcation period" of about 18 hrs (Podsiadlowski et.al., 2002). A natural point that arises, therefore, is about the role of UCXBs in our study, and the general importance of the above channels of formation in relation to the ones we have described above, which we now consider in brief.

The key feature of UCXBs from the point of view of our study is that the number of UCXBs N_{UC} is a tiny fraction of the total number of XBs in a GC, and so of little importance as far as N_{XB} is concerned. This is a general, robust feature, which follows from the basic point that the UCXBs are extremely short-lived because of their extreme brightness, so that N_{UC} is small at any given epoch despite their considerable birthrate. To see this in more detail, consider the UCXB birthrate of about one every 2×10^6 year per $10^7 M_\odot$ of the mass of a GC, as given by (Bildsten & Deloye, 2004), which, together with their estimated lifetimes of $(3 - 10) \times 10^6$ years, yields an estimate of $N_{UC} \sim 1 - 5$ in a $10^7 M_\odot$ GC at any given time. Actually, the observed GCs in our galaxy have lower masses, in the range $\sim (10^5 - 10^6)M_\odot$ (Ivanova et.al., 2005). Thus a Galactic GC of $10^6 M_\odot$ like 47 Tuc will have $N_{UC} \sim 0.1 - 0.5$, remembering that the birthrate scales down appropriately with the GC mass, but the lifetime remains the same. This is to be compared with the observed number of XBs in 47 Tuc of 45 (Pooley et al., 2003), which yields a fraction $N_{UC}/N_{XB} \sim 2 \times 10^{-3} - 1.1 \times 10^{-2}$. We can double-check this and put it on a systematic basis with the aid of Table 1 of Ivanova et.al. (2005), wherein these authors have listed the minimum expected number of UCXBs in a number of Galactic GCs, by combining this with the total number of observed XBs obtained from Pooley et al. (2003) and other sources. For 47 Tuc, with 0.23 UCXBs and 45 XBs, the ratio is $N_{UC}/N_{XB} \sim 5 \times 10^{-3}$, very similar to above, and those for other sources are also similar. For example, Terzan 5 has a ratio $\sim 2 \times 10^{-3}$, and NGC 6652 has a ratio $\sim 8 \times 10^{-4}$.

We see from the above that UCXBs constitute such a tiny fraction of the total XB populations of Galactic GCs in terms of numbers that their effect is negligible for this work. However, in a study of the X-ray luminosity functions of GCs, their effect is expected to be crucial: if a GC contains even one UCXB, its luminosity may dominate over the combined output of all other XBs. It is the extension of this idea which has been used in recent years to argue that the luminosity function of XBs in ellipticals may be dominated by UCXBs in their GCs (Bildsten & Deloye, 2004).

3.4.3 X-ray source numbers in globular clusters

The filled squares in Fig. 3.8 represent globular clusters with significant numbers of X-ray binaries in them. These points generally lie near the surface in this three-dimensional plot, mostly in the vicinity of the fold described above. This is more clearly seen in the two-dimensional plot of Fig. 3.9, where the bulk of the observational points are indeed seen to be near the upward "knee" of the computed curves. To facilitate comparison with observations further, we show in Fig. 3.10 contours of constant N_{XB} in the $\Gamma - \gamma$ (Verbunt parameters) plane. Overplotted on these are the above observed clusters (filled squares), where the number in the parentheses next to each indicates the total number of X-ray binaries observed in it (Pooley et al., 2003). The contours are seen to be qualitatively rather similar in shape to the curves in Fig. 3.9. The trend in the observed N_{XB} values generally follows the contours, with one exception. This is most encouraging (also see Sec. 2.4 for a discussion) for the construction of more detailed models, and indeed rather remarkable in view of the fact that no particular attempt has been made to fit the data at this stage.

3.5 Discussion

In the present chapter, we have explored the results of a Boltzmann study of the evolution of compact-binary populations in globular clusters in the continuous limit, and made preliminary contacts with observations of X-ray binaries in Galactic globular clusters. Our Boltzmann approach has built into it the rates of the essential dynamical processes that occur due to star-star and star-binary encounters in dense clusters, *viz.*, collisional hardening, binary formation by tidal capture and exchange, and binary destruction by dissociation and other mechanisms, as obtained by previous numerical studies of large numbers of such individual encounters. We stress that our Boltzmann scheme is not a Fokker-Planck one, wherein the cumulative effects of a large number of small changes in distant encounters is described as a slow diffusion in phase space. We can and do handle both small and large changes in the framework of the original Boltzmann visualization of motion through phase space (at a computational cost which is quite trivial compared to that required for N-body simulations). Indeed, the continuous limit of collisional hardening used in this chapter may be looked upon as an example of a slow diffusion in a-space, while some of the formation and destruction processes are examples of faster and more radical changes. Of course, all these processes are episodic in nature, and we are studying their continuous, probabilistic limit in this introductory work. As already pointed out, we will describe an explicit treatment of the stochasticity of these processes within the framework of stochastic PDEs in the following chapter, which the Boltzmann equation becomes under such circumstances.

3.5.1 Conclusions

We find the indications from this preliminary study to be sufficiently encouraging to attempt several steps of improvement, most of which we have already indicated in the previous sections. To recapitulate briefly, we need to provide an appropriate description of the stochastic processes, which we do in Chap. 4. We need to introduce a mass function for the background stars in the globular cluster core, and handle non-circular orbits formed in the encounter processes. We need to assess the possible importance of binary-binary interactions in this problem, which we have neglected altogether so far. We need to include essential aspects of stellar evolution of the companion in our orbital-evolution scheme, particularly for LMXBs. In a more ambitious vein, we need to consider the evolution of the stellar background representing the cluster core, which we do in Chap. 5. As the core collapses, the collapse stalls due to binary heating, and possible gravothermal oscillations occur, the core parameters ρ and r_c evolve appropriately, and so do the Verbunt parameters Γ and γ. Binary-population evolution with such evolving GC parameters is an interesting problem in itself, even if we do not explicitly consider the back reaction of binary evolution on the evolution of its background.

The scaling of N_{XB} with the two Verbunt parameters we already found here seems to be among the basic building blocks of our understanding of how globular clusters cook up their gross overabundance of X-ray binaries through an interplay between dynamical formation and destruction. It remains to be seen if there are other such building blocks which have not been investigated so far.

Chapter 4

Evolution of Compact-Binary Populations in Globular Clusters: A Boltzmann Study. Introducing Stochasticity

4.1 Introduction

In the previous chapter, we introduced the Boltzmann scheme, and studied the evolution of compact-binary populations of globular clusters with the aid of this scheme. The Boltzmann scheme follows compact-binary evolution as a result of both (a) those processes which determine compact-binary evolution in isolation (*i.e.*, outside globular clusters), *e.g.*, angular momentum loss by gravitational radiation and magnetic braking, as also orbital evolution due to mass transfer, and (b) those processes which arise from encounters of compact binaries with the dense stellar background in globular clusters, *e.g.*, collisional hardening (Heggie, 1975; Shull, 1979; Banerjee & Ghosh, 2006), binary formation through tidal capture and exchange processes, and binary destruction (Fabian et.al., 1975; Press & Teukolsky, 1977; Lee & Ostriker, 1986; Di Stefano & Rappaport, 1992, 1994; Spitzer, 1987; Hut & Bahcall, 1983). We treat all of the above processes simultaneously through our Boltzmann scheme, the aim being to see their combined effect on the compact-binary population as a whole, in particular on the evolution of (a) the total number of X-ray binaries as the formation and destruction processes continue to operate, and, (b) the orbital-period distribution of the population. As stressed in Chap. 3, our scheme is the original Boltzmann one (not the Fokker-Planck reduction of it), which, by definition, is capable of handling both the *combined* small effects of a large number of frequent, weak, distant encounters and the *individual* large effects of a small number of rare, strong, close encounters *on the same footing*. We note here that, although Monte Carlo Fokker-Planck approaches were normally thought to be capable of handling only the former effects, schemes for including the latter have been proposed and studied recently (Fregeau et.al., 2003; Fregeau & Rasio, 2007).

In Chap. 3, we studied the problem in the continuous limit, wherein we used continuous representations for both kinds of processes described above, *i.e.*, those of category (a) above, which are inherently continuous, and also those of category (b), which are inherently stochastic. For the latter category, therefore, we used the *continuous limit* of the above stochastic processes, wherein the probability or cross-section of a particular such process happening with a given set of input and output variables was treated as a continuous function of these variables. These cross-sections were, of course, those that had been determined from extensive numerical experiments with two-body and three-body encounters performed earlier (Heggie, Hut & McMillan, 1996; Portegies Zwart et.al., 1997b).

In this chapter, we address the next question, namely, how is the inherent stochasticity of the processes of category (b) to be introduced into our scheme, to be handled simultaneously with the inherently continuous nature of those of category (a)? As stressed in Chap. 3, this step is of great importance, since it is a simultaneous operation of the above continuous and stochastic processes in globular clusters that leads to the observed properties of compact-binary populations in them. To this end, we introduce stochasticity into our Boltzmann study in this chapter in the following way. For a first look, we consider the rates of the processes of category (b) as *randomly fluctuating* about the mean rates described in Sec. 3.2, while those of the processes of category (a) remain continuous, as before. We model these fluctuations as a *Wiener process* (see Appendix B and references therein), which is the mathematical description of Brownian motion.

With this prescription, the Boltzmann equation governing the evolution of the distribution function $n(a,t)$ of compact binaries in time t and orbital radius a becomes a *stochastic* partial differential equation (henceforth SPDE), instead of the ordinary partial differential equation (henceforth OPDE) which it was in the continuous limit. We handle the solution of this SPDE with the aid of techniques developed largely during the last fifteen years (Kloeden et.al., 1994; Gaines, 1995; Øksendal, 2004). These techniques involve the use of the *Itô calculus* (see Appendix C and references therein), instead of ordinary calculus, for handling the stochastic terms.

Our results show that the full solutions with stochasticity included have fluctuations which vary from one "realization" to another of the stochastic processes, as expected. However, the full results show trends which generally follow those in the continuous limit. Furthermore, the average result over many realizations comes very close to the continuous limit, showing the importance of the latter limit for understanding mean trends. On the other hand, understanding fluctuations in a typical full run is also very important, as this gives us a first idea of the magnitude of fluctuations we can expect in the data on X-ray binaries in globular clusters as a result of the stochastic processes, as also the expected trends in the fluctuations with the essential globular-cluster parameters, *e.g.*, the Verbunt parameters introduced in Chap. 3 (also see below).

Comparison of our computed trends in the number N_{XB} of X-ray binaries in Galactic globular clusters with the Verbunt parameters on the one hand, with observed trends in recent CHANDRA data on Galactic globular clusters on the other, shows that our full results are in good agreement with observation. We have thus constructed a straightforward, very inexpensive scheme for following the evolution of compact-binary populations in globular clusters, including essential, fluctuating, encounter processes that are thought to operate in such clusters, as also those continuous processes which operate in isolated binaries and so apply here as well. We can also follow the evolution of N_{XB}, as also that of the orbital-period distribution of compact binaries in globular clusters. For the latter study, however, proper modeling of stellar-evolutionary effects still remains to be done for parts of the parameter space, as explained in Sec. 3.4, which is also discussed in Sec. 4.4.

We organize this chapter as follows. In Sec. 4.2, we introduce stochasticity explicitly through our prescription, explaining the details of Wiener processes and the Itô calculus in the Appendices. We describe our generalization of the Lax-Wendorff scheme, introduced in Sec. 3.2.6, to handle the solution of the SPDE which the Boltzmann equation has become now. In Sec. 4.3, we describe the results of our full calculations including stochasticity, and compare these with the continuous-limit results. In Sec. 4.3.3, we compare our full results with observations. Finally, In Sec. 4.4, we discuss our results, putting them in the context of previous studies in the subject, and indicating some additional physical effects to be included by stages in future versions of our scheme, as well as some future problems to be tackled.

4.2 Introducing Stochasticity

In order to study the behavior of the inherently stochastic terms in the full Boltzmann equation

$$\frac{\partial n(a,t)}{\partial t} = R(a,t) - n(a,t)D(a,t) - \frac{\partial n(a,t)}{\partial a} f(a,t), \tag{4.1}$$

we must explicitly include stochastic, fluctuating parts in these terms, in addition to their mean values studied in Sec. 3.2, as above. We do so by expressing the above rates $R(a,t)$, $D(a,t)$, and $f(a,t)$ as their earlier mean values $\overline{R}(a)$, $\overline{D}(a)$ and $\overline{f}(a)$, augmented by fluctuating components as below:

$$\left.\begin{array}{l} R(a,t) = \overline{R}(a) + \zeta^t_{atc} + \zeta^t_{aex1} \\ D(a,t) = \overline{D}(a) + \zeta^t_{aex2} + \zeta^t_{adss} \\ f(a,t) = \overline{f}(a) + \zeta^t_{acoll} \end{array}\right\} \tag{4.2}$$

Here, ζ^t_{aX} is the random fluctuation rate of events of type X from their mean rates, and X = tc, ex1, ex2, dss, coll by turn, these notations having been introduced above. In general, ζ^t_{aX} is a function of both a and t, of course.

The crucial question is that of modeling ζ^t_{aX} appropriately. In this introductory work, we use the standard normally-distributed model

$$\zeta^t_{aX} = S_X(a)\eta^t, \tag{4.3}$$

where $S_X^2(a)$ is the variance of ζ_{aX}^t at a given a and η^ts at each t are independent random numbers distributed in a standard normal distribution. This separable form is appropriate since the dynamical processes of binary formation and destruction at a given value of a are inherently independent of those at other values of a. The "flow" or "current" of binaries from larger to smaller values of a due to the hardening described above and in Chap. 3 does not affect this independence, but merely changes the number of binaries in an infinitesimal interval of a around a given value of a at a given instant t, which is automatically taken into account by the Boltzmann equation (also see below). Indeed, the hardening process itself has this independence, *viz.*, that its rate at a given value of a is independent of that at other values of a, and so is separable in the same way. By contrast, the number distribution $n(a,t)$ of the binaries *cannot* be written in this form, since, at a particular a, it is determined both by the binary formation and destruction rates at that a, *and* by the rates of binary arrival from (and also departure to) other values of a due to hardening, as described above. All of this is, of course, automatically included in the Boltzmann equation by definition.

The essence of the physics of these fluctuations is contained in the adopted model for η^t. By adopting a normally-distributed variation, we are, in effect, considering a *Wiener process* (see Appendix B and references therein), which is the standard mathematical description of Brownian motion. In other words, we are studying a situation wherein the variations in the above dynamical rates about their respective mean values constitute a Brownian motion. We return to Wiener processes later in more detail.

4.2.1 Variances of stochastic-process rates

How do we estimate the variance of a stochastic process of type X whose mean value is $\overline{R}_X(a)$? To answer this question, consider first how it is addressed in Monte Carlo simulations, which have been performed in this subject by several authors (see, *e.g.*, Sigurdsson & Phinney (1993), Portegies Zwart et.al. (1997a), or Fregeau et.al. (2003)). These works have uniformly used the so-called *rejection method* for determining whether an event of a given type occurs in a given time interval or not. The method works as follows.

For events of type X, if the mean rate of event occurrence is $\overline{R}_X$, then the timescale for occurrence of such events is

$$\Delta t_X = \frac{1}{\overline{R}_X} \tag{4.4}$$

Hence, during a time step $\Delta t < \Delta t_X$, the quantity $p_X = \overline{R}_X \Delta t < 1$ is the *expected mean number of events* during this interval. $p_X < 1$ can also be interpreted as the *probability* of occurrence of an event X within this time step (Portegies Zwart et.al., 1997a), and the actual number of such events within Δt will then follow a binomial distribution with the following mean and variance:

$$\left.\begin{array}{rl} \text{mean} = & \overline{R}_X(a)\Delta t \\ \text{variance} = S_X^2(a)\Delta t^2 = & \overline{R}_X(a)\Delta t(1 - \overline{R}_X(a)\Delta t). \end{array}\right\} \tag{4.5}$$

Note that the above variance depends on a, since the mean rates depend on a. When several different types of events are considered simultaneously, as in the present problem, we must, of course, so choose Δt that it is shorter than the shortest event-occurrence timescale appearing in the problem. We discuss this point below.

4.2.1.1 Time step

The mean rates depend on a as detailed in Chap. 3 (see Fig. 3.3). $\overline{R}_{tc}(a)$ is a decreasing function of a, and so attains its maximum at $a = a_{min}$. All other rates are either constant (ex2), or increasing functions of a, so that their maximum values can be thought to occur at $a = a_{max}$. Accordingly, if we make the following choice for our computational time step Δt_d:

$$\Delta t_d < \min\left\{\frac{1}{\overline{R}_{tc}(a_{min})}, \frac{1}{\overline{R}_{ex1}(a_{max})}, \frac{1}{\overline{R}_{ex2}(a_{max})}, \frac{1}{\overline{R}_{dss}(a_{max})}, \frac{1}{\overline{\dot{a}_{coll}}(a_{max})}\right\}, \tag{4.6}$$

this will ensure that Δt_d is smaller than the shortest of the above event-occurrence timescales.

However, as is well-known, this time step must also obey the *Courant condition* (Press et.al., 1992) throughout the range of a under consideration (*i.e.*, $0.6R_\odot$-$60R_\odot$):

$$\Delta t_c = \epsilon \frac{\Delta a}{\overline{f}_{\max}}, \qquad \epsilon < 1. \tag{4.7}$$

Here, Δa is the step-size in a, and $\overline{f}_{\max}$ is the largest value of $\overline{f}(a)$ over the range of a under consideration (see above and Chap. 3). Satisfaction of this condition is essential for the stability (Press et.al., 1992) of the solution of Eqn. (4.1).

To ensure that both of the above conditions are satisfied, we choose the time step Δt for solving Eqn. (4.1) to be

$$\Delta t = \min\{\Delta t_d, \Delta t_c\}. \tag{4.8}$$

4.2.2 Solution of Stochastic Boltzmann Equation

The Lax-Wendorff scheme (Press et.al., 1992) used by us for numerical solution of the Boltzmann equation in the continuous limit has been introduced in Sec. 3.2.6. The stochastic version of this equation, *viz.*, Eqn. (4.1) can be looked upon as the earlier continuous equation with additional stochastic terms, which turns it into a SPDE (see Sec. 4.1). We now discuss our method of solving this SPDE[1].

It it well-known that ordinary calculus cannot be applied to the handling of stochastic terms in SPDEs, since these terms are non-differentiable in the ordinary sense, and the ordinary definition of an integral does not apply to them. Rather, one has to modify the methods of calculus suitably, and redefine appropriate integrals. As summarized in Appendix C, one such modified calculus is the *Itô Calculus*, which has been used widely for solution of SPDEs in recent years (Øksendal, 2004; Kloeden et.al., 1994). The corresponding integrals involving the stochastic terms are then called *Itô integrals*, which have properties appropriately different from those of ordinary integrals, as indicated in Appendix C.

4.2.2.1 Numerical Method

In solving an SPDE like Eqn. (4.1), one integrates the continuous terms in the usual way, but the stochastic terms must be integrated using Itô calculus (Gaines, 1995). This means that, in advancing the solution at t by a time step dt — which

[1] In SPDE literature, the continuous terms are sometimes called *drift* terms and the stochastic terms *diffusion* terms, but we shall *not* use this terminology here, since stochastic terms in our problem do not always represent diffusion, and furthermore since there is a possibility with such usage of confusion with the Fokker-Planck approach, which does represent diffusion in phase space.

is essentially a Taylor expansion of the solution $n(a,t)$ about t — the expansions of the stochastic terms in Eqn. (4.1) are to be performed using the stochastic Taylor expansion (Eqn. (C.7)), as discussed in Appendix C.

A variety of numerical algorithms have been explored by various authors for numerical solution of SPDEs. The particular algorithm we use is a hybridization of the two-step Lax-Wendorff scheme for the continuous terms, as utilized in the continuous-limit study in Chap. 3, and the second-order stochastic Taylor expansion according to the *Milshtein scheme* for the stochastic terms (Milshtein, 1974; Gaines, 1995), *i.e.*, Eqn. (C.13), as explained in Appendix C. In this scheme, there is only one stochastic path to be solved for in our case *viz.*, that of $n(a,t)$ (corresponding to X_k) and the continuous terms (*i.e.*, the σ_ps), the variances in tc, ex1, ex2, dss and coll rates being as given above. Note that, in each of the two steps in the Lax-Wendorff scheme, the expansion (C.13) needs to be applied, whereupon we arrive at the following discretization scheme[1] for Eqn. (4.1):

$$
\begin{aligned}
&\text{Half step :}\\
&n_{j+1/2}^{N+1/2} = \tfrac{1}{2}\left(n_{j+1}^{N} + n_{j}^{N}\right) + \left[\overline{R}(a_{j+1/2}) - \overline{D}(a_{j+1/2})\left(\tfrac{n_{j+1}^{N}+n_{j}^{N}}{2}\right)\right]\tfrac{\Delta t}{2}\\
&+\left(\mathcal{W}_{j+1/2_{tc}}^{N} + \mathcal{W}_{j+1/2_{ex1}}^{N}\right) - \left(\mathcal{W}_{j+1/2_{ex2}}^{N} + \mathcal{W}_{j+1/2_{dss}}^{N}\right)\left(\tfrac{n_{j+1}^{N}+n_{j}^{N}}{2}\right)\\
&+\left[\left((\mathcal{W}_{j+1/2_{ex2}}^{N})^2 - S_{ex2}^2(a_{j+1/2})\right) + \left((\mathcal{W}_{j+1/2_{dss}}^{N})^2 - S_{dss}^2(a_{j+1/2})\right)\right]\left(\tfrac{n_{j+1}^{N}+n_{j}^{N}}{4}\right)\\
&+\left(\mathcal{W}_{j+1/2_{ex2}}^{N}\mathcal{W}_{j+1/2_{dss}}^{N}\right)\left(\tfrac{n_{j+1}^{N}+n_{j}^{N}}{2}\right)\\
&-\tfrac{\overline{f}(a_{j+1/2})\Delta t}{2\Delta a}(n_{j+1}^{N} - n_{j}^{N}) - \tfrac{\mathcal{W}_{j+1/2_{coll}}^{N}}{2\Delta a}(n_{j+1}^{N} - n_{j}^{N}),\\
&\text{Full step :}\\
&n_{j}^{N+1} = n_{j}^{N} + \left(\overline{R}(a_j) - \overline{D}(a_j)n_{j}^{N}\right)\Delta t\\
&+\left(\mathcal{W}_{j\ tc}^{N} + \mathcal{W}_{j\ ex1}^{N}\right) - \left(\mathcal{W}_{j\ ex2}^{N} + \mathcal{W}_{j\ dss}^{N}\right)n_{j}^{N}\\
&+\left[\left((\mathcal{W}_{j\ ex2}^{N})^2 - S_{ex2}^2(a_j)\right) + \left((\mathcal{W}_{j\ dss}^{N})^2 - S_{dss}^2(a_j)\right)\right]\tfrac{n_{j}^{N}}{2}\\
&+\left(\mathcal{W}_{j\ ex2}^{N}\mathcal{W}_{j\ dss}^{N}\right)n_{j}^{N}\\
&-\tfrac{\overline{f}(a_j)\Delta t}{\Delta a}\left(n_{j+1/2}^{N+1/2} - n_{j-1/2}^{N+1/2}\right) - \tfrac{\mathcal{W}_{j\ coll}^{N}}{\Delta a}\left(n_{j+1/2}^{N+1/2} - n_{j-1/2}^{N+1/2}\right).
\end{aligned}
\tag{4.9}
$$

Here, $\mathcal{W}_{j\ X}^{N} \equiv S_X(a_j)\eta^N\Delta t$, where η^N is the value of a standard normal variate at the Nth time step.

[1] It can be shown that the commutation condition (C.15) is satisfied in this case.

For any particular run, we compute the $\mathcal{W}^N_{j\ X}$s ($\mathcal{W}^N_{j+1/2_X}$s) for a particular a_j ($a_{j+1/2}$) over the a and t intervals of integration, and repeat it for all a_js. The standard normal variate η^Ns are generated using the well-known *polar method* (Press et.al., 1992). All values of $\mathcal{W}^N_{j\ X}$ and $\mathcal{W}^N_{j+1/2_X}$ are stored in a two dimensional array (*i.e.*, a *Wiener sheet*), which serves as the input for solving Eqn. (4.9). Because of the fluctuations in the collisional hardening rate (as contained in $\zeta^t_{a coll}$), it is not impossible that the value of the total hardening rate f might occasionally exceed $\overline{f}_{max}$, which would violate the Courant condition, possibly making the solution procedure unstable. To avoid this, we have so restricted the variations in $\mathcal{W}^N_{j\ coll}$s and $\mathcal{W}^N_{j+1/2_{coll}}$s that the *amplification factor* $\epsilon \equiv f\Delta t/\Delta a$ always lies between zero and unity (Press et.al., 1992).

4.3 Results

We now present the results obtained from our above computations of the cases which we studied in Chap. 3 in the continuous limit. As before, we study (a) the evolution of the distribution function $n(a,t)$, and, (b) the dependence of the computed number of XBs N_{XB} on the Verbunt parameters. We choose exactly the same values of all GC parameters as we did in there, for ease of comparison.

4.3.1 Evolution of compact-binary distribution

In Fig. 4.1, we show a typical evolution of the compact binary population distribution $n(a,t)$. The GC parameters were chosen, as in Chap. 3, to be $\rho = 6.4 \times 10^4 M_\odot \mathrm{pc}^{-3}$, $r_c = 0.5$ pc and $v_c = 11.6$ km sec^{-1}, similar to those of the well-known Galactic cluster 47 Tuc. As the figure shows, the surface representing the evolution fluctuates randomly throughout, but it does show a clear overall evolution which is of the same nature as that in the continuous limit (cf. Fig. 3.5). In particular, the population grows with time predominantly at shorter radii ($a < 10R_\odot$). As before, we start with a small number of primordial compact binaries with various initial distributions, and find that, by $t \sim 1-1.5$ Gyr, the distribution "heals" to a form which is independent of the initial choice of distribution. The fluctuations differ in detail from run to run, of course, as we

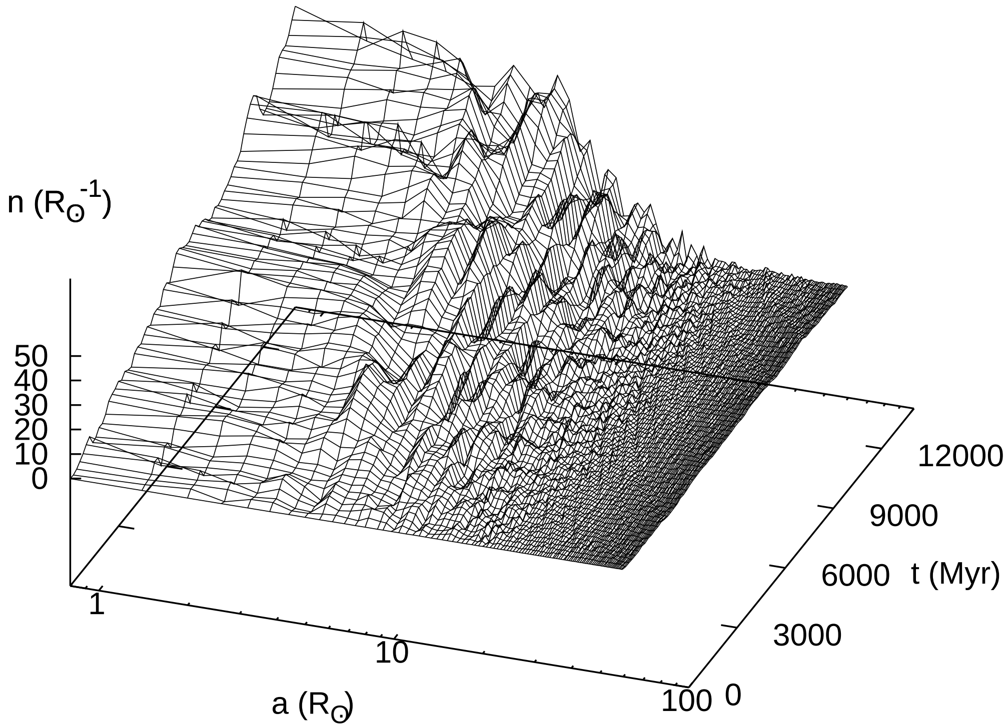

Figure 4.1: *A typical example, i.e., one "realization" of the evolution of the binary distribution function* $n(a,t)$*. Globular cluster parameters are chosen to be roughly those of* 47 Tuc*, as explained in text (also see Fig. 3.5).*

choose different seeds for random number generation, but the overall nature of the evolution remains the same for all runs. Indeed, the results for different runs seem to represent different variations about a *mean* surface, which is very close to that in the continuous limit, as in Chap. 3. We explicitly demonstrate this below by displaying temporal and radial slices through the above surface $n(a,t)$ (see Figs. 3.6 & 3.7) for different runs, and also displaying their averages over a number of runs, which we show to be close to the continuous limit.

To do this, we first show in Fig. 4.2 typical time slices, *i.e.*, $n(a)$ at fixed t, (solid lines) through the surface in Fig. 4.1, for a *single* run, overplotting the continuous limit from Chap. 3 for comparison. The distribution with fluctuations does indeed follow the continuous-limit distribution generally, the same gross features being visible through fluctuations, in particular that $n(a)$ is roughly constant $a \leq 7R_\odot$, and falls off sharply at larger radii. The overall nearly-self-similar evolution at large times, described in Chap. 3, can also be vaguely discerned through the fluctuations. We have discussed possible causes of such self-similar evolution in Sec. 3.3.1. Next, in Fig. 4.3, we show radial slices corresponding to the evolution in Fig. 4.1, representing the behavior of $n(t)$ at a fixed radius a, overplotted with the continuous limit. Again, the curves from a single run follow, in a statistical sense, the corresponding continuous limits. In particular, it can be seen that the radial slices corresponding to larger values of a tend to saturate by about 6 Gyr, while those for smaller values of a do not show such saturation.

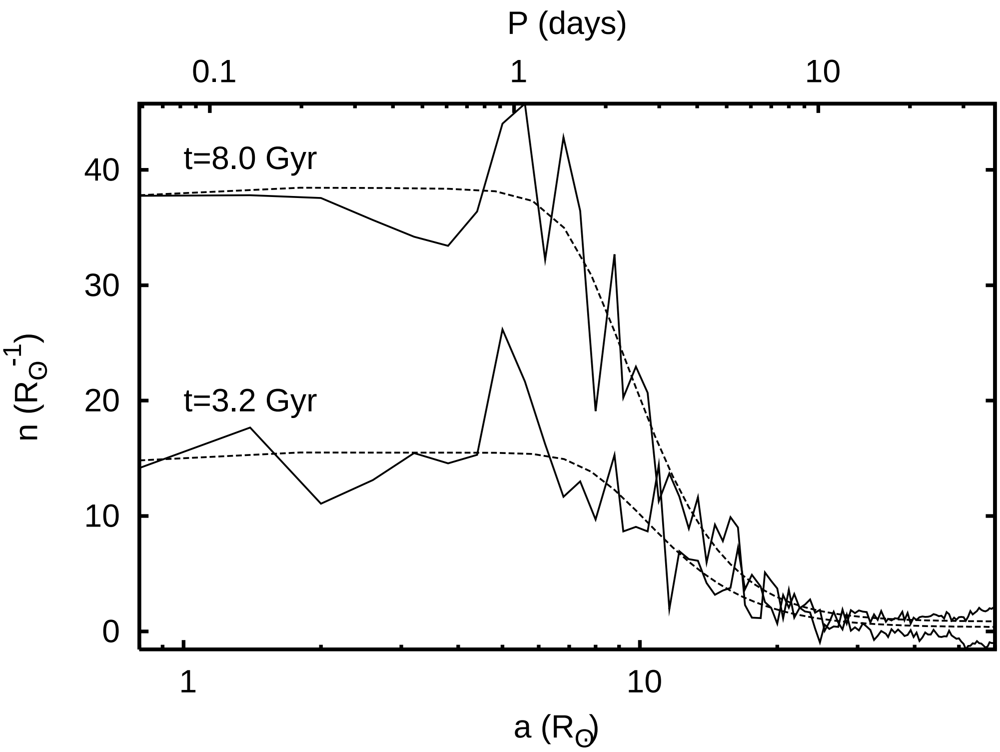

Figure 4.2: *Typical time slices, i.e., $n(a)$ at specified times, for the evolution shown in Fig. 4.1 (solid lines). Overplotted are the same time slices in the continuous limit (dashed lines) from Chap. 3 (cf. Fig. 3.6).*

Finally, in Figs. 4.4 and 4.5, we show the above temporal and radial slices of the average of 12 different runs, overplotted with the the corresponding continuous

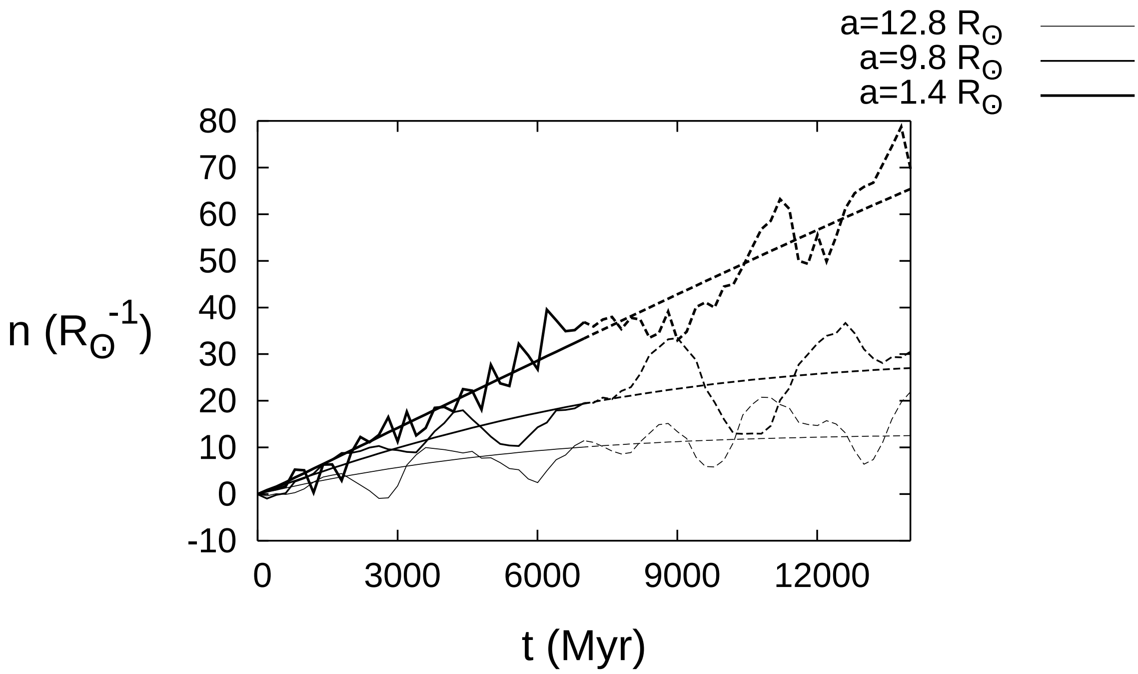

Figure 4.3: *Typical radial slices, i.e., $n(t)$ at fixed values of binary radius for the evolution shown in Fig. 4.1. Overplotted are the same radial slices in the continuous limit from Chap. 3. As in that case, we show the evolution beyond 8 Gyr by dashed lines to indicate that such long evolution times may not be applicable to Galactic GC, but are included here to demonstrate the timescales (cf. Fig. 3.7).*

limits. These figures clearly demonstrate how the fluctuations average out over many runs, so that the mean result approaches the continuous limit.

4.3.2 Number of X-ray binaries

The total number of GC X-ray binaries N_{XB} at a particular time was computed from Eq. (3.40), as in Chap. 3. We determined N_{XB} for a representative evolution time of $\sim$ 8 Gyr, and studied its dependence on the Verbunt parameters Γ and γ, so as to relate our computational results with the systematics of recent

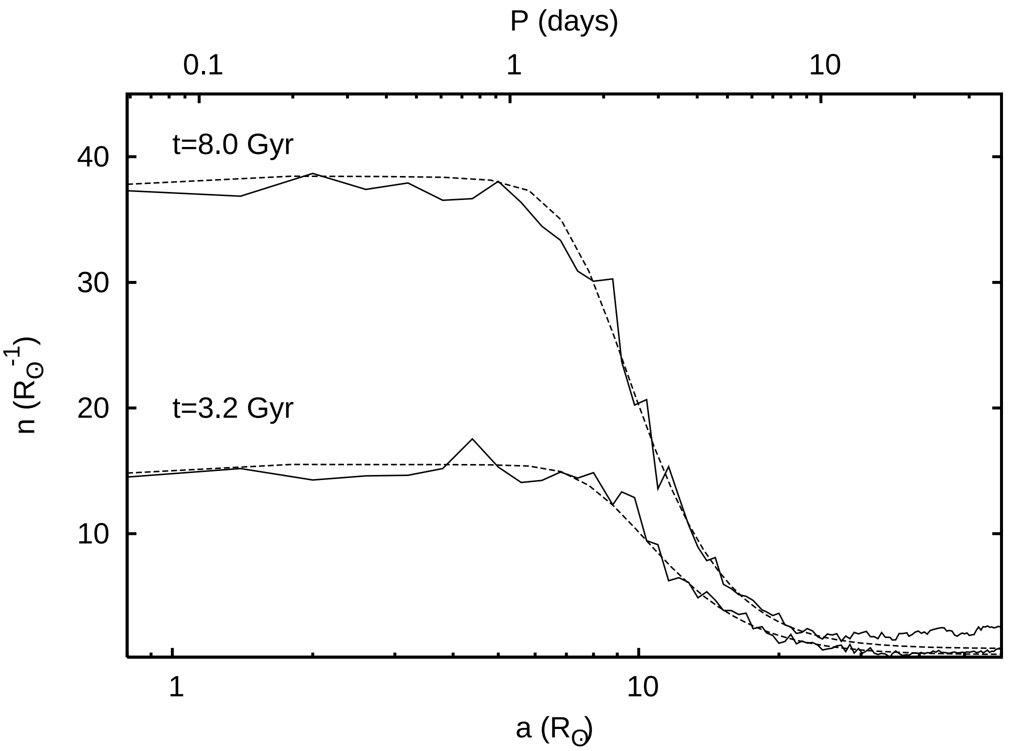

Figure 4.4: *Typical time slices through the average evolutionary surface of 12 different "realizations" of the evolution represented in Fig. 4.1, all with the same GC parameters (solid line). Overplotted are the corresponding time slices in the continuous limit from Chap. 3 (dashed line).*

observations of X-ray binaries in globular clusters (Pooley et al., 2003). For this, we computed, as in Chap. 3, values of N_{XB} over a rectangular grid in $\Gamma - \gamma$ space, spanning the range $\gamma = 1 - 10^6$ and $\Gamma = 10^3 - 10^8$, which encompasses the entire range of Verbunt parameters over which Galactic GCs have been observed (see Fig. 3.1). Although the GCs actually observed so far lie along a diagonal patch over this grid, as explained there, computational results over the whole grid are useful for clarifying the theoretically expected trends.

At a specific grid point (Γ, γ), the values of ρ, r_c and v_c are evaluated using the definitions of Verbunt parameters and the virialization condition (see Sec. 3.3.2 for a detailed discussion). Also as before, we take representative values of primordial stellar binary fraction (k_b) and compact-star fraction (k_X) to be 10 percent and 5 percent respectively.

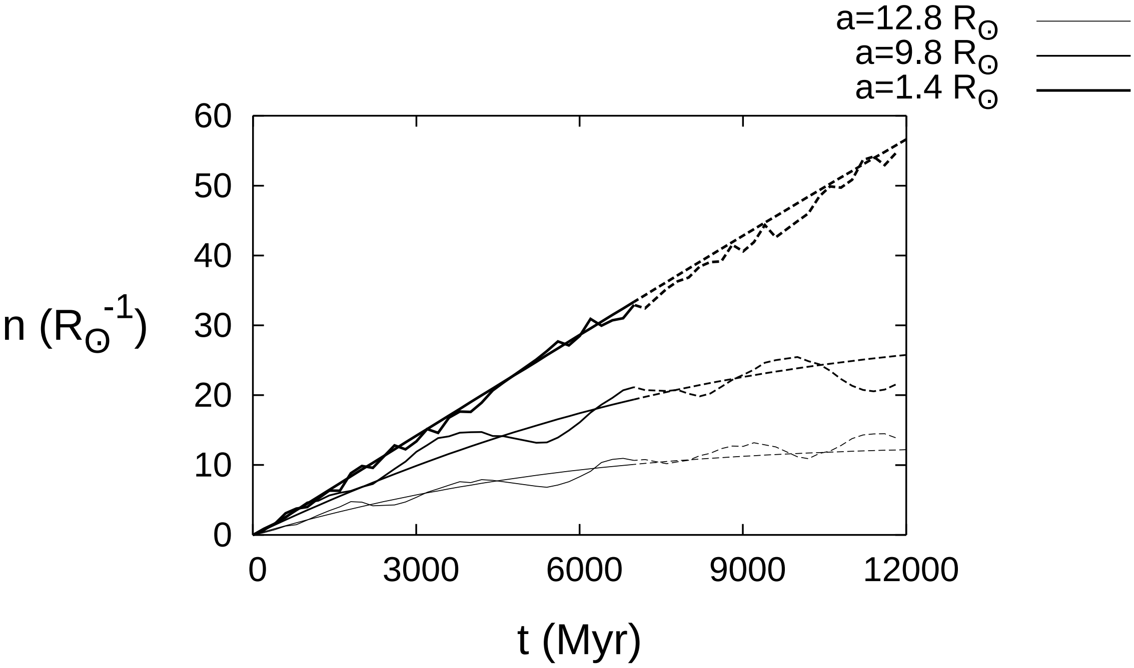

Figure 4.5: *Typical radial slices of the same average evolutionary surface as in Fig. 4.4. Overplotted are the corresponding radial slices in the continuous limit from Chap. 3.*

Fig. 4.6 shows the resulting $N_{XB}(\Gamma, \gamma)$ surface. As indicated in Sec. 3.3.2, the overall fall-off in this surface for $\gamma > 3 \times 10^3$ is a signature of the increasing rates of compact-binary destruction rates with increasing γ, and the above specific value of γ represents an estimate of the threshold above which destruction rates are very important. Further, the trend in N_{XB} with Γ is simple — N_{XB} increases with Γ monotonically, since the dynamical formation rate of compact binaries scales with Γ. What we notice in fig. 4.6 is that this surface also shows random fluctuations due to the stochastic processes, but it generally follows the N_{XB} surface corresponding to the continuous limit, shown overplotted in the same figure. This is similar to what was discussed above for the compact-binary

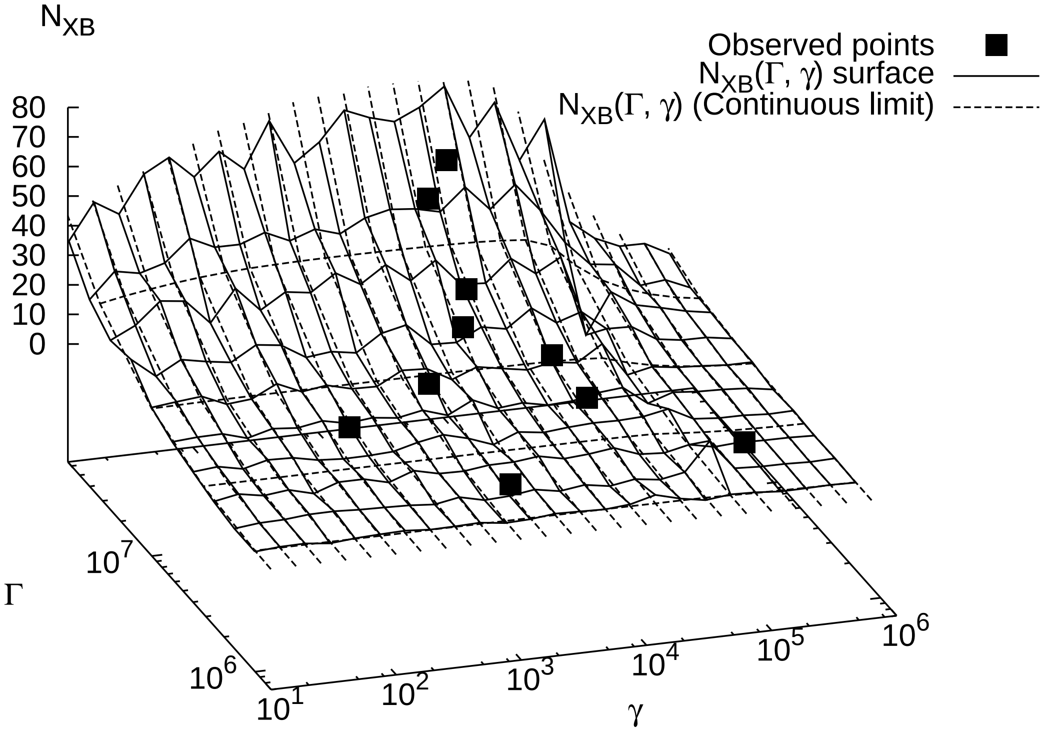

Figure 4.6: *$N_{XB}(\gamma, \Gamma)$ surface (solid line). The observed GCs with significant number of XBs (Pooley et al., 2003) are shown overplotted. Also shown overplotted is the continuous-limit result (dashed line) which is same as in Fig. 3.8.*

distribution, and the point about the mean surface corresponding to the average of many realizations of the stochastic processes being very close to the continuous limit also holds here. We also note that the *total* fluctuations in N_{XB} increase with increasing value of Γ. However, as will become evident from results discussed below, the *relative* fluctuations actually decrease with increasing Γ.

To further clarify the trends and to make comparisons with the results of the "toy" model in Chap. 2 and with those in Chap. 3, we plot the quantity Γ/N_{XB} for a *fixed* value of Γ against γ in Fig. 4.7, displaying the curves for several values of Γ as indicated. As can be seen, the fluctuating Γ/N_{XB} vs. γ curves for various values of Γ follow the same mean trend, although the details of the

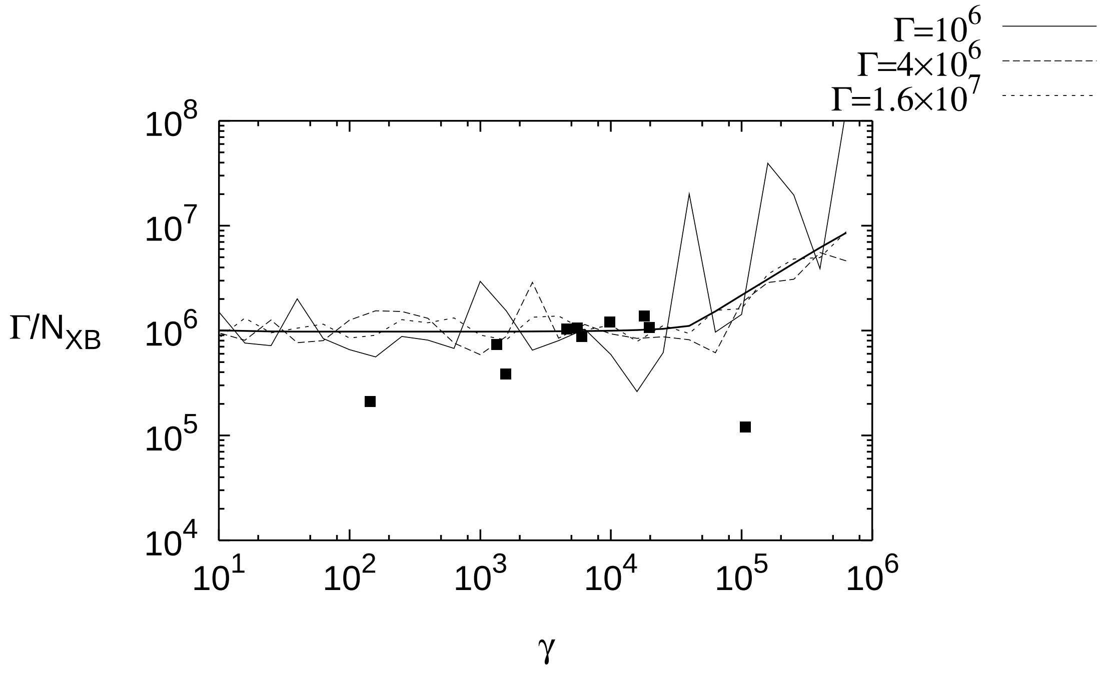

Figure 4.7: *Computed* Γ/N_{XB} *as a function of* γ, *for values of* Γ *as indicated. The continuous-limit result for* $\Gamma = 10^7$ *is shown overplotted (thick line, cf. Fig. 3.9). Also shown overplotted are the positions of Galactic GCs with significant numbers of X-ray sources, as in Fig. 3.9.*

fluctuation are different in different cases. This mean trend is in fact very close to the mean "universal" curve corresponding in the continuous limit evolution of Chap. 3, and is overplotted in the figure. Thus, as in the continuous limit case, the basic scaling of the toy model, *viz.*, $N_{XB} \propto \Gamma g(\gamma)$, where $g(\gamma)$ is a "universal" decreasing function (representing the increasing binary destruction rate with increasing γ, as explained above), does essentially carry over to this detailed model with stochasticity included, suggesting a robust feature of the scaling between different clusters which is expected to be further confirmed by future observations.

Another feature of Fig. 4.7 is that the relative fluctuations in the curves increase with decreasing value of Γ. This is consistent with the intuitive notion that, in all phenomena of this nature, the relative fluctuations in N_{XB} are expected to increase at smaller values of N_{XB}, which occur at smaller values of Γ. More formally, this can be seen as follows. From Eqn. (4.5), it is clear that, over an interval Δt, the relative variance in the number of events of type X is:

$$r_X(a) = (1 - \overline{R}_X(a)\Delta t).$$

For the range of Γ and γ considered in this work, we found that Δt was actually close to Δt_c in most cases, so that $\Delta t \sim \gamma^{-1}$ roughly. Since the formation rates scale as $R_X \sim \Gamma$, we have:

$$r_X(a) = \left(1 - \mathcal{O}\frac{\Gamma}{\gamma}\right).$$

Therefore, for a fixed γ, $r_X(a)$ increases as Γ (and hence N_{XB}) decreases.

4.3.3 Comparison with observations

In Secs. 4.3.1 and 4.3.2 we saw that the basic trends of the results, as obtained from the stochastic Boltzmann equation (4.1), are the same as those obtained from the Boltzmann equation in the continuous limit. Therefore, as in Chap. 3, the results from the stochastic Boltzmann equation are consistent with the observations of XB populations in Galactic GCs. Indeed, since fluctuations *are* present in the dynamical processes under study here, we should ideally compare theoretical trends including fluctuations with observational results, as we do here, where Fig. 4.6 shows the positions of the observed GCs with significant numbers of X-ray sources from Pooley et al. (2003) in the $\gamma - \Gamma - N_{XB}$ co-ordinates. The observational points do lie near the computed $N_{XB}(\gamma, \Gamma)$ surface. In Fig. 4.7, we compare the $\Gamma/N_{XB} - \gamma$ curves with the positions of the observed points, showing that most points do indeed lie near the curves.

In Fig. 4.8 we plot the computed contours of constant N_{XB} in the plane of Verbunt parameters, similar to what we did in Fig. 3.10, but now with the fluctuations included. The fluctuations are clearly seen to be larger for smaller values

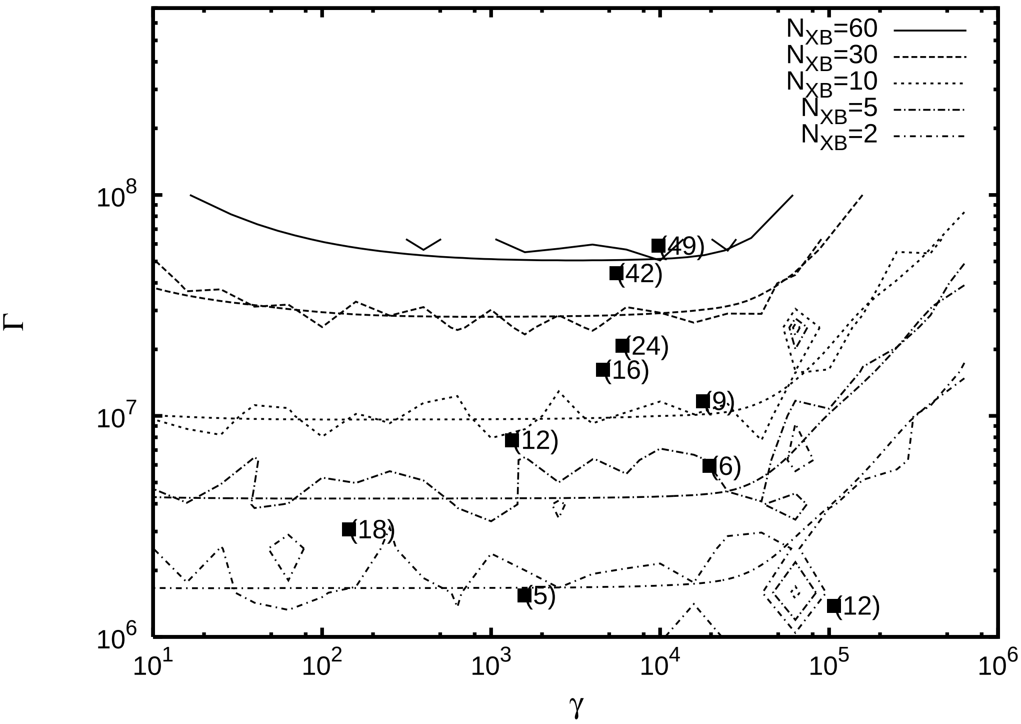

Figure 4.8: *Contours of constant N_{XB} in the plane of Verbunt parameters. Corresponding contours in the continuous-limit case are shown overplotted, using the same line-styles for easy comparison. Positions of GCs with significant numbers of X-ray sources are also overplotted, with the corresponding N_{XB} in parentheses, as in Fig. 3.10.*

of N_{XB}, as expected, and as mentioned above. Again, the observed numbers generally agree well with the present contours which include fluctuations, and these contours do generally follow the continuous-limit contours of Chap. 3, which are shown overplotted.

4.4 Discussions

We have described in this chapter a scheme for introducing stochasticity into the Boltzmann study of compact-binary evolution in globular clusters that we began in Chap. 3. Our scheme involves the use of stochastic calculus (for the first time in this subject, to the best of our knowledge), whereas previous studies in the subject have normally used Monte-Carlo methods of various descriptions — depending on the particular aspect of the problem being studied — for handling stochasticity (see, *e.g.*, Hut, McMillan & Romani (1992); Di Stefano & Rappaport (1994); Fregeau et.al. (2003); Fregeau & Rasio (2007)). With the aid of this scheme, we have demonstrated that the joint action of inherently stochastic and continuous processes produces evolutionary trends which necessarily contain fluctuations that vary between individual "realizations" of the stochastic processes, as expected. However, these trends do generally follow those found in the continuous-limit approximation of Chap. 3, and when trends are averaged over more and more realizations, the mean trend comes closer and closer to the continuous-limit one. In this sense, the continuous limit is very useful as an indicator of the expected mean trend. On the other hand, the magnitude of the fluctuations seen in any given realization, particularly in certain parts of parameter space, suggest that one should compare the results of a typical realization to observations, in order to get a feel for expected fluctuations in the data from stochastic dynamical processes alone, *i.e.*, apart from those coming from uncertainties in the observational methods of obtaining the data.

Boltzmann approach in its original form appealed to us because of its ability by definition to handle weak, frequent, distant encounters and strong, rare, close encounters on the same footing. Of course, the approach is of practical use only when probabilities or cross-sections of such encounters are known from detailed studies of individual encounters through numerical experiments, as is the case for our current use of this approach. It was generally believed that, since Fokker-Planck methods were normally used for handling only the weak, frequent, distant encounters above, treating their cumulative effect as a diffusion in phase space, this argument would also apply to Monte-Carlo Fokker-Planck methods. However, in a novel feature included recently by Fregeau, Rasio and co-authors (Fregeau et.al., 2003; Fregeau & Rasio, 2007) in their Monte-Carlo method, both of the above types of encounters are handled in the following way.

The dynamical evolution of the cluster is treated by a basically Hénon-type Monte-Carlo method, which describes this evolution as a sequence of equilibrium models, subject to regular velocity perturbations which are calculated by the standard Hénon method for representing the average effect of many weak, frequent, distant encounters (see Fregeau et.al. (2003) and references therein). In addition, the strong, rare, close encounters are by handled by (a) keeping track of the (Monte-Carlo-realized) positions of the objects in the cluster, and so deciding whether two given objects will undergo a strong, close encounter or not, by a *rejection method* very similar to that described above in Sec. 4.2.1, and then (b) treating these encounters first (i) through cross-sections compiled from analytic fits to numerical scattering experiments (Fregeau et.al., 2003), exactly as we have done throughout our approach, and then, (ii) in a more detailed approach, through a direct integration of the strong interaction at hand using standard two- and three-body integrators (Fregeau & Rasio, 2007).

A direct comparison of our results with those of above authors is, for the most part, not possible, since we focused primarily on the formation, destruction and hardening of a compact binary population in a given GC environment, while Fregeau et. al focused primarily on the dynamical evolution of the GC environment in the presence of a given *primordial* binary population. However, there is one feature on which we were able to roughly compare our results with those obtained by these and earlier authors. This is the problem of hardening of primordial binaries in GCs, pioneering studies which were performed through direct Fokker-Planck integration by Gao et.al. (1991), and through Monte-Carlo method by Hut, McMillan & Romani (1992), and again recently through the above Monte-Carlo method by Fregeau et.al. (2003). In an early test run of our scheme, we studied this problem by “turning off” the binary formation and destruction terms in our scheme, thereby studying only the hardening of the primordial binary population through our Boltzmann approach. The results we obtained for the progressive hardening of the binary a-distribution profile (from an initial profile which was uniform in $\ln a$, as in all the above references, and in our work) were, indeed, very similar to those given in the above references.

In a pioneering study, Di Stefano & Rappaport (1992, 1994) explored the tidal-capture formation and subsequent evolution of compact binaries in GCs, concentrating on recycled, millisecond pulsars in the first part of the study (Di Stefano & Rappaport, 1992), and on CVs in the second part (Di Stefano & Rappaport, 1994). These authors followed the histories of many neutron stars against a given background representing a GC core (parameters corresponding to 47 Tuc and ω

Cen were used as typical examples), employing Monte-Carlo methods to generate tidal-capture events in this environment. They followed the subsequent orbital evolution of these binaries due to hardening by gravitational radiation and magnetic braking, until Roche lobe contact occurred. In those cases where such contact occurred through orbit shrinkage before the low-mass companion could reach the giant phase due to its nuclear evolution, these authors did not follow further evolution of the binary, while they did so when the contact occurred due to the evolutionary expansion of the companion.

From the above considerations, Di Stefano and Rappaport estimated the expected number of recycled pulsars and CVs in GCs like 47 Tuc and ω Cen, and also gave the orbital-period distribution of the above binaries at two points, *viz.*, (a) just after tidal capture and orbit circularization, and (b) at Roche-lobe contact. However, their orbital-period distributions cannot be compared directly with those given here (or Chap. 3) for the following reason. In the Monte-Carlo method of these authors, tidal capture occurs at different times for different binaries, as does Roche-lobe contact. Thus, showing the orbital-period distribution at any of the above two points means, in effect, that the period-distributions at different times are being mixed. By contrast, we have studied the evolution of the orbital period-distribution in time, displaying "snapshots" of the whole distribution at various times, which we called "time slices" above and also in Chap. 3. In our display, for example, at any given time, some binaries are in Roche-lobe contact and some are not. Indeed, it seems that the orbital period-distributions just after tidal capture, as given by Di Stefano & Rappaport (1992), should be compared with corresponding N-body results given in Portegies Zwart et.al. (1997b), and indeed they appear rather similar. We have, of course, pointed out in Sec. 3.4, and stress the point here again, that our orbital period-distributions are to be regarded at this stage as intermediate steps in our calculation — rather than final results to be compared with future data on orbital period-distributions of X-ray binaries in GCs — because stellar-evolutionary effects on binary evolution have not been included yet in our scheme (also see below). With this inclusion, the aim would be to produce the GC-analogue of such orbital period-distributions as have been computed by Pfahl et.al. (2003) for LMXBs *outside* GCs.

In addition to the above improvement, we listed in Secs. 3.4 & 3.5, various other improvements and extensions that are to be implemented in our scheme in future. For example, the compact-binary distribution function above can be looked upon as one obtained by integrating the full, multivariate distribution function which includes other variables, *e.g.*, the binding energy of the binary in the gravitational potential of the GC — the so-called *external* binding energy (or, equivalently, the position of the binary within the GC potential well (Hut, McMillan & Romani, 1992)), over these other variables. It would be most instructive to be able to follow the evolution in these additional variables in a more elaborate future scheme.

Encouraged by the veracity of the continuous limit, as presented in this chapter, we plan to conclude our program of the first stage of exploration of our Boltzmann scheme by studying one more problem in the same spirit of demonstration of feasibility as we have followed here and in Chap. 3. This is the question of compact-binary evolution in the environment of an *evolving* GC. Whereas, in keeping with the tradition of numerous previous studies, we have so far treated the GC environment as a fixed (*i.e.*, unchanging in time) stellar background, in reality a GC is believed to undergo considerable evolution following the long, quasi-static, "binary-burning" phase, passing through phases of deep core collapse, (possible) gravothermal oscillations, and so on. In this study, which we take up in the next chapter, we demonstrate that, at the current level of approximation in our scheme, and in the continuous limit, it is possible to follow the evolution of compact-binary populations of GCs through these phases of GC evolution, at the expense of only a modest amount of computing time.

Chapter 5

Evolution of Compact-Binary Populations in Globular Clusters: A Boltzmann Study. Evolving Clusters in the Continuous Limit

5.1 Introduction

In this chapter, we study the effect of GC evolution on that of its compact-binary population through the Boltzmann scheme introduced in Chaps. 3 & 4. As a first exploration, we study here the evolution of the compact-binary population in an evolving GC core in the *continuous-limit* approximation introduced in Chap. 3, deferring the inclusion of stochastic effects to a future work. The basic generalization involved in handling an evolving core is that the essential core parameters ρ, v_c and r_c now evolve with time (and so do the Verbunt parameters Γ and γ), while rates of individual formation, destruction, and hardening processes remain as they were in Chap. 3. We so model the time-evolution of the core parameters analytically that they roughly mimic that found in numerical simulations of GC evolution.

In Sec. 5.2.1, we discuss the essential features of the evolution of a GC core (with binaries), and in Sec. 5.2.2, we present a simple analytical model for mimicking the actual evolution found by previous numerical simulations. In Sec. 5.3, we discuss the appropriate generalization of our Boltzmann scheme, and our numerical methods. In Sec. 5.4, we describe our results on the evolution of compact-binary populations in an evolving GC in the continuous-limit approximation. We conclude by discussing our results in Sec. 5.5.

5.2 Evolution of globular clusters

In this section, we briefly describe first the essential features of the dynamical evolution of a GC containing a significant number of primordial binaries, as inferred from numerical simulations of GC evolution. We then discuss the analytical model we use to mimic this evolution for our purposes in this work.

5.2.1 Nature of GC evolution

A GC evolves dynamically as a result of two-body relaxation (Spitzer, 1987; Heggie & Hut, 2003). Simulations of the evolution of such many-body systems have been performed by several authors with the aid of Monte-Carlo and Fokker-Planck schemes (Spitzer (1987) and references therein) or through more detailed and computationally-intensive N-body codes (Makino & Aarseth, (1992)) in special-purpose supercomputers (Makino & Taiji, 1998). Such simulations show that, beginning from an initial model like the Plummer or King model (Heggie & Hut, 2003), a GC containing a significant fraction of stars in binaries evolves through three distinct phases (Gao et.al. (1991), henceforth GGCM91), *viz.*, (a) an initial phase of *core contraction*, (b) a subsequent *quasi-steady* phase of "binary-burning" (see below), and (c) finally a phase of deep *core collapse* and *gravothermal oscillation* (GTO). We briefly discuss these below.

In the above core-contraction phase, the GC core undergoes gravitational contraction rapidly due to two-body relaxation process (Heggie & Hut, 2003), wherein the kinetic energy of the stars in the core is transferred to those in the the surrounding envelope through two-body encounters. Such a phase lasts for about 10 initial half-mass relaxation time t_{rh}. The latter quantity refers to the two-body relaxation timescale (Spitzer, 1987) at the Lagrangian radius containing half of the GC mass. As the core contracts, the stellar density in

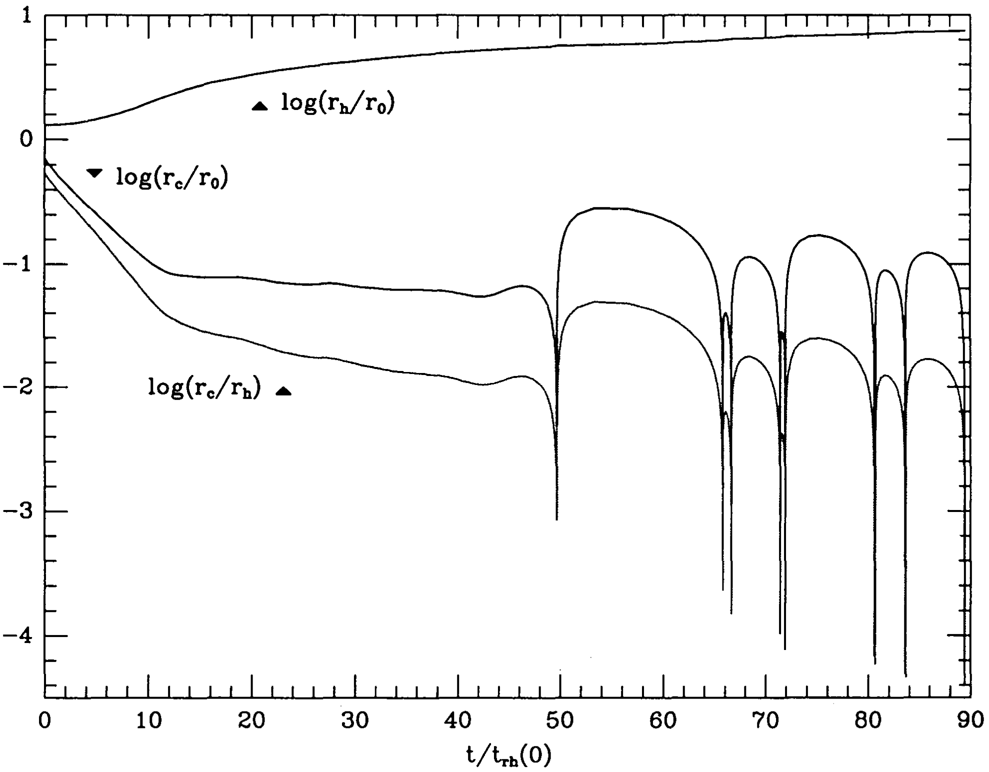

Figure 5.1: *Fig. 1 of GGCM91 reproduced, showing the evolution of the core radius* r_c *and the half-mass radius* r_h *in their Fokker-Planck calculation. The evolution has been computed for an initial plummer sphere of scale-length* r_0 *with 10% primordial binaries. The time has been measured in the calculation in units of the initial half-mass relaxation time* $t_{rh}(0)$*, which we denote by* t_{rh} *here. See GGCM91 for details.*

the core increases, and the primordial binaries in the GC preferentially segregate into the core due to *dynamical friction* (Chandrasekhar, 1942), which refers to the effective retarding force experienced by a individual moving star or binary due to the gravitational forces of the surrounding stars. At a certain point, the core density becomes large enough that significant amounts of kinetic energy are imparted to the core stars due to the recoils they receive during the process of collisional hardening of the binaries through binary-single star encounters in the core. This process of "binary heating" of the core eventually becomes significant enough to stop further core contraction and so end the first phase, leading to a quasi-steady phase during which the core radius remains roughly constant. In an obvious analogy with nuclear burning during stellar evolution, this phase is often referred to as the "binary burning" phase of a GC core.

Typically after several tens of t_{rh}, most of the hard binaries are ejected out of the system due to the large recoil velocities they receive in the above star-binary encounters, thus depleting the energy source which was keeping the core in the above quasi-steady phase. The GC then undergoes deep core-collapse, entering the third phase of its evolution. It was found in the above simulations (Sugimoto & Bettwieser, 1983; Makino, 1996), if the number of stars in the GC is sufficiently large ($N \geq 7000$, say), the core undergoes gravothermal oscillations (GTO) following its first deep core-collapse. These oscillations consist of alternate deep collapses and large expansions of the core. They arise essentially due to the large difference between the relaxation times of the core and the envelope (Heggie & Hut, 2003). As demonstrated by the above numerical simulations (GGCM91 and references therein, as also later work), the core can expand by an order of magnitude during these GTO, and the typical duration of the expanded phase is usually much longer than that of the collapsed phase. This GTO phase may continue for several tens of t_{rh}. The ultimate fate of the GC is decided by the processes of dissolution which act on it, *e.g.*, (a) continual escape of stars from the GC envelope, and (b) tidal stripping of the GC in its orbit in the galactic potential, when it passes (repeatedly) through parts of the orbit where galactic tidal forces are the strongest, *e.g.*, at or near the bar of a barred spiral galaxy.

5.2.2 An analytical model

We now present a simple analytical model for the time-variations of r_c, v_c and ρ which is based on the above numerical simulations of GC evolution, and which captures the essential features of a typical evolution of these parameters through the above three phases. For this introductory work, we chose the results of the GGCM91 simulations as a template, which have been cited widely, and confirmed generally by other simulations in the same time frame. This template is shown in Fig. 5.1, reproduced from Fig. 1 of GGCM91.

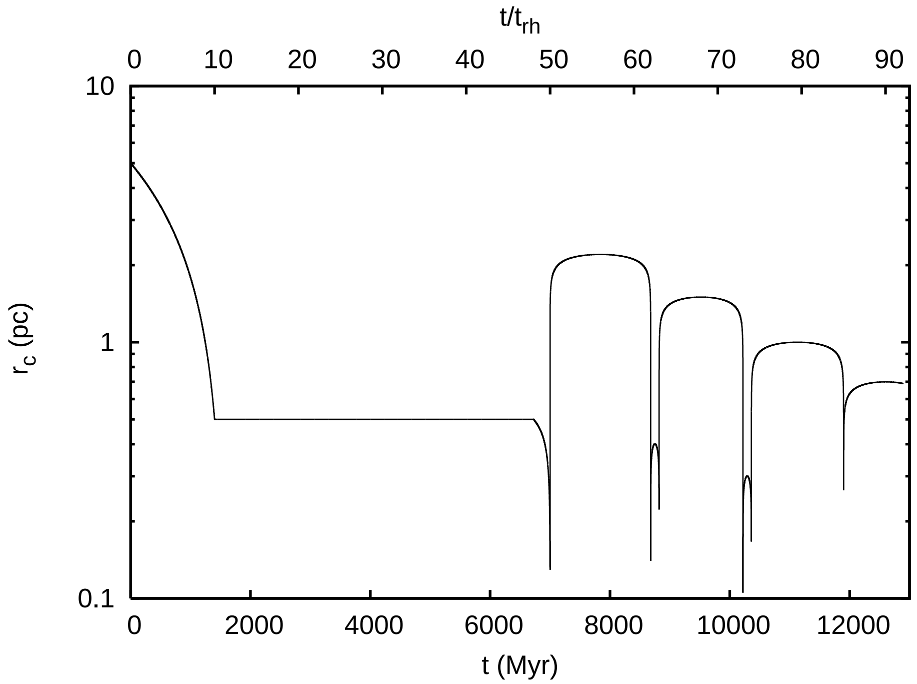

Figure 5.2: *The template evolution $r_c(t)$ according to Eqn. (5.1), which has been constructed to follow that of GGCM91. We take the core density $\rho_c = 6.4 \times 10^4 M_\odot$ pc^{-3} and the radius $R_c = 0.5$ pc in the quasi-steady phase (represented by the horizontal line), which are similar to those observed for the GC* 47 Tuc *(see text). For convenience of the reader, the time axis is labelled both in absolute terms (bottom axis) and in units of t_{rh} (top axis).*

We have constructed a simple, analytic description of this template which is qualatitatively correct, and adequate for our purposes here. We display this analytical template in Fig. 5.2. Its mathematical description in terms of the model core radius $r_c(t)$ is as follows:

$$r_c(t) = \begin{cases} r_c[10 - (9/10t_{rh})t] & (t \leq 10t_{rh}) \\ R_c & (10t_{rh} < t < 48t_{rh}) \\ (r_c/\log(2t_{rh}))\log(50t_{rh} - t) & (48t_{rh} \leq t < 50t_{rh}) \\ \vdots & \vdots \\ A(r_c/5t_{rh})[\log(t - 63t_{rh}) + \log(73t_{rh} - t)] & (63t_{rh} < t < 73t_{rh}) \\ \vdots & \vdots \end{cases} \tag{5.1}$$

The first piece of the above analytical model represents the initial phase of contraction of the core, during which its radius decreases by about an order of magnitude, settling at a value of R_c which corresponds to the quasi-steady phase of binary burning, represented by the constant value R_c in Fig. 5.2. The latter phase is, of course, that of constant core parameters which we evoked in Chaps. 3 & 4, as had been done by many previous authors (see references in Chap. 3). This phase continues upto $\sim 48t_{rh}$, at which point deep core-collapse starts, subsequently developing into GTO. We mimic these with the aid of the relatively simple analytic forms given above, roughly representing the amplitudes and durations of the GTO seen in the GGCM91 results as displayed in Fig. 5.1.

From the above evolutionary profile of R_c, we obtain that of the core density $\rho(t)$ with the aid of the assumption that the mass of the core remains roughly constant. Finally, the evolutionary profile of the velocity dispersion is obtained from the condition of virialization. These profiles are shown in Fig. 5.3. With the aid of these profiles, the evolutionary profiles of the Verbunt parameters $\Gamma(t)$ and $\gamma(t)$ can be readily obtained from the expressions for these parameters given in Sec. 3.2.1. Evolution of the Verbunt parameters are shown in Fig. 5.4. Note that our analytical model has basically only two input parameters, *viz.*, the core radius R_c and the core density ρ_c in the quasi-steady phase, the scale of all other core parameters following from these. For these two parameters R_c and ρ_c, we adopt the values corresponding to 47 Tuc, as we did in the previous chapters. For the timescale t_{rh}, we adopted an approximate value of ~ 140 Myr, which corresponds to the median value of the observed half-mass relaxation times of the Galactic GCs (see GGCM91 and references therein). The dimensionless amplitudes A of the oscillations in Eq. (5.1) were, of course, determined by the requirement of roughly reproducing the GGCM91 results.

5.3 Boltzmann scheme with evolving core

Generalization of the Boltzmann scheme for an evolving stellar background is straightforward: one replaces the constant Verbunt parameters of Chap. 3 & 4 with the time-evolving ones described above. The formal Boltzmann equation

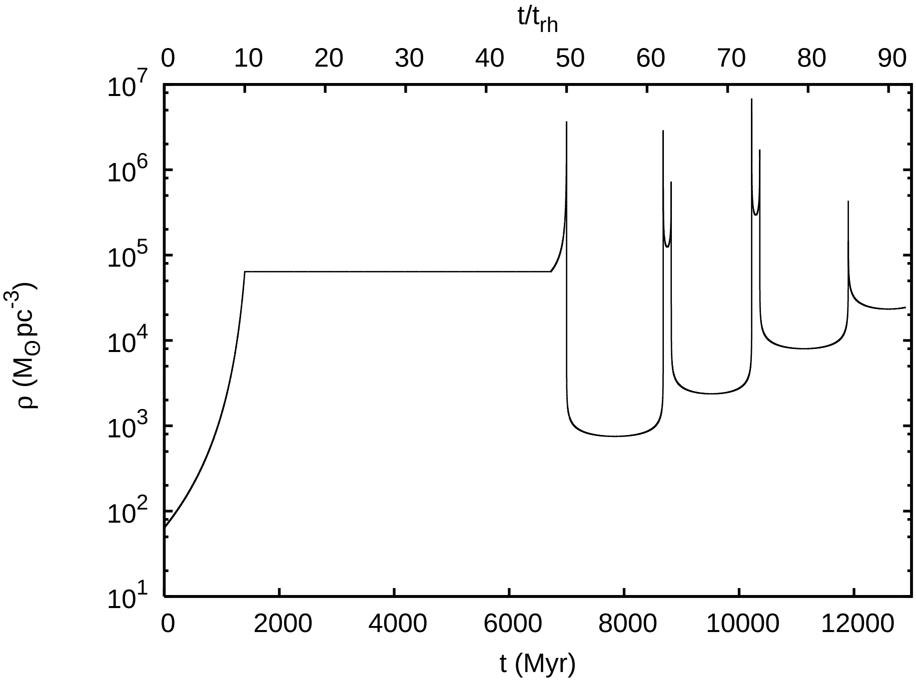

(a)

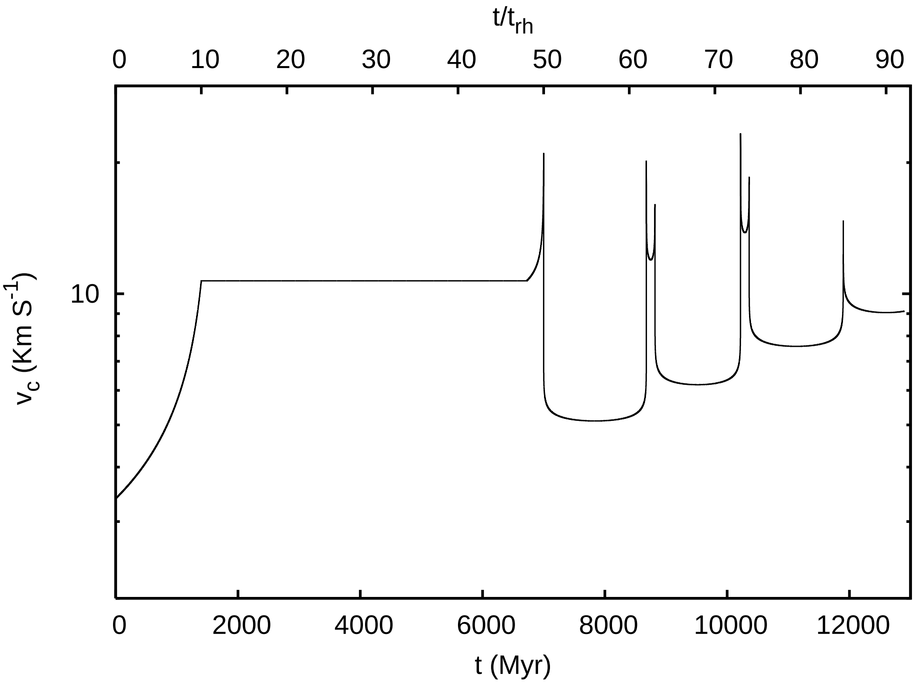

(b)

Figure 5.3: *Core density evolution $\rho(t)$ (top panel) and core dispersion velocity evolution $v_c(t)$ (bottom panel) corresponding to the $r_c(t)$ in Fig. 5.2. $\rho(t)$ has been obtained from mass conservation in the core and $v_c(t)$ is derived assuming that the core is virialized. For convenience, the time axis is labelled both in Myrs and in units of t_{rh} (see text).*

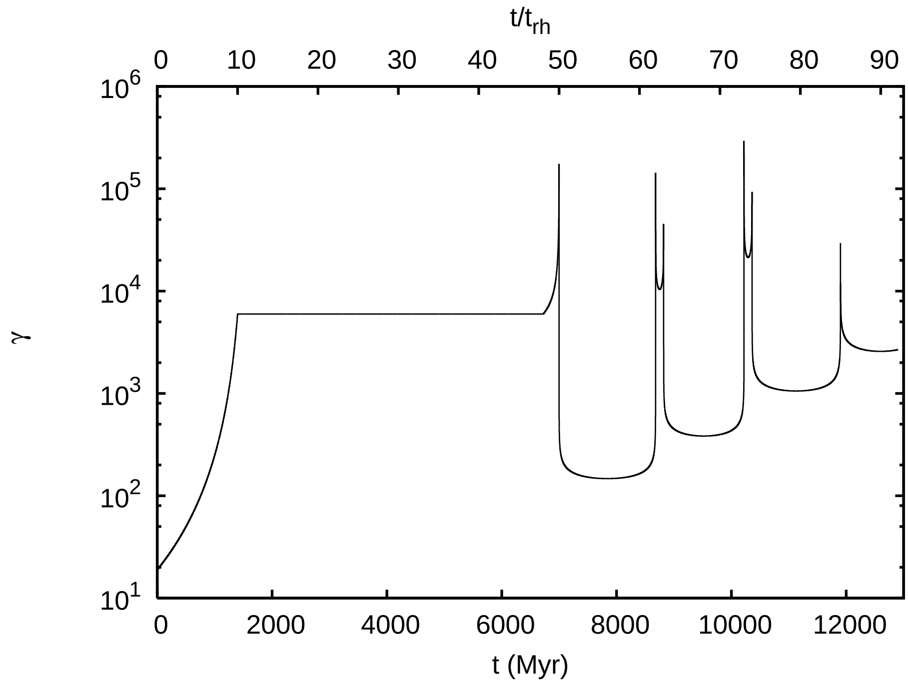

(a)

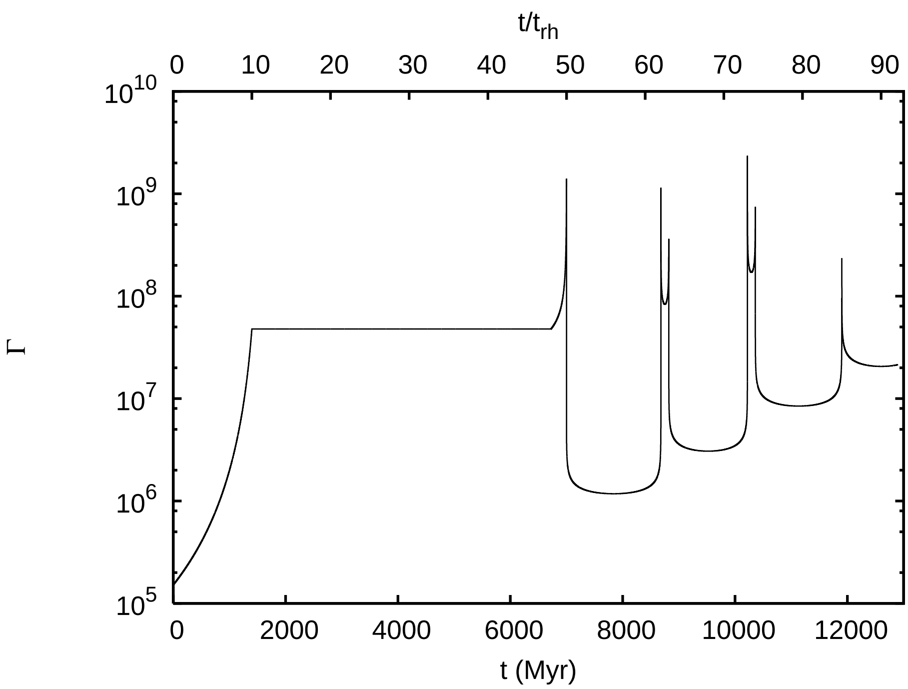

(b)

Figure 5.4: *Evolution of the Verbunt parameters $\gamma(t)$ (top panel) and $\Gamma(t)$ (bottom panel) corresponding to the evolutions of the core parameters in Figs. 5.2 & 5.3.*

remains the same as before, *viz.*,

$$\frac{\partial n(a,t)}{\partial t} = R(a,t) - n(a,t)D(a,t) - \frac{\partial n(a,t)}{\partial a} f(a,t), \tag{5.2}$$

The formation rate $R(a,t)$ consisting of the tidal capture ("tc") rate $r_{tc}(a,t)$ and the "ex1" exchange rate $r_{ex1}(a,t)$ as

$$R(a,t) = r_{tc}(a,t) + r_{ex1}(a,t), \tag{5.3}$$

remains formally as before, but we have to remember now that these rates are now time-dependent even in the continuous limit, since they follow the evolution of the Verbunt parameters, $\Gamma(t)$ and $\gamma(t)$. Similar arguments hold for the destruction rate $D(a,t)$, consisting of the "ex2" exchange rate $r_{ex2}(a,t)$ and the dissociation ("dss") rate $r_{dss}(a,t)$ as

$$D(a,t) = r_{ex2}(a,t) + r_{dss}(a,t). \tag{5.4}$$

These arguments also hold, of course, for the collisional hardening rate (which is part of the total hardening rate $f(a,t)$), wherein the fixed value of γ in the earlier calculations is now replaced by the $\gamma(t)$, as above.

In this work, we only consider compact-binary evolution with an evolving GC core in the *continuous limit*, *i.e.*, the analogue of what we did in Chap. 3 for a static core. The purpose is to identify those essential new features which enter due to the evolution of the core.

We solve Eqn. (5.2) using the two-step Lax-Wendorff method (Press et.al., 1992) as before (see Sec. 3.2.6, where we described the advantages of this method). In the present case, one has to so vary the time-step Δt for solving Eqn. (5.2) during the computation as to ensure stability and convergence. A necessary condition to be satisfied for this is the (time-dependant) Courant condition (Press et.al., 1992):

$$\Delta t(t) = \eta \frac{\Delta a}{f_{max}(t)}, \qquad \eta < 1 \tag{5.5}$$

Here, Δa is the mesh interval in a for solving Eqn. (5.2) and $f_{max}(t)$ is the maximum value of $f(a,t)$ at time t within the range of a over which the integration is performed.

5.4 Results

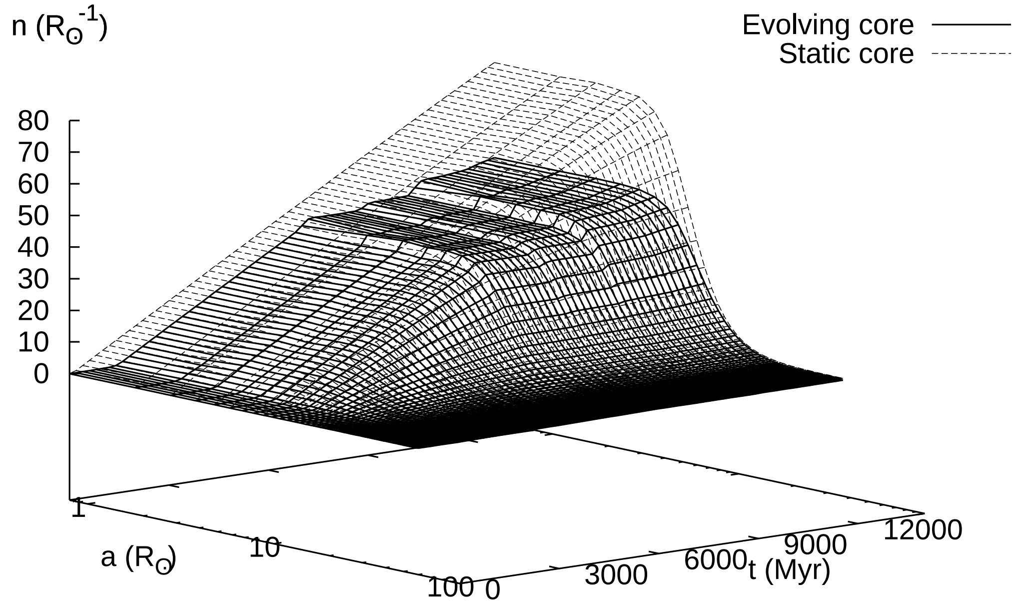

Figure 5.5: $n(a,t)$ *surface corresponding to the evolution represented in Figs. 5.2 & 5.3 (solid line). For comparison, the corresponding evolution of* $n(a,t)$ *for a static core is overplotted (dashed line) where the core parameters are taken to be same as those in the quasi-steady phase, i.e.,* $\rho = \rho_c = 6.4 \times 10^4 M_\odot\ \mathrm{pc}^{-3}$, $r_c = R_c = 0.5$ *pc and* $v_c = V_c = 10.7$ *Km* S^{-1}.

The surface traced out by the solid lines in Fig. 5.5 shows $n(a,t)$ resulting from Eqn. (5.2) using the evolutionary model described in Sec. 5.2. The GC core parameters are chosen such that in the quasi-steady phase they are similar to those of 47 Tuc, *i.e.*, $\rho_c = 6.4 \times 10^4 M_\odot\ \mathrm{pc}^{-3}$ and $R_c = 0.5$ pc (see Sec. 5.2.2). It is seen that the shape of the time slices remains similar to that in the static case, but that of the radial slices is significantly modified (cf. Fig. 3.5). In other words, the orbital-radius distribution of the binary population is not qualitatively modified by core evolution, but the *time-evolution of this distribution is.* To elucidate this point, the static-core cases with $\rho = \rho_c$, $r_c = R_c$ and $v_c \approx 10.7$ Km S^{-1} are overplotted in Fig. 5.5 (dashed lines) for various orbital radii. (The above value of v_c is obtained by applying virial theorem with the assumed values of ρ_c and R_c and is therefore equal to that for the evolving-core model during its quasi-steady phase, which we henceforth denote by V_c. It is interesting to note that this value is nearly equal to that actually observed for 47 Tuc, *viz.*, 11.4 Km S^{-1} Pryor & Meylan (1993). This may suggest that virialization holds, at least approximately, for this GC, making it an appropriate choice for illustrating our model.)

Figures. 5.5 & 5.6 demonstrate that, in the beginning, the growth of the compact-binary population is delayed by roughly the time taken for the initial core-contraction phase. This is so because the core density is sufficiently low over most of this phase that the Verbunt parameter Γ is small, and so are the dynamical formation rates (see Fig. 5.4). Only as this phase approaches the quasi-steady phase do the encounter rates become large enough to initiate rapid binary formation. Because of this delay in growth initiation, the size of the compact-binary population with an evolving core is always somewhat smaller than what it would be if we started with a static core with the same parameters as those which are relevant to the quasi-steady phase. During the quasi-steady phase, the binary population builds up in a way which is very similar to that found for the static core (cf, Fig. 5.6), as expected. It is in the deep core-collapse and GTO phase, however, that the most remarkable new features appear. After a very brief interval of rapid increase of the binary population during the first deep core-collapse, corresponding to the first kink in the radial slice at $t \approx 7.5$ Gyr in Fig. 5.6, the population growth is essentially halted during the subsequent GTO phase, with a few more upward, generally smaller kinks visible at later times. Crudely speaking, therefore, the binary population *saturates* at the value it attains at the beginning of the deep core-collapse and GTO phase.

These last features are easy to understand in the light of the evolutionary behavior of the essential core parameters given earlier. During the deep core-collapse and GTO phase, the core spends most of its time in expanded, low-density phases, as is clear from Figs. 5.1, 5.2, and 5.3. Consequently, the Verbunt parameter Γ also has low values (with accompanying low binary-formation rates) over most of

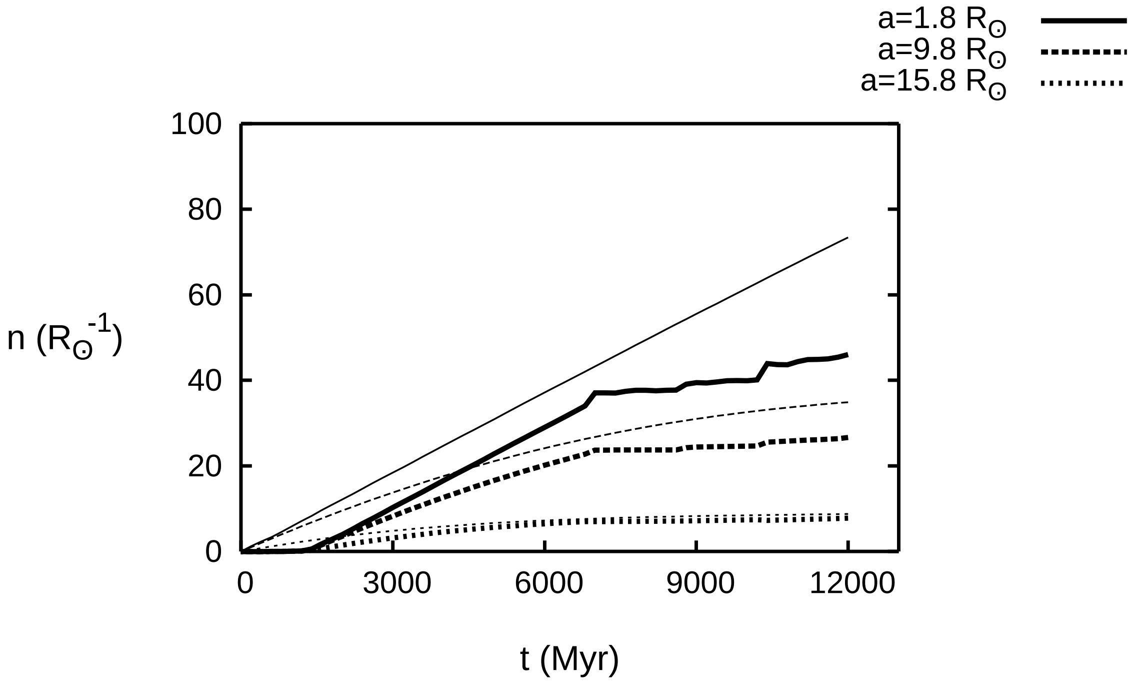

Figure 5.6: *Radial slices of the $n(a,t)$ surfaces from Fig. 5.5. Note that, while there is a monotonic rise in the population for the static core (thin line) with time, compact-binary formation practically ceases after $t \sim 7.5$ Gyr for the evolving core (thick line), where the deep core-collapse and GTO phase starts. Small upward kinks in the population correspond to sharp spikes in the Verbunt parameters during the very short-lived, deep core-collapses (see text).*

this phase, interspersed with very brief, sharp spikes of large value (with accompanying high binary-formation rates) corresponding to the repeated episodes of deep core collapse, as seen in Fig. 5.4. The features seen in Fig. 5.6 during this phase are now clear: the upward kinks in the binary population correspond to the latter spikes in Γ, and the plateaus or saturation phases correspond to the former lows in Γ. As the durations of the spikes are very small compared to those of the extended lows (see Fig. 5.4), there is little overall growth in the binary population during this entire phase, making it an overall "saturation" phase.

Figures 5.5 & 5.6 further demonstrate that, except for an initial delay in starting binary production as described above, the build-up of the binary population for an evolving core is very similar to that for the static core upto $t \sim 7.5$ Gyr. It follows that, upto about this age of the GC, the results of a static-core calculation (with core parameters corresponding to the quasi-steady phase of the evolving GC) are expected to give a reasonable representation of the actual results for an evolving core. For comparison, note that we used an evolutionary time of $t \sim 8$ Gyr in our calculations in Chaps. 3 & 4. It is clear that if the static-core calculations are continued considerably beyond such limiting times, they would lead to a considerable overestimate of the compact-binary population, in view of the saturation effect found here during the deep core-collapse and GTO phase.

5.5 Conclusions & Discussion

In this chapter, we have introduced a generalization of our Boltzmann scheme for describing compact-binary evolution in the *evolving* core of a GC. This generalization is quite straightforward and remains computationally inexpensive. We have restricted ourselves here to an exploration of the results of the above generalization of the continuous-limit approximation, in order to identify the basic features. A more complete description would be one including the stochastic effects as in Chap. 4: this is deferred to a future project.

Our main result from the above generalization is that the formation of compact binaries in a GC core is primarily restricted to the quasi-steady or binary-burning phase. In the deep core-collapse and GTO phase that follows this phase, binary production almost stops because the core spends most of this phase at low values of the Verbunt parameter Γ, which dominantly determines the rate of binary production. Indeed, since it is clear from Fig. 5.4 that the other Verbunt parameter γ, which determines the rate of binary destruction and also that of collisional hardening (see Sec. 3.2.1), is similarly low over most of this phase, it is roughly correct to say that star-star and star-binary encounter rates have little overall effect on the compact-binary population in this phase. (They do have strong but very short-lived effects during the spikes in the Verbunt parameters described above and evident in Fig. 5.4, of course.) Thus, crudely speaking, the overall behavior of this phase is as if the GC core has vanished, so that the population of compact binaries already produced reaches saturation, and simply "coasts along", *i.e.*, evolves as if it were outside a GC.

We also find that the nature of the orbital radius/period distribution $n(a)$ of the compact binaries at any time t is not substantially affected by the evolution of the GC core. As pointed out in earlier chapters, we have not yet taken into account detailed stellar evolution of the companion to the compact star, direct collision with red giants, and so on, so that our description is currently applicable to CVs and short-period LMXBs. However, the above conclusion about the insensitivity to GC evolution is likely to remain valid even after the inclusion of these effects, since GC evolution timescale is generally much longer than those on which these effects occur.

To some extent, our results here put in the proper context the widespread previous use (including our own in the last two chapters) of a static (*i.e.*, constant in time) stellar background (Hut, McMillan & Romani, 1992; Portegies Zwart et.al., 1997b). The simple evolving-core model studied here suggests that the essential connection is that between an assumed static background and the quasi-steady binary-burning phase of a GC core. For typical half-mass relaxation times ($\sim$ 140 Myr) of Galactic GCs, this phase lasts upto $t \sim 7.5$ Gyr, so that a static-core calculation over a similar duration is likely to give a reasonable account of the evolving-core results, while one continued considerably beyond this duration is likely to lead to a considerable overestimate. Sine our own calculations in Chaps. 3 & 4 were over a duration of $t \sim 8$ Gyr, we were roughly self-consistent within the confines of our model.

Chapter 6

Summary and Discussions

6.1 Summary

In this section, we summarize the results that we described in the previous chapters. This thesis deals with the evolution of compact binary population in GCs as they are formed and destroyed dynamically and evolve at the same time. All the important dynamical processes have been considered, *viz.*, tidal capture (tc), exchange (ex1 & ex2) and dissociation (dss) (see Sec. 1.5 for a discussion). The main objective was to study the nature of evolution of a compact-binary population in a dense stellar environment like the core of a GC and estimate quantities like the number of X-ray binaries N_{XB} that can be directly compared with observations (see Sec. 1.4.2). Throughout this work, we have characterized the GC core through two observable quantities, *viz.*, the star-star encounter rate Γ and the binary-single-star encounter rate γ (see Chap. 3 and references therein), for which we coined the name Verbunt parameters. We obtained our results in terms of these parameters to make a direct connection between the compact-binary population evolution as obtained from our model and the dynamical nature of the GC and also to compare the results with the observations.

A dynamically formed binary may in general be detached and become an X-ray binary after the non-degenerate companion fills its Roche-lobe (commonly known as Roche-lobe overflow or RLO) through evolution of the binary (see Sec. 1.4.1). Evolution of such pre X-ray binaries or PXBs are not only governed by "natural" mechanisms, *viz.*, orbital angular momentum loss, but as well by repeated encounters with the surrounding stars in the GC core, which we call collisional hardening.

We develop our approach in a step by step manner. We begin with a simple-minded approach for modelling the PXB hardening upto the Roche-lobe contact phase and infer a scaling in the PXB hardening timescale (Chap. 2). We then demonstrate a qualitative comparison of this scaling with the observed Galactic GC X-ray binary population using a "toy" model for evolution of GC X-ray binaries. In a much more detailed approach, we develop a Boltzmann scheme for compact binary population evolution in a GC, wherein we utilize a collisional Boltzmann equation for evolving the compact-binary population. In the first step, we develop this scheme for a static stellar background in the continuous limit, in which we ignore the discrete and stochastic nature of dynamical encounters and model all the rates corresponding to dynamical encounters as continuous functions (Chap. 3). In the next step, we incorporate the stochasticity in the dynamical processes by considering dynamical rates that randomly fluctuate about their means in a stochastic Boltzmann equation (Chap. 4). The fluctuations are modelled to have similar nature as that in a Monte-Carlo simulation. Finally, we consider the effect of the dynamical evolution of the host GC by modelling the evolution of the stellar background according to the results obtained from simulations of GC evolution and follow the compact-binary population evolution in this evolving background using the Boltzmann equation (in the continuous limit) (Chap. 5).

6.1.1 Collisional hardening of compact binaries in GCs

In a preliminary attempt, we consider essential mechanisms for orbit-shrinkage or "hardening" of compact binaries in GCs to the point of Roche-lobe contact and X-ray emission phase, focussing on the process of "collisional hardening" due to encounters between binaries and single stars in the cluster core (Chap. 2). The interplay between this kind of hardening and that due to emission of gravitational radiation produces a characteristic scaling of the orbit-shrinkage time τ_{PXB} with the Verbunt parameter γ representing binary-single-star encounter rate, *viz.*, $\tau_{PXB} \propto \gamma^{-4/5}$ (see Sec. 2.2). We then investigate possible effects of this scaling on populations of X-ray binaries N_{XB} in GCs within the framework of a simple "toy"scheme for describing the evolution of PXBs in GCs. We find that the expected qualitative trends sufficiently supported by the observed Galactic GC X-ray binary population (Pooley et al., 2003) to encourage us toward a more quantitative study (see Fig. 2.4).

6.1.2 Evolution of compact-binary populations in GCs: A Boltzmann Study. The continuous limit

In a more detailed study as described in Chap. 3, we explore a "Boltzmann scheme" for studying the evolution of compact binary populations in GCs, wherein we utilize a bivariate Boltzmann equation in compact binary radius a and time t (Eqn. (3.5)) for studying the evolution of compact binary population in an unevolving GC core. The compact binary population is described by a combined distribution function $n(a, t)$, which, for a smaller than the Roche-lobe contact point ($a_L \approx 2R_\odot$) represents LMXBs and larger a represents PXBs. We include processes of compact-binary formation by tidal capture and exchange encounters, their destruction by dissociation and exchange mechanisms, and binary hardening by encounters (*i.e.*, collisional hardening), gravitational radiation and magnetic braking, and also mass transfer following the Roche-lobe contact. The rates of all these dynamical events have been estimated using the cross sections of these events (see Secs. 3.2.4 & 3.2.5), that have been determined either theoretically (Heggie, 1975) or by detailed numerical experiments by several authors in the literature (Spitzer (1987); Heggie, Hut & McMillan (1996) and references therein). However, the dynamical processes are intrinsically stochastic in nature, and we study the non-probabilistic, continuous limit in this first step.

In this work, we particularly focus on two aspects, *viz.*, (a) the evolution of the period distribution of GC compact binaries and (b) the number of X-ray sources N_{XB} in GCs as a function of the Verbunt parameters. From our computations, we find that the period distribution of the X-ray binaries is such that $n(a) = dN_{XB}/da$, the number of X-ray binaries per unit interval of the orbital radius a, is roughly constant for a smaller than the Roche-lobe overflow point $a_L \approx 2R_\odot$. For $a > a_L$, which represent PXBs, $n(a)$ remains constant with a upto $a \approx 7R_\odot$, and falls off sharply for larger a (see Figs. 3.5 & 3.6). Using typical values of Galactic GC parameters, *e.g.*, binary fraction in the core, the compact star fraction and the age of the cluster (see Chap. 3), we find that the model number of X-ray binaries N_{XB} and its expected scaling with Verbunt parameters are in good agreement with the observations of Galactic globular clusters (Pooley et al. (2003), see Sec. 1.4), as demonstrated in Fig. 3.8. We also find that for a *given* Γ, the $\Gamma/N_{XB}(\gamma)$ curve is nearly *independent* of the choice of Γ over the observed ranges of Γ and γ, indicating a *universal* behavior with γ (see Fig. 3.9), as already indicated by the toy model in Chap. 2.

6.1.3 Evolution of compact-binary populations in GCs: A Boltzmann study. Introducing stochasticity

In Chap. 3, a major simplification that has been adapted is the assumption of "smoothed" rates of the dynamical processes which represents their mean rates in a continuous limit. As an important development over the continuous-limit model, we take into account in Chap. 4, the discrete and stochastic nature of the dynamical processes by considering all the dynamical rates as randomly fluctuating about their means. We model these fluctuations (see Sec. 4.2.1) as those would have been in Monte-Carlo simulations using the so called "rejection method" as performed earlier by several authors. The mean rate functions are of course taken to be same as those in the continuous limit in Chap. 3. We apply the the existing methods of stochastic calculus (see Sec. 4.2.2), also known as the Itô calculus (see Appendix C), to compute the (stochastic) evolution of $n(a,t)$ using the stochastic version of the Boltzmann equation given by Eqns. (4.1) & (4.2).

To make a direct comparison with the continuous-limit case, we perform the same set of computations as in that case with identical sets of parameters. All the results are found to statistically agree with the continuous-limit results in the sense that the former represent random fluctuations about the latter results in all the cases. Specifically, we find that the resulting $n(a,t)$ surface fluctuates randomly about the continuous-limit surface (see Figs. 4.2 & 4.3), the details of the fluctuations being different for different runs (*i.e.*, runs with different random number seeds). This is further evident from the observation that an average surface of several independent runs are much smoothed out and tends to coincide with the continuous-limit surface (see Figs. 4.4 & 4.5). The XB distribution function dN_{XB}/da is, in this case, a randomly fluctuating distribution about the corresponding uniform mean distribution. As in the case of the continuous limit described above, we also explored the dependence of computed number of XBs N_{XB} on the Verbunt parameters using the same choices of GC parameters as in that case, and found similar trends and agreement with observations (Fig. 4.6).

6.1.4 Evolution of compact-binary populations in GCs: A Boltzmann Study. Evolving clusters in the continuous limit

In Chaps. 3 & 4, we have ignored the evolution of the host GC itself by assuming a static stellar background. In a realistic GC, the core evolves due to two body relaxation, the kinetic energy deposited in the core due to collisional hardening (binary heating), escape of stars and binaries and winds from massive stars (mass-loss heating) (see Sec. 5.2.1). The effect of all these competing clauses in a GC has been studied extensively through Fokker-Planck, Monte-Carlo and direct N-body simulations. The evolution of the GC core results in time variation of the Verbunt parameters, which in turn affects the evolution of the compact binary population. To take into account the effect of dynamical evolution of the GC, we utilize the continuous-limit Boltzmann equation to compute the evolution of GC compact binary population using the same models for binary formation, destruction and hardening as in Chap. 3, but now with time-varying GC core parameters (Chap. 5). We analytically model the time-evolution of the core-radius r_c to have its overall characteristics similar to that obtained in earlier simulations of GC evolution (Gao et.al., 1991) and the resulting evolution of core density ρ and dispersion velocity v_c are derived from the simplifying assumptions of constancy of core-mass and virialization respectively (see Sec. 5.2.2).

We find that the formation of the compact binaries begins approximately when the core shrinks to the quasi-steady state and the compact binary population grows as in the case of a static core. However, the formation of compact binaries practically halts as soon as the gravothermal oscillation (GTO) phase (see Sec. 5.4) starts. In other words, the dynamical formation of compact binaries is primarily restricted to the quasi-steady phase. The reason for this is during GTO, the GC core spends most of the time in an expanded phase when the core radius is considerably larger than its quasi-steady value, so that the core density becomes much smaller and the encounter rates drop appropriately. Assuming typical values of half-mass relaxation time of GCs, the compact binaries can be formed only upto $\sim 8-10$ Gyrs, although the lifetime of the GC itself can be longer — of the order of a Hubble time. This implies that the assumption of static core would overestimate the compact binary population, if the evolution were continued with this assumption well beyond $8-10$ Gyr, say upto a Hubble time. This, then justifies our extending the static-core evolution only upto ≈ 8 Gyr, as in Chaps. 3 & 4 (see Sec. 5.5).

6.2 Discussions

The study of X-ray binaries and other kinds of compact binaries in GCs are among the areas in astrophysics which currently receive primary attention both theoretically and observationally. Studying compact binary populations in GCs is essential for understanding the dynamics of GCs. In particular, the density of X-ray binaries is much higher in GCs than that compared to the field as *Chandra* observations indicate (Angelini et.al., 2001; Pooley et al., 2003). It fact, it has been argued that all the X-ray binaries in a galaxy might have been formed in its GCs (White et.al., 2002; Sarazin et al., 2003). Therefore, it is extremely important to make theoretical studies of the X-ray binary population in GCs to interpret these very interesting observations and hence to understand the X-ray binary population in a galaxy. Pioneering contribution has already been provided by several authors in this direction (Di Stefano & Rappaport, 1992, 1994; Hut, McMillan & Romani, 1992; Portegies Zwart et.al., 1997b).

While the use of Boltzmann equation is popular in various branches of physics, *e.g.*, fluid dynamics, kinetic theory of gases, plasma physics, magnetohydrodynamics, and particle physics, our formulation of a Boltzmann scheme for evolving the binary population in a dense stellar system is a new approach in this relatively recent branch of astrophysics. Particularly, to the best of our knowledge, we believe that our use of stochastic calculus for evolving a compact-binary population, as we do in our stochastic formulation, is a pioneering one in this branch of stellar dynamics. There are several important advantages of the Boltzmann scheme. First, this scheme takes into account the distant, frequent and the close, rare encounters in the *same footing*, by the very definition of the Boltzmann equation. In fact, no other techniques (see Sec. 1.6) can handle both of these kinds of encounters in such a natural way, and separate treatments are necessary to incorporate the close encounters. Note that the Fokker-Planck equation is also derived from the Boltzmann equation, but it extracts out only the distant, frequent encounters by approximating the encounter term as a sum of diffusion coefficients (see Sec. 1.6.1). Second, the Boltzmann method is very fast and computationally much inexpensive compared to N-body and also Monte-Carlo methods. For the computations discussed here, it typically takes less than a minute to 1-2 minutes (in the case of evolving background) wall-clock time for a single run, in an ordinary workstation. Third, the Boltzmann scheme is a general and versatile framework and not necessarily limited to the particular analytical model for dynamical formation, destruction and compact-binary evolution that we have adapted in our work. Any suitable model for dynamical encounters and more detailed model for compact-binary evolution can in principle be incorporated in the Boltzmann scheme. We discuss the limitations of our approach below. In Sec. 6.3, we indicate the prospects of the Boltzmann scheme for further developments and also its applications for investigating other interesting and open questions in astrophysics.

6.2.1 Limitations

The work described in this thesis is the application of the Boltzmann scheme for the first time where we limit ourselves to simplified pictures of dynamical encounters and binary evolution. It serves as a feasibility demonstration for this approach and already provides enough interesting results to encourage us to pursue further development of this approach.

There are several limitations in our model. First, we do not take into account the nuclear evolution of the "normal" companion stars in these compact binaries (also see discussions in Chap. 3 & 4). Hence, we restrict ourselves only to "CV-like" X-ray binaries, where the mass-transfer occurs in the main-sequence phase of the companion, so that its nuclear evolution is unimportant. Such kinds of X-ray binaries are CVs and short-period LMXBs (see Chap. 1). When we consider other kinds of X-ray binaries, *e.g.*, wide LMXBs, in which the mass-transfer occurs in the RG phase, we must include nuclear evolution of the companion. However, our comparison with the observations is still justified since the X-ray binaries in the Pooley et al. (2003) sample are mostly CVs. Second, we limit the binary evolution upto the point of period-minimum ($P_{orb} \approx 80$ min), and hence do not consider the "degenerate branch" (van den Heuvel, 1991, 1992) representing ultracompact X-ray binaries (UCXB). Also, we do not incorporate the formation of UCXBs through RG-NS collisions (Verbunt, 1987; Lombardi et.al., 2006). UCXBs consist of a very important class of X-ray binaries (see Sec. 1.4 and references therein) which has recently attracted significant interest, both from theoretical point of view and observationally, so that it is very important to study their population, particularly when one is interested in the GC X-ray luminosity function (also see discussions in Chap. 3). Although UCXBs are very bright X-ray sources ($L_X \sim 10^{36} - 10^{39}$ erg s^{-1}), so that they may completely dominate the bright end of the GC X-ray luminosity function (Bildsten & Deloye, 2004), they are much fewer in number compared to other types of GC X-ray binaries (Ivanova et.al., 2005), making their contribution unimportant when we are comparing only the total population, as in the present work. Among other limitations, we do not consider hydrodynamic effects in our model, *e.g.*, mass-loss during tidal capture, role of multiple exchanges and stellar mass-function in our model, although they are not expected to affect our results severely.

6.3 Outlook

One of the important improvements over the work described in this thesis would be the inclusion of the nuclear evolution of the companion. This would enable us to study the population of various kinds of X-ray binaries in GCs. In particular, a significant fraction of the known bright X-ray binaries consists of wide LMXBs, for which the nuclear evolution of the companion is a key feature. Stellar evolution can be incorporated in the Boltzmann scheme in various ways; those used by previous authors have involved “synthetic” stellar and binary evolution routines like “BSE” (Hurley et.al., 2002) and “SeBa” (Portegies Zwart et.al., 2001). Another important extension would be to consider UCXBs. This is particularly important when one is interested in the GC X-ray luminosity function (see above). To include this kind of binaries, one has to model their formation through RG-NS collisions appropriately, utilizing the results of simulations of RG-NS encounters (*e.g.*, Lombardi et.al. (2006)).

Apart from the above X-ray binaries, other related binary systems of much recent interest in GCs are millisecond radio pulsar (MRP) and double neutron-star (DNS) systems. A significant number of MRPs have been discovered in GCs from radio observations. As discussed in Chap. 1, MRPs are descendants of LMXBs, so that the MRP population evolution can also be studied using our scheme, with appropriate extensions. The study of the DNS population is also very important, since inspiralling double neutron stars are promising sources of gravitational waves. Such DNS systems are produced in significant numbers in GCs through the “ex2” type of exchange (in our terminology) described in earlier parts of this thesis, which can also be looked upon as a double-exchange with neutron stars in a binary initially consisting of two normal, low-mass GC stars (Grindlay et.al., 2006). A study of DNS population of GCs using our Boltzmann scheme will make important contact with planned observations by future gravitational-wave observatories. Finally, inclusion of a mass function for the GC stars would represent an important step towards making the stellar background in the GC more realistic, which would be particularly relevant when nuclear evolution of the companion star is introduced into the scheme. We plan to take up some of the above projects in near future.

Appendix A

Analytical expression for $\tau(\gamma)$

We drop the magnetic braking term in the integral on right-hand side of Eqn. (2.7), as explained in the text, and obtain:

$$\tau_{PXB}(a_i, \gamma) \approx \int_{a_f}^{a_i} \frac{da}{\alpha_{\mathrm{GW}} a^{-3} + \alpha_{\mathrm{C}} a^2 \gamma} = \frac{1}{\alpha_{\mathrm{GW}}} I_1, \tag{A.1}$$

where,

$$I_1 \equiv \int_{a_f}^{a_i} \frac{da}{a^{-3} + B a^2 \gamma}, \qquad B \equiv \frac{\alpha_{\mathrm{C}}}{\alpha_{\mathrm{GW}}} \tag{A.2}$$

Defining $\delta \equiv B\gamma$ and substituting $\delta a^5 \equiv b^5$ in the above, we get

$$I_1 = \delta^{-\frac{4}{5}} [I]_{b_f}^{b_i}, \tag{A.3}$$

where the indefinite integral $I(x)$ is given by,

$$I = \int \frac{x^3 dx}{1 + x^5} \tag{A.4}$$

Standard expressions for integrals of type I are given in Gradshteyn & Ryzhik (1980) (also, see Dennery & Krzywicki (1996)), from which we get,

$$\begin{aligned} I(x) = -\frac{1}{5}\ln(1+x) - \frac{1}{5}\left[\cos\frac{\pi}{5}\ln\left(1 - 2x\cos\frac{\pi}{5} + x^2\right)\right. \\ \left. + \cos\frac{2\pi}{5}\ln\left(1 + 2x\cos\frac{2\pi}{5} + x^2\right)\right] \\ + \frac{2}{5}\left[\sin\frac{\pi}{5}\tan^{-1}\left(\frac{x - \cos\frac{\pi}{5}}{\sin\frac{\pi}{5}}\right) + \sin\frac{2\pi}{5}\tan^{-1}\left(\frac{x + \cos\frac{2\pi}{5}}{\sin\frac{2\pi}{5}}\right)\right] \end{aligned} \tag{A.5}$$

From equations (A.1), (A.2), (A.3), (A.5),

$$\tau_{PXB}(a_i, \gamma) = \alpha_{\mathrm{C}}^{-\frac{4}{5}} \alpha_{\mathrm{GW}}^{-\frac{1}{5}} \gamma^{-\frac{4}{5}} \left[I \right]_{x=b_f}^{x=b_i} \tag{A.6}$$

Appendix B

Wiener Processes

The *Wiener process* is a formal mathematical description of Brownian motion, a classic example of a stochastic process, wherein a particle (*e.g.*, pollen grain) on the surface of water undergoes random motion due to stochastic bombardment of it by water molecules. A standard description of such a particle is given by the following differential form due to Langevin:

$$dX_t = a(t, X_t)dt + \sigma(t, X_t)\zeta_t dt. \tag{B.1}$$

Here, X_t is one of the components of the particle velocity at time t, $a(t, X_t)$ is the retarding viscous force. The second term on the right-hand side represents the random molecular force, represented as a product of an intensity factor $\sigma(t, X_t)$ and a random noise factor ζ_t, the latter at each time t being a random number, suitably generated.

A standard Wiener process $W(t)$ is often defined as a continuous Gaussian process with independent increments, satisfying the following properties:

$$W(0) = 0, \qquad E(W(t)) = 0, \qquad \mathrm{Var}(W(t) - W(s)) = t - s, \tag{B.2}$$

for all $0 \leq s \leq t$. Here, E represents the expectation value and 'Var' the variance of the indicated stochastic variable[1]. Note that a Wiener process $W_t(\omega)$, can also be thought of as a "pure" Brownian motion with $a = 0$ in Eq. (B.1)

[1]Strictly speaking, the first equation should be written as $W(0) = 0$, w.p.1, where 'w.p.1' stands for 'with probability one', since we are dealing with random variables here. But we shall not go into mathematical rigor here, referring the reader to Kloeden et.al. (1994)

(Kloeden et.al., 1994), wherein the increments $dW_t(\omega)$ for any sample path ω represents a Gaussian white noise.

Eqn. (B.1) can then be rewritten in terms of the *symbolic differential* (see below) $dW_s(\omega) \equiv \zeta_s(\omega)ds$ of a Wiener process, and its integral form

$$X_t(\omega) = X_{t_0}(\omega) + \int_{t_0}^{t} a(s, X_s(\omega))ds + \int_{t_o}^{t} \sigma(s, X_s(\omega))dW_s(\omega) \qquad \text{(B.3)}$$

represents a path integral over the trajectory of the particle for the sample path $X_t(\omega)$, where ω is a particular trajectory of the Brownian particle.

Appendix C

Itô calculus

The problem with the second term on the right-hand side of Eqn. (B.3), which represents an integral along a *Wiener path*, is that it is not defined in ordinary calculus, since $W_t(\omega)$ is not differentiable in the ordinary sense. Such an integral along a Wiener path has to be *redefined* suitably to become acceptable mathematically, and the Itô integral is an example of this. The classical limit-of-sum definition of an integral does not hold for an Itô integral like

$$X_t(\omega) = \int_{t_0}^{t} f(s,\omega)dW_s(\omega), \tag{C.1}$$

since the corresponding finite sum will be divergent over a Wiener path, as sample paths of a Wiener process do not have bounded variance (see above). However, it can be shown that such a sum is *mean-square convergent* under very general conditions (Øksendal, 2004), owing to the well-behaved mean-square properties of Wiener processes. Accordingly, Eqn. (C.1) is defined only in the sense of *mean-square convergence*, with the result that the integral (C.1) is a random variable $X_t(\omega)$ with the following properties:

$$E(X_t) = 0, \qquad E(X_t^2) = \int_{t_0}^{t} E(f(s)^2)ds \tag{C.2}$$

Consider now the well-known *Itô formula* for the transformation of a function $f(X_t)$ of stochastic variable X_t (Gaines, 1995). For simplicity, first assume that X_t follows a stochastic equation of the form

$$X_t = X_{t_0} + \int_{t_0}^{t} a(X_t)dt + \int_{t_0}^{t} \sigma(X_t)dW_t, \tag{C.3}$$

(*i.e.*, the same as Eqn. (B.3) without the explicit time dependence in the continuous and stochastic terms. For brevity, we drop the symbol ω, representing the sample path, from now on. Let us divide the entire time span into time-steps at $t_1, t_2, \ldots t_k, \ldots$ of length $h_1, h_2, \ldots h_k, \ldots$ with the largest step size h_{max}. Then X_t at times t_k and t_{k+1} are related by

$$X_{k+1} = X_k + \int_{t_k}^{t_{K+1}} a(X_t)dt + \int_{t_k}^{t_{K+1}} \sigma(X_t)dW_t, \tag{C.4}$$

where we write $X_k \equiv X_{t_k}$ and $X_{k+1} \equiv X_{t_{k+1}}$ for brevity. The Itô formula states (Øksendal, 2004) that:

$$f(X_t) = f(X_k) + \int_{t_k}^{t} \mathcal{L}f(X_s)ds + \int_{t_k}^{t} f'(X_s)\sigma(X_s)dW_s, \tag{C.5}$$

where the operator $\mathcal{L}$ is defined by:

$$\mathcal{L}f(X_s) \equiv f'(X_s)a(X_s) + \frac{1}{2}f''(X_s)\sigma^2(X_s). \tag{C.6}$$

For explicitly time-dependent continuous and stochastic terms, the Itô formula can be generalized suitably.

We can use Eqn. (C.5) in Eqn. (C.4) to expand $a(X_t)$ and $\sigma(X_t)$ around t_k:

$$\begin{aligned} &X_{k+1} = X_k + a(X_k)h_{k+1} + \sigma(X_k)\Delta W_{k+1} \\ &+ \textstyle\int_{t_k}^{t_{k+1}} \int_{t_k}^{t} \mathcal{L}a(X_s)dsdt + \int_{t_k}^{t_{k+1}} \int_{t_k}^{t} a'(X_s)\sigma(X_s)dW_sdt \\ &+ \textstyle\int_{t_k}^{t_{k+1}} \int_{t_k}^{t} \mathcal{L}\sigma(X_s)dsdW_s + \int_{t_k}^{t_{k+1}} \int_{t_k}^{t} \sigma'(X_s)\sigma(X_s)dW_sdW_t \end{aligned} \tag{C.7}$$

Now, if we discard all terms in Eqn. (C.7) of $\mathcal{O}(h^\alpha)$ for $\alpha > 1$, we obtain

$$X_{k+1} = X_k + a(X_k)h_{k+1} + \sigma(X_k)\Delta W_{k+1} + \frac{1}{2}\sigma'(X_k)\sigma(X_k)\left((\Delta W_{k+1})^2 - h_{k+1}\right), \tag{C.8}$$

which is known as the *Milshtein scheme*. This is the stochastic analogue of the second-order Taylor expansion of ordinary calculus. The Milshtein scheme can be shown to be *strongly* or *pathwise* convergent (Kloeden et.al., 1994) to order h, in the sense that the solution converges to the actual Brownian path as $h_{max} \to 0$. If we restrict the expansion upto the $\mathcal{O}(h^{1/2})$ terms, *i.e.*, upto the first three terms in the right-hand side of (C.7), we obtain a slower ($\sim h^{1/2}$) pathwise convergence, which is known as the *Euler-Maruyama scheme*.

For higher dimensions, with $X_k \in \mathcal{R}^{\mathcal{N}}$ and $W_t \in \mathcal{R}^{\mathcal{D}}$, the second-order stochastic Taylor expansion of X_k^i is given by (see Gaines (1995) and references therein):

$$X_{k+1}^i = X_k^i + a^i(X_k)h_{k+1} + \sum_{j=1}^{\mathcal{D}} \sigma_j^i(X_k)\Delta W_{k+1}^j + \sum_{j=1}^{\mathcal{N}} \sum_{p,q=1}^{\mathcal{D}} \frac{\partial \sigma_p^i}{\partial X^j} \sigma_q^j(X_k) I_{pq}(k, k+1) + R, \tag{C.9}$$

where

$$I_{pq}(k, k+1) \equiv \int_{t_k}^{t_{k+1}} \int_{t_k}^{t} dW_s^p dW_t^q \tag{C.10}$$

and R contains all terms of $\mathcal{O}(h^\alpha)$ for $\alpha > 1$. If $\mathcal{D} \le p, q$ $(p \neq q)$, we obtain upon integration by parts:

$$I_{pq}(k, k+1) + I_{qp}(k, k+1) = \Delta W_{k+1}^p \Delta W_{k+1}^q \equiv B_{pq}(k, k+1). \tag{C.11}$$

If we further define

$$A_{pq}(k, k+1) \equiv I_{pq}(k, k+1) - I_{qp}(k, k+1), \tag{C.12}$$

then we can, with the aid of Eqns. (C.12) and (C.11), express I_{pq} in terms of A_{pq} and B_{pq}. Substituting the result in Eqn. (C.9), we finally obtain,

$$\begin{aligned}
X_{k+1}^i = & X_k^i + a^i(X_k)h + \sum_p \sigma_p^i(X_k)\Delta W_{k+1}^p \\
& + \frac{1}{2} \sum_{j=1}^{\mathcal{N}} \sum_{p=1}^{\mathcal{D}} \frac{\partial \sigma_p^i}{\partial X^j} \sigma_p^j(X_k) \left((\Delta W_{k+1}^p)^2 - h_{k+1} \right) \\
& + \sum_{j=1}^{\mathcal{N}} \sum_{0<p<q\le\mathcal{D}} \frac{1}{2} \left(\frac{\partial \sigma_q^i}{\partial X^j} \sigma_p^j + \frac{\partial \sigma_p^i}{\partial X^j} \sigma_q^j \right) (X_k) B_{pq}(k, k+1) \\
& + \sum_{j=1}^{\mathcal{N}} \sum_{0<p<q\le\mathcal{D}} \frac{1}{2} \left(\frac{\partial \sigma_q^i}{\partial X^j} \sigma_p^j - \frac{\partial \sigma_p^i}{\partial X^j} \sigma_q^j \right) (X_k) A_{pq}(k, k+1) + R
\end{aligned} \tag{C.13}$$

If $\forall\ i, p, q$

$$\sum_{j=1}^{\mathcal{N}} \left(\frac{\partial \sigma_q^i}{\partial X^j} \sigma_p^j - \frac{\partial \sigma_p^i}{\partial X^j} \sigma_q^j \right) = 0, \tag{C.14}$$

then the A_{pq} terms drop out of Eqn. (C.13). Equation (C.14) is called the *commutavity condition* and is usually written as,

$$[\sigma_p, \sigma_q] = 0. \tag{C.15}$$

When the above commutavity condition is not satisfied, the quantities A_{pq}, known as the *Levy areas*, have to be calculated in order to achieve second-order accuracy.

References

Aarseth, S.J., 1963, MNRAS, 126, 223. 30

Aarseth, S.J., 1999, PASP, 111, 1333. xxxi, 30

Aarseth, S.J., 2003, “Gravitational N-Body Simulations”, Cambridge University Press. 23, 31

Antia, H.M., 2002, “Numerical Methods for Scientists and Engineers”, Hindustan Book Agency. 82, 83

Ahmad, A. and Cohen, L., 1973, J. Comput. Phys., 12, 389. 31

Angelini, L., Loewenstein, M. and Mushotzky, R.F., 2001, ApJ, 557, L35. xvii, 2, 8, 14, 15, 35, 140

Ashman, K.M. and Zepf, S.E., 1998, “Globular Cluster Systems”, Cambridge Univ. Press. ix, xv, 6, 7, 15

Bailyn, C.D., 1995, Ann. Rev. Astron. Astrophys., 33, 133. 7

Banerjee, S. and Ghosh, P., 2006, MNRAS, 373, 1188. (BG06) xx, xxi, xxiii, xxiv, xxv, 18, 22, 34, 56, 99

Banerjee, S. and Ghosh, P., 2007, ApJ, 670, 1090. (Paper I) xviii, xix, xxvi, xxvii, 17, 32

Banerjee, S. and Ghosh, P., 2008a, ApJ, 680, 1438. (Paper II) xxviii, xxix, xxx, 32

Banerjee, S. and Ghosh, P., 2008b, in preparation. (Paper III) xxiii, 32

Baumgardt, H., Hopman, C., Potegies Zwart, S. and Makino, J., 2006, MNRAS, 372, 467. 31

Becker, L., 1920, MNRAS, 80, 590. 18

Belleman, R.G., Bédorf, J. and Portegies Zwart, S.F., 2008, NewA, 13, 103. 32

Bildsten, L. and Deloye, C.J., 2004, ApJ, 607, L19. xviii, 17, 93, 94, 95, 142

Bolte, M. and Hogan, C.J., 1995, Nature, 376, 399. 1

Chandrasekhar, S., 1942, "Principles of Stellar Dynamics", University of Chicago Press, Chicago. xxxi, 3, 123

Chang, J. S. and Cooper, G., 1970, J. Comput. Phys., 6, 1. 25

Clayton, D., 1968, "Principles of Stellar Evolution and Nucleosynthesis", McGraw-Hill, New York. 7, 45

Cohn, H., 1979, ApJ, 234, 1036. 23, 25

Cohn, H., 1980, ApJ, 242, 765. 23, 25

Côté, P., Welch, D.L., Fischer, P., Da Costa, G.S., Tamblyn, P., Seitzer, P. and Irwin, M.J., 1994, ApJS., 90, 83. 10

Côté, P. and Fischer, P., 1996, Astron. J., 112, 565. 10

Davies, M.B. and Hansen, B.M.S., 1998, MNRAS, 301, 15. 7

Dennery, P. and Krzywicki, A., 1996, "Mathematics for Physicists", Dover Publications, Inc., New York. 145

Dewi, J.D.M., Podsiadlowski, Ph. and Sena, A., 2006, MNRAS, 368, 1742. 7

d'Inverno, R., 1992, "Introducing Einstein's Relativity", Oxford Univ. Press. xx, 12, 36, 37

Di Stefano, R. and Rappaport, S., 1992, ApJ, 396, 587. 2, 29, 99, 118, 119, 140

Di Stefano, R. and Rappaport, S., 1994, ApJ, 423, 274. 99, 117, 118, 140

Drukier, G.A., Cohn, H.N., Lugger, P M. and Yong, H., 1999, ApJ, 518, 233. 26

Edmonds, P.D., Gilliland, R.L., Guhathakurta, P., Petro, L.D., Saha, A. and Shara, M.M., 1996, ApJ, 468, 241. 9

Eggleton, P.P., 1983, ApJ, 268, 368. 68

Elson, R., Fall, S.M. and Freeman K.C., 1987, ApJ, 323, 54. 2, 6

Fabian, A. C., Pringle, J. E. and Rees, M. J., 1975, MNRAS, 172, 15P. xix, 18, 72, 75, 77, 99

Fregeau, J.M., Gürkan, M.A., Joshi, K.J. and Rasio, F.A., 2003, ApJ, 593, 772. 29, 34, 100, 103, 117, 118

Fregeau, J. M., Cheung, P., Portegies Zwart, S. F. and Rasio, F. A., 2004, MNRAS, 352, 1. 29

Fregeau, J.M. and Rasio, F.A., 2007, ApJ, 658, 1047. 29, 100, 117, 118

Gaines J.G., 1995, in "Stochastic Partial Differential Equations", ed. Etheridge, A., Cambridge University Press. xxx, 33, 101, 105, 106, 149, 151

Gao, B., Goodman, J., Cohn, H. and Murphy, B., 1991, ApJ, 370, 567. (GGCM91) xxiii, xxxi, 3, 5, 25, 26, 33, 56, 58, 118, 122, 139

Ghosh, P. and White, N.E., 2001, ApJ, 559, L97. xxiv, 51

Ghosh, P., 2007, "Rotation and Accretion Powered Pulsars", World Scientific Publications, Hackensack. 11, 12

Gilliland, R,L., Edmonds, P.D., Petro, L., Saha, A. and Shara, M.M., 1995, ApJ, 447, 191. 9

Goodman, J., 1987, ApJ, 313, 576. xxxi

Goodman, J. and Hut, P., 1993, ApJ, 403, 271. 25

Gradshteyn, I.S. and Ryzhik, I. M., 1980, "Table of Integral, Series, and Products", Academic Press, San Diego. 145

Grindlay, J., Portegies Zwart, S. and McMillan, S., 2006, Nature Physics, 2, 116. 2, 20, 143

Grindlay, J.E., 1988, in "The Harlow-Shapley Symposium on Globular Cluster Systems in Galaxies" (Proc. IAU Symp. 126), eds. Grindlay, J.E. and Philip, A.G.D. (Kluwer, Dordrecht). 8

Gunn, J.E. and Griffin, R.F., 1979, Astron. J., 84, 752. 5, 9

Gürkan, M.A., Fregeau, J.M. and Rasio, F.A., 2006, ApJ, 640, L39. xvi, 7

Harris, W.E., 1996, "Globular Clusters in the Milky Way" (Harris, 1996), VizieR On-line Data Catalog: VII/195. x, xv, 2, 62

Heggie, D.C., 1975, MNRAS, 173, 729. xxi, 10, 18, 21, 36, 38, 55, 56, 79, 99, 137

Heggie, D.C. and Hut, P., 1993, ApJS, 85, 347. 26

Heggie, D.C. and Ramamani, N., 1995, MNRAS, 272, 317. 5

Heggie, D.C., Hut, P. and McMillan, S.L.W., 1996, ApJ, 467, 359. xxvi, xxvii, 19, 33, 56, 57, 77, 79, 100, 137

Heggie, D.C. and Hut, P., 2003, "The Gravitational Millon-Body Problem: A Multidisciplinary Approach to Star Cluster Dynamics", Cambridge University Press, Cambridge, UK. xv, xvi, xix, xxiii, xxxi, 3, 4, 5, 10, 14, 19, 22, 26, 30, 55, 122, 124

Hénon, M., 1971a, Ap. Space Sci., 13, 284. 23, 26, 28

Hénon, M., 1971b, Ap. Space Sci., 14, 151. 23, 26, 28

Hills, J.G., 1975a, Astron. J., 80, 809. 10, 18, 22

Hills, J.G., 1975b, Astron. J., 80, 1075. 10, 18

Hills, J.G. and Day, C.A., 1976, Astrophys. Lett., 17, 87. 7

Hurley, J.R., Tout, C.A. and Pols, O.R., 2002, MNRAS, 329, 897. 31, 143

Hut, P., 1983, ApJL, 272, L29. x, 22

Hut, P. and Bahcall, J.N., 1983, ApJ, 268, 319. ix, xxvii, 18, 19, 20, 21, 33, 55, 56, 80, 81, 99

Hut, P. and Verbunt, F., 1983, Nature, 301, 587. 35, 36

Hut, P., 1985, IAUS, 113, 231H. 25, 35, 36, 38

Hut, P. et. al., 1992, PASP, 104, 981. xvii, 10, 14, 35, 36, 56

Hut, P., McMillan, S. and Romani, R.W., 1992, ApJ, 389, 527. xxiii, 29, 33, 56, 58, 59, 117, 118, 120, 134, 140

Hut, P., 1993, ApJ, 403, 256. 18

Hut, P., 2001, in "Astrophysical Supercomputing Using Particles", IAU Symposium, Vol. 208, eds. Makino, J. and Hut, P. 56

Ivanova, N. et. al., 2005, ApJ, 621, L109. xviii, 17, 94, 142

Joshi, K.J., Rasio, F.A. and Portegies Zwart, S.F., 2000, ApJ, 540, 969. 27, 29, 33

Joshi, K.J., Nave, C.P. and Rasio, F.A., 2001, ApJ, 550, 691. 29

Frank, J., King, A. and Raine, D., 2002, "Accretion power in Astrophysics", Cambridge University Press, Cambridge, UK. 12

Kaluzny, J., Kubiak, M., Szymanski, M., Udalski, A., Krzeminski, W., Mateo, M. and Stanek, K.Z., 1998, A&AS, 128, 19. 9

King, I., 1962, Astron. J, 67, 471. 4

Kippenhan, R. and Weigert, A., 1990, "Stellar Structure and Evolution", Springer-Verlag, Berlin. 7, 13, 45

Kloeden, P.E., Platen, E. and Schurz, H., 1994, "Numerical Solution of SDE Through Computer Experiments", Springer-Verlag. xxx, 33, 101, 105, 147, 148, 150

Kraicheva, Z.T., Popova, E.I., Tutukov, A.V. and Yungelson, L.R., 1978, in "Non-stationary Evolution of Close Binaries", ed. Zytkow, A., Polish Academy of Sciences, p.25 xxvii, 46, 80

Kundu, A., Maccarone, T.J. and Zepf, S.E., 2002, ApJ, 574 L15. xvii, 15

Kustaanheimo, P. and Stiefel, E., 1965, Reine Angew. Math., 218, 204. 31

Lanadu, L.D., and Lifshitz, E.M., 1962, "Classical Theory of Fields", Butterworth-Heinemann. 12, 37, 65

Latham, D.W., Hazen-Liller, M.L. and Pryor, C.P., 1985, in "Stellar Radial Velocities" (IAU Colloquium 88), eds. Phillip, A.G.D. and Latham, D.W., Schenectady: L. Davis. 9

Lee, H.M. and Ostriker, J.P., 1986, ApJ, 310, 176. xix, 19, 75, 76, 99

Lee, H.M., 1987a, ApJ, 319, 772. 25

Lee, H.M., 1987b, ApJ, 319, 801. 25

Leonard, P.J.T., 1996, in "The Origins, Evolution and Densities of Binary Stars in Clusters", eds. E.F. Milone and J.C. Mermilliod (ASP, San Francisco). 7

Lightman, A. P. and Shapiro, S. L., 1977, ApJ, 211, 244. 28

Liu, Q.Z., van Paradijs, J. and van den Heuvel, E.P.J., 2001, A&A, 368, 1021.

Lombardi, J.C.Jr., Rasio, F.A. and Shapiro, S.L., 1996, ApJ, 468, 797. 7

Lombardi, J.C., Proulx, Z.F., Dooley, K.L., Theriault, E.M., Ivanova, N. and Rasio, F.A., 2006, ApJ, 640, 441. 142, 143

Lynden-Bell, D. and Wood, R., 1968, MNRAS, 138, 495. 4

Lyne, A.G. and Lorimer, D.R., 1995, Nature, 369, 127. 7

Maccarone, T.J., Kundu, K., Zepf, S.E. and Rhode, K.L., 2007, Nature, 445. xvi, 7

Mackey, A.D., Wilkinson, M.I., Davies, M.B. and Gilmore, G.F., 2007, MNRAS, 379, L40. 7

Mackey, A. D. and Gilmore, G. F., 2003a, MNRAS, 338, 85. 6

Mackey, A. D. and Gilmore, G. F., 2003b, MNRAS, 338, 120. 6

Makino, J., 1996, ApJ, 471, 796. xxxi, 3, 5, 34, 56, 124

Makino, J. and Aarseth, S.J., 1992, PASJ, 44, 141. 30, 55, 122

Makino, J. and Taiji, M., 1998, "Scientific Simulations with Special-Purpose Computers–the GRAPE Systems", Wiley-VCH. 32, 56, 122

Marchal, C., 1990, "The Three-Body Problem", Elsevier, Amsterdam. 18

Marchant, A.B. and Shapiro, S.L., ApJ, 234, 317. 26, 28

McMillan, S.L.W., McDermott, P.N. and Taam, R.E., 1987, ApJ, 318, 261. 75

McMillan, S.L.W. and Hut, P., 1996, ApJ, 467, 348. 10

Michie, R.W. and Bodenheimer, P.H., 1963, MNRAS, 126, 267. 5

Merritt, D., Piatek, S., Portegies Zwart, S. and Hemsendorf, M., 2004, ApJ, 608, L25. 7

Meylan, G. and Heggie, D.C., 1996, A&A. Rv., 8, 1. 10

Mikkola, S., 1984a, MNRAS, 207, 115. 26

Mikkola, S., 1984b, MNRAS, 208, 75. 26

Mikkola, S. and Aarseth, S. J., 1996, Celest. Mech. Dyn. Astron., 64, 197. 31

Miller, M.C., 2007, in "The Multicolored Landscape of Compact Objects and Their Explosive Origins", AIP Conference Proceedings, Volume 924, American Institute of Physics. xvi

Milshtein, G.N., 1974, Th. Prob. Appl., 19, 557. xxx, 106

Murphy, B. and Cohn, H., 1988, ApJ, MNRAS, 232, 835. 25

Narlikar, J.V., 1993, “Introduction to Cosmology”, Cambridge University Press. xv

Øksendal, B., 2004, “Stochastic Differential Equations: An Introduction with Applications”, 6th ed., Springer International Edition. xxx, 33, 101, 105, 149, 150

Paczyński, B., 1971, ARA&A, 9, 183. 45, 68

Paczyński, B., 1990, ApJ, 348, 485. 7

Peters, P.C., 1964, Phys. Rev. B., 136, 1224. 65

Pfahl, E.D., Rappaport, S. and Podsiadlowski, P. 2003, ApJ, 597, 1036. 93, 119

Plummer, H.C., 1911, MNRAS, 71, 460. 5

Podsiadlowski, P., Rappaport, S. and Pfahl, E.D., 2002, ApJ, 565, 1107. 13, 41, 77, 92, 94

Pooley, D. et.al., 2003, ApJ, 591, L131. ix, x, xiii, xvii, xxv, xxviii, 8, 14, 15, 16, 34, 35, 52, 53, 55, 61, 62, 77, 88, 93, 94, 95, 111, 113, 115, 137, 138, 140, 142

Portegies Zwart, S.F. and Meinen, A.T., 1993, A&A, 280, 174. 31

Portegies Zwart, S. F., Hut, P. and Verbunt, F., 1997a, A&A, 328, 130. xxix, 29, 63, 103, 104

Portegies Zwart, S.F., Hut, P., McMillan, S.L.W. and Verbunt, F., 1997b, A&A, 328, 143. xxiii, 29, 33, 41, 45, 46, 57, 58, 65, 74, 77, 100, 119, 134, 140

Portegies Zwart, S., Hut, P., Makino, J. and McMillan, S.L.W. 1998, A&A, 337, 363. 26

Portegies Zwart, S.F., McMillan, S.L.W., Hut, P. and Makino, J., 2001, A&A, 321, 199. 19, 30, 31, 93, 143

Portegies Zwart, S., Baumgardt, H., Hut, P., Makino, J. and McMillan, S.L.W., 2004, Nature, 428, 724. xvi, 2, 7

Portegies Zwart, S.F., Belleman, R.G. and Geldof, P.M., 2007a, NewA, 12, 641. 32

Portegies Zwart, S.F., McMillan, S.L.W., Groen, D., Gualandris, A., Sipior, M. and Vermin, W., 2007b, NewA (in press), arXiv:0711.0643. 32

Press, W.H., and Teukolsky, S.A., 1977, ApJ, 213, 183. 19, 75, 99

Press, W.H., Teukolsky, S.A., Vetterling, W.T., Flannery, B.P., 1992, "Numerical Recipes in C", Cambridge University Press. xxvii, xxix, 82, 83, 104, 105, 107, 129

Pryor, C., McClure, R.D., Fletcher, J.M. and Hesser, J.E., 1989, Astron. J., 98, 596. 9

Pryor, C. and Meylan, G., 1993, in "Structure and Dynamics of Globular Clusters", ASP Conference Series, vol. 50, eds. Djorgovski, S.G., and Meylan, G. xv, 2, 131

Reed, L.G., Harris, G.L.H., and Harris, W.E., 1994, Astron. J., 107, 555. 2

Rosenbluth, M.N., MacDonald, W.M. and Judd, D.L., 1957, Phys. Rev., 107, 1. 25

Rubenstein, E.P., and Bailyn, C.D., 1997, ApJ, 474, 701. 10

Sarazin, C.L., Kundu, A., Irwin, J.A., Sivakoff, G.R., Blanton, E.L. and Randall, S.W., 2003, ApJ, 595, 743. xvii, 15, 16, 17, 140

Shakura, N.I. and Sunyaev, R.A., 1973, A&A, 24, 337. 12

Shapiro, S.L. and Marchant, A.B., 1978, ApJ, 225, 603. 26, 28

Shapiro, S.L., 1985, in "Dynamics of Star Clusters", IAU Symposium 113, eds. Goodman, J. and Hut, P., Dordrecht: Reidel. 25

Shapiro, S.L. and Teukolsky, S.A., 2004, "Black Holes, White Dwarfs and Neutron stars", Wiley-VCH. 11

Shull, J.M., 1979, ApJ, 231, 534. xxi, 23, 38, 39, 40, 53, 56, 66, 99

Sigurdsson, S. and Phinney, E.S., 1993, ApJ, 415, 631. xxix, 10, 33, 56, 58, 59, 103

Sigurdsson, S. and Phinney, E.S., 1995, ApJS, 99, 609. 56, 58, 59

Skumanich, A., 1972, ApJ, 171, 565. 38

Spitzer, L.Jr. and Härm, R., 1958, ApJ, 127, 544. 23

Spitzer, L.Jr. and Hart, M. H., 1971a, ApJ, 164, 399. 28

Spitzer, L.Jr. and Hart, M.H., 1971b, ApJ, 166, 483. 28

Spitzer, L.Jr. and Thuan, T.X., 1972, ApJ, 175, 31. 23, 26

Spitzer, L.Jr. and Shull, J.M., 1975, ApJ, 200, 339. 5

Spitzer, L.Jr., 1987, "Dynamical Evolution of Globular Clusters", Princeton Univ. Press. xvi, xix, xxv, xxvi, xxxi, 3, 5, 8, 10, 14, 18, 19, 21, 24, 26, 27, 33, 36, 70, 71, 72, 75, 99, 122, 137

Spruit, H.C. and Ritter, H., 1983, A&A, 124, 267. 41

Statler, T.S., Ostriker, J.P. and Cohn, H., 1987, ApJ, 316, 626. 25

Stuntzeff, N.B., Schommer, R.A., Olszewski, E.W. and Walker, A.R., 1992, Astron. J., 104, 1743. 2

Sugimoto, D. and Bettwieser, E., 1983, MNRAS, 204, 19. xxxi, 58, 124

Takahashi, K., 1995, PASJ, 47, 561. 26

Takahashi, K., 1996, PASJ, 48, 691. 26

Takahashi, K. and Portegies Zwart, S. F., 1998, ApJ, 503, L49. 26

Takahashi, K. and Portegies Zwart, S. F., 1999, in "Galaxy Dynamics" (ASP Conference Series vol. 182), eds. Merritt, David R., Valluri, Monica and Sellwood, J.A., San Francisco: ASP. 26

Tauris, T. M. and van den Heuvel, E.P.J., 2006, in "Compact stellar X-ray sources" (Cambridge Astrophysics Series, No. 39), eds. Lewin, W. and van der Klis, M., Cambridge, UK, p.623. 13, 14

Trager, S.C., King, I.R. and Djorgovski, S., 1995, Astron. J., 109, 218. 5

Tripicco, M.J., 1993, in "The Globular Cluster-Galaxy Connection", eds. Smith, G.H. and Brodie, J.P. 1

van den Bergh, S., 1991, ApJ, 369, 1. 2

van den Heuvel, E.P.J., 1991, in "Neutron Stars: Theory and Observation", eds. Ventura, J. and Pines, D., Kluwer, Dordrecht, p.171. xviii, 11, 13, 14, 36, 41, 69, 142

van den Heuvel, E.P.J., 1992, in "X-Ray Binaries and Recycled Pulsars", eds. van den Heuvel, E.P.J. and Rappaport, S.A., Kluwer, Dordrecht, p.233. xxii, 11, 13, 36, 41, 69, 70, 142

van der Sluys, M.V., Verbunt, F. and Pols, O.R., 2005, A&A, 440, 973. xx, 42, 66

Verbunt, F. and Zwaan, C., 1981, A&A, 100, L7. xx, 12, 37, 38, 39, 66

Verbunt, F., 1987, ApJ, 312, L23. xviii, 17, 142

Verbunt, F. and Hut, P., 1987, IAUS., 125, 187V. 8, 35

Verbunt, F., 2003, in "New horizons in globular cluster astronomy", ASP conf. series 296, ed. Piotto, G. et.al., San Francisco: ASP. xviii, 34, 38, 40, 60, 61

Verbunt, F. and Lewin, W.H.G., 2004, in "Compact Stellar X-ray Sources", eds. Lewin, W.H.G. and van der Klis, M., Cambridge Univ.Press. 35

Verbunt, F., 2006, in Highlights of Astronomy, Volume 14, XXIVth IAU General Assembly, August 2006, ed. van der Hucht, K.A. 60, 61

von Hoerner, S., 1960, Zeitschrift fuer Astrophysik, 50, 184. 1, 23

White, N.E. and van Paradijs, 1996, ApJL, 473, L25. 7

White, N.E. and Ghosh, P., 1998, ApJ, 504, L31. xxiv, 51

White, R.E., Sarazin, C.L. and Kulkarni, S.R., 2002, ApJ, 571, L23. xvii, 16, 140

Zwaan, C., 1981, in "Solar Phenomena in Stars and Stellar Systems", eds. Bonnet, R.M. and Dupree, A.K., D. Reidel, Dordrecht, Holland. 37